1998

Numerical simulation of the hydrodynamic behavior of a gas-solid fluidized bed with and without an electric field

Forhad Md Hossain
Iowa State University

INFORMATION TO USERS

This manuscript has been reproduced from the microfilm master. UMI films the text directly from the original or copy submitted. Thus, some thesis and dissertation copies are in typewriter face, while others may be from any type of computer printer.

The quality of this reproduction is dependent upon the quality of the copy submitted. Broken or indistinct print, colored or poor quality illustrations and photographs, print bleedthrough, substandard margins, and improper alignment can adversely affect reproduction.

In the unlikely event that the author did not send UMI a complete manuscript and there are missing pages, these will be noted. Also, if unauthorized copyright material had to be removed, a note will indicate the deletion.

Oversize materials (e.g., maps, drawings, charts) are reproduced by sectioning the original, beginning at the upper left-hand corner and continuing from left to right in equal sections with small overlaps. Each original is also photographed in one exposure and is included in reduced form at the back of the book.

Photographs included in the original manuscript have been reproduced xerographically in this copy. Higher quality 6" x 9" black and white photographic prints are available for any photographs or illustrations appearing in this copy for an additional charge. Contact UMI directly to order.

UMI

A Bell & Howell Information Company
300 North Zeeb Road, Ann Arbor MI 48106-1346 USA
313/761-4700 800/521-0600

Numerical simulation of the hydrodynamic behavior of a gas-solid fluidized bed with and without an electric field

by

Forhad Md Hossain

A dissertation submitted to the graduate faculty

in partial fulfillment of the requirements for the degree of

DOCTOR OF PHILOSOPHY

Major: Mechanical Engineering

Major Professor: G.M. Colver

Iowa State University

Ames, Iowa

1998

Graduate College
Iowa State University

This is to certify that the Doctoral dissertation of

Forhad Md Hossain

has met the dissertation requirements of Iowa State University

Signature was redacted for privacy.

Major Professor

Signature was redacted for privacy.

For the Major Program

Signature was redacted for privacy.

For the Graduate College

TABLE OF CONTENTS

LIST OF FIGURES

LIST OF TABLES

NOMENCLATURE

The variables used in this dissertation are listed below. Where appropriate, some symbols may have more than one meaning.

A_t Cross section area of fluidized bed, m^2

C_D Drag coefficient

d_p Diameter of solid particles, cm

E Electrical field strength, V/m(or kV/m)

E_o Reference electrical field strength, kV/m

E_{mb} Electric field strength of minimum bubbling, kV/m

E_{max} Breakdown electrical field strength between particle contact, kV/m

$F_{J\text{-}DC}$ Electrical force due to the DC current effect, N

$F_{J\text{-}AC}$ Electrical force due to the AC current effect, N

F_{vdw} Van der walls force, N

F_{el} Electrical force, N

g Gravitational force per unit mass, cm/sec^2

$G(\varepsilon)$ Modulus of elasticity, N/m^2

J Current density

K_{el} Constant due to electrical force, N

K_a permittivity constant, $8.85x10^{-12}$ F/m

K_b Ratio of permittivity

M Mass of particles in the bed, kg

P	Pressure, pa
ΔP	Pressure across the fluidized bed, pa
Re_s	Solids Reynolds number
R_c	Particle contact resistance, ohm
R_s	Surface contact resistance, ohm
t	Time, sec
T	Temperature, k
U	Superficial velocity, cm/s
u_g	Lateral gas velocity, cm/s
u_s	Lateral solid particle velocity, cm/s
U_b	Bubble rise velocity, cm/s
U_{mf}	Minimum fluidized velocity, cm/s
v_g	Vertical gas velocity, cm/s
v_s	Vertical solid particle velocity, cm/s
x	Co-ordinate in lateral direction, cm
y	Co-ordinate in vertical direction, cm
U_{mb}	Minimum bubbling velocity, cm/s
$U_{mb.E}$	Minimum bubbling velocity under electric field, cm/s
U_o	Gas velocity, cm/s
U	Superficial gas velocity, cm/s
Y	Elasticity of the fluidized bed under electric field, N/m^2

Y_{mb} Elasticity of the bed under minimum bubbling. N/m^2

Y_{vdw} Elasticity due to van der walls force. N/m^2

$Y_{vdw.el}$ Elasticity due to van der walls force with electrical . N/m^2

c Velocity of sound in gas phase m/s

d_p Particle diameter. cm

g Acceleration of gravity. 9.81 m/s^2

k Constant from the Richardson-Zaki relationship

n Constant from the Richardson-Zaki relationship

p_b Pressure inside the bubble. N/m

r Radius coordinate. cm

r_b Bubble radius. cm

t Time. s

u Velocity of fluid phase. m/s

u_b Relative fluid/particle interstitial fluid velocity far. cm/s

from the bubble. m/s

v Velocity of disperse (or particle) phase. m/s

x Distance between two particles. m

Greek

α Resistivity of the bed. Ohms

$\beta_o(\varepsilon)$ Permeability constant

β $\left(\frac{dp}{dD}\right)$, cm^2/s^2

β_x Fluid-particle friction coefficient in the x direction

β_y Fluid-particle friction coefficient in the y direction

ε_g Fluid void fraction

ε_s Solid void fraction

$\varepsilon_{em.o}$ Permittivity of free space, 8.854×10^{-12} F/m

ε_{mf} Voidage of the fluidized bed under minimum fluidization

ε_{mb} Voidage of the fluidized bed under minimum bubbling

ε_{packed} Voidage of the packed bed

ϕ Electrical field potential, V

ϕ_s Particle sphericity

μ Viscosity, $N.s/m^2$

γ Constant

λ Eigen value of the characteristic equation

ρ_f Fluid density, gm/cm^3

ρ_p Particle density, gm/cm^3

σ Stress of the fluidized bed, N/m^2

τ_c Time constant for particle contact resistance, s

τ_s Time constant for surface contact resistance, s

ω	Angular velocity, radian/s
δt	Time Step, s
$\delta r, \delta z$	Mesh size, cm

1. INTRODUCTION

The objective of the study is to simulate numerically the behavior of a fluidized bed with and without an electric field. The effects studied include bed circulation in particulate (bubble-free) fluidization, bubble development, and jet propagation. Fluidization is an operation which involves the flow of solids in contact with a gas, liquid, or both a gas and liquid. Fluidization technology has been applied in chemical, petrochemical, metallurgical, mineral, and bio-chemical operations. Classical applications of gas-solid fluidized beds can be exemplified by the following: synthesis reactions such as the production of phallic anhydrite, polyethylene, acrylonytrite, and hydrocarbons such as fluid catalytic cracking (FCC), thermal cracking, fluid coking, the reduction and oxidization reactions of ores such as roasting of sulfide ores, reduction of iron ores, and carbonization and gasification process such as coal and coke gasification and activated carbon production. State-of-the-art applications of gas-solid fluidized beds include material processing such as the production of silicon, silicon carbide, tungsten carbide and particles with metallic coatings, clean fossil fuel technology such as control of No_x , So_2 , N_2 O, air toxins, liquid and solid wastes, and other emissions resulting from coal use as well as high pressure circulating fluidized bed incineration of solid waste (Fan, 1996).

Fundamental research on gas bubbles and fluid dynamics associated with bubble flows in gas-solid fluidization was the focus of considerable research carried out in the 60's, and 70's. Since the beginning of the 80's, substantial research (Fan, 1996) has been shifted to high velocity fluidization. Examples of fundamental topics of current research interest in

gas-solid fluidization include the elasticity behavior of particulate phase or solid stress. fluidization stability analysis. flow behavior in the bubble wakes and voidage distribution around the bubbles in the analysis of gas flow division. Other topics of interest include bubble coalescence and break up. gas kinetics theory (Gidaspow. 1994) in the dilute and dense phase pneumatic transport simulation. mechanisms of the cluster formation and dynamics of the solids flow in the core and annular regions of fluidized beds and their interaction in fast fluidization. characterization of fluidization with fine powders. scale-up criteria and fluidization at high temperatures and pressures.

A hydrodynamic approach to fluidization was developed by Davidson (Davidson. 1985) in 1961. Davidson's model accurately predicted many features of bubble motion in a fluidized bed. He analyzed a single bubble motion in an infinite fluid bed using two continuity equations and an expression for relative velocities in terms of Darcy's law for flow in porous media. Davidson assumed that the flow of solids around a bubble was irrotational He predicted the existence of a spherical surface of zero velocity. called a cloud. Shortly after his prediction. the existence of a cloud was verified experimentally by inserting O_2 into a bubble injected into a fluidized bed near minimum fluidization. The concept of a cloud is so important that one actually denotes it to be a phase in the transfer coefficient models of Levenspiel and others (Ettehadieh. 1982).

The modeling of fluidized beds using hydrodynamic equations also started with the Davidson model in 1961. During the following years several investigators attempted hydrodynamic modeling of a fluidized bed (Jackson. 1963. Murray. 1965.Pigford and Baron.

1965, Soo, 1967, Ruckenstein and Tzeculescu, 1967). The models became more detailed and hence analytically intractable.

In recent years, extensive experiments were conducted in Mechanical Engineering at ISU to observe the bubble control phenomenon by applying both ac and dc electric fields across the two-phase fluidized bed (solid-gas). It was reported that the electric field has strong effects on the dynamics of a bubbling fluidized bed. For example, heat and mass transfer can either be decreased or increased as a result of ac and dc fields. Experiments have confirmed that bubble formation and calming of a gas in a fluidized bed (reduced circulation) can be attained with fields (e.g. Colver and Bosshart,1979). Work previously carried out in this laboratory shows that expansion of a bubbling bed to 15% (compared to 1-2% for a field free bed) is possible with ac fields. Bed control with electric fields depends on the dynamic conditions of the bed, the properties of the material as well as the strength and frequency of the applied field. It was observed that with increased particle size, bubble control is diminished probably as a result of the increase in the ratio of fluid dynamics and gravitational forces to electrostatically induced forces.

An attempt has been made to predict the bed behavior with electric field forces. A new model for cohesive force between particles leads to the concept of the bed modulus of elasticity. This modulus of elasticity has been added to the existing solids stress term in the code. The effects of the stress of solids on bed circulation, bubble growth, and jet propagation with field is investigated. The relevant bed parameters including pressure, velocity, and void fraction for each phase have been calculated numerically using the modified K-FIX

multiphase FORTRAN computer code. In this study the transient dynamics of two-dimensional, two phase flow with interfacial exchange are calculated. The program solves a set of partial differential equations to describe the flow of a gas-solid mixture. Each phase is described in terms of its own density, velocity, and voidages. The program allows the description of the flow of solid particles of different sizes. Each size of particle is treated as a continuum - a particulate phase with a characteristic diameter.

2. DESCRIPTION OF PHYSICAL MECHANISMS

Gas fluidization is the levitation of a mass (bed) of solid particles by an upward flowing gas. In this state, the particle mass behaves like a fluid in that it tends to establish a level and flow in response to pressure gradients. In this state, this there is a balance between the hydrodynamic drag force and the gravitational force acting on the particle. The gas velocity required to achieve this state is known as the minimum fluidization. The pressure drop through any section of the fluidized bed equals the weight of the solid particles and the gas divided by the cross-sectional area of the bed. Different regimes of gas-solid two phase fluidization may include particulate, bubbling, turbulent, and fast fluidization.

A velocity higher than the critical velocity causes the formation of bubbles. The velocity at which bubbles first appear is called the minimum bubbling velocity. The fluidized bed is now divided in to two regions, one region containing bubbles, while the other is a mixture of fluid and particles in a state of minimum fluidization. Further increases in the superficial velocity move the fluidized bed into a fast transporting regime where slugs dominate in the bed. In the limit that the superficial velocity exceeds the terminal velocity of the largest particle in the fluidized bed, all the particles in the fluidized bed would be carried out of the bed.

Formation of Bubbles

Gas flow in excess of the minimum bubbling velocity, forms voids called bubbles. Bubbles grow, diminish or coalescence with other bubbles as they move up from the bottom of the bed. There is intense mixing and gas solids contact as the particles are carried and

released by the bubbles. This intense mixing makes it easy to have an isothermal system with good mass transfer. When bubbles reach the free surface of the bed, they erupt and throw particles into the freeboard (the level of the solids is the bed height and the vertical space above the bed height is called the freeboard). Smaller particles are carried out by the gas, while larger particles drop back into the bed. This carry-over behavior is called elutriation. When the superficial velocity of the fluidized bed exceeds the terminal velocity of a particle, the particle is elutriated out of the fluidized bed.

Previous Studies

The formation of bubbles in a fluidized bed depends primarily on the properties of the particles and the fluid (Geldart,1986).

Katz and Sears (1969), and Johnson and Melcher (1975) reported bed expansion without bubble formation with a electric field, using gel particles and sand particles. Dietz and Melcher (1978) reported that an electric force was required to gain bubble control after investigating interparticle electrical forces in packed and fluidized beds.

In the case of an electric field, Dietz (1977) studied the fields and forces on a microscopic sphere above a ground plane in a sinusoidal varying electric field. He found that there were three regimes of interest: conduction, polarization and intermediate cases. He also showed that the electric force is a function of frequency. Moissis and Zahn (1986) carried out a theoretical approach to an electrofluidized bed that responded to a small ac electric fields. It was concluded that bed expansion would occur in a co-flow condition. However, they reported no effect on the fluidized bed for the cross flow condition.

Colver (1979) showed that the best stabilization could be achieved by using smaller diameter particles (e. g. smaller than 100 μ m) and a horizontally directed alternating electric field in a fluidized bed. Also he reported the superiority of an ac electric field over a dc field in controlling bubble formation.

Colver and Basshart (1980) reported up to 30% expansion in bed height without bubbling for a bed of 60 μm particles in a field alternating at 20 Hz and an rms field strength of 9.05 kilo-volt per centimeter, kV/cm. It was also reported that high relative humidity could dramatically increase the conductivity and reduce the effect of bubble control.

Colver (1976) found that an electric field strength of order kV/cm was required to control bubble formation and was effective on a variety of particulate materials including both good conductors and semiinsulators. Donahoe and Colver (1984) conducted experiments by injecting a single bubble into an electrofluidized bed. It was found that applying an electric field altered the bubble volume and rise velocity. In the dc case, the bubble could easily be immobilized by the field. Also, the required electric field strength to gain bubble control was higher for the ac than for the dc electric field due to charge relaxation.

Mechanism of Bubble Control

To gain an insight into the mechanism of bubble control, the interparticle and hydrodynamic forces on particles must be investigated. Colver (1976) first conducted a series of experiments to understand the dynamics and stationary charging of heavy metallic and dielectric particles against the conducting wall in the presence of a dc applied electric field.

He reported that the charge had the form $Q = 4\pi\varepsilon_{em,o} a^2 kE$. where k=1.64. Colver (1980) investigated different interparticle forces, including Van der Waals, capillary, electrostatic contact dipole, and electrostatic. Different charge relaxation time constants were also determined for 62 μm glass beads at 30% relative humidity.

Colver (1983) also proposed equations for estimating different charge relaxation time constants. From this time constant the void fraction of an electrofluidized bed could be predicted.

Rietema (1991) proposed a criteria for the minimum bubbling velocity using perturbation analysis for the bed elasticity modulus. Xie and Geldart (1992, 1993) examined the effect of Van der Waals force on the fluidized bed without an electric field. It was reported that the voidage of minimum bubbling decreased with the increasing particle diameter and temperature.

Gidaspow (1994) derived a relationship for the particle drag force from kinetic energy dissipation analysis. He developed the same function as the well known Ergun equation.

3. THEORETICAL STUDIES

In a field-free fluidized bed, the independent variable is the gas throughput (superficial velocity) for given conditions in the bed of particle size, temperature, etc. However, for a given superficial velocity, the dynamics of the bed, as reflected in bubble formation and particle circulation, heat transfer, and mass transfer, etc., can also be readily altered by varying the intensity and frequency of the electric field. The role of the field is thus seen to be an independent variable along with the superficial velocity. Fields must be applied in a balanced way so that an acceptable state of fluidization is maintained. Thus, previous investigators attempting to use dc fields on a fluidized bed often reported conditions of bed freezing, spouting, and generally poor quality of fluidization. It seems clear that for a bed to maintain a state of fluidization, particle forces cannot overwhelm other stabilizing forces in the bed. This is precisely what can happen with dc fields if not carefully controlled. However, with ac fields, locking and unlocking of particles (or simply relaxing interparticle forces) apparently accommodates adjustments of the particles to normal fluidization forces of fluid drag and gravity is such a way as to maintain good fluidization Colver,1977b).

Inter-Particle Forces and Bed Expansion

Limited bed expansion in field-free gas fluidized beds is observed for small particles. An equation representing this expansion as reflected as an increase in bed viodage ε with superficial gas velocity U is the Richardson-Zaki equation (Davidson and Harrison,1971), $\frac{U}{U_i} = \varepsilon^n$ where U_i is approximately the free fall velocity of the particles.With ac fields, bed expansions of an additional 5-15% are possible beyond field free expansions depending on

particle size and superficial velocity. This expansion is accompanied by a reduction in circulation in the bed and diminished bubble formation.

One might have anticipated another effect with fields, such as a contraction of the particle packing resulting in a decrease volume of the fluidized bed. This might in fact be expected in beds with negligible wall effects and with $U\langle U_{mb}$, but to date the effect has not been reported in smaller beds except perhaps with dc fields where contraction of particles into a spouting bed can readily be observed. The additional bed expansion observed with external fields is simply explained by the decrease in gas by passing with a corresponding increase in interstitial gas velocity leading to greater particle drag. These events lead to a distribution and increase in the bed viodage until a balance between particle drag and gravity is again established. Bed expansions of up to 15% and more are observed with small particles, say $\langle 50\mu m$.

Forces on Particles

To begin to model the observed behavior of an electrofluidized bed, it is necessary to gain an understanding of the possible types of forces that act on particles as a consequence of an applied electric field. The forces acting on particles in a gas fluidized bed are summarized in Table 3.1 (Colver, 1980).

Dipole forces in Table 3.1 can be usually be neglected compared to induced electrostatic forces for slightly conductive particles. We will not consider the permanent forces of Van der Waals, capillary or electrostatic contact here. To be consistent with the

Table 3.1: Electrostatic forces between particles

Types of Equation	**Functional Relationships**
Van der Waals	$F_{vdw} = K_1\left[\frac{d_1 d_2}{d_1 + d_2}\right]$
Capillary	$F_{vdw} = K_2 d$
Electrostatic Contact	$F_{el} = K_{el} A\left(\frac{\phi}{Z_0}\right)^2$
Dipole	$F_D = Kd^2E^2$
Electrostatic	$F_j = K_a d^2\left[\frac{E^2}{2} - K_b\left(\frac{JK_c}{\sigma}\right)^{\beta}\right]$

assumption of no free charge in the bed, the first term of the electrostatic force Table 3.1 is taken as zero.The electrostatic force equation due to current in the fluidized bed takes the form.

$$F_{j\text{-}dc} = -K_a K_b d^2\left(\frac{JK_c}{\sigma}\right)^{\beta} \qquad (3.1)$$

where the K's and β are constants and J, d, and σ are the current density, particle diameter, and bed electrical conductivity respectively. The "dc" subscript has been added to eqn. (3.1) to remind us that this was developed for a dc field current.

An extension of the Davidson field-free model was proposed for the hydrodynamic behavior of bubbles formed in the fluidized bed (Colver et al., 1992b). In this model a spherical bubble was assumed already to be formed in the bed. It was then postulated that electrostatic forces must be of the same order of magnitude as particle-fluid forces for effective control. For an incipiently fluidized bed, gravitational forces acting on the particles were just balanced by the forces of fluid drag. In this regime ($U_{mf} < U < U_{mb}$), applied electric fields had little effect on the overall bed behavior except to induce oscillations if it is an ac field. But in a bubbling bed ($U > U_{mb}$), the mechanism was different. Two bubble models would be incorporated, one was for the fluid dynamics and another for the electrostatics. The well known Davidson model was used for an isolated spherical bubble since it offered a closed form solution of the pressure distribution as well as the fluid and particle velocity distributions around the bubble. For the electrostatic model, the maximum electric field induced particle-particle force would be determined by a similar spherical bubble. Bubble control would be postulated to be effective when the maximum electrostatic forces were made comparable to the maximum fluid dynamic forces. In this case, only the electrostatic force was important by comparing it to the hydrodynamic forces. The following assumptions and equations describe the Davidson bubble model (Davidson, Clift, and Harrison, 1985).

Assumptions:

- spherical bubble
- incompressible flow for the particle and fluid phases
- negligible particle-particle friction (potential flow of

particle phase)

- pre-determined particle path around the spherical bubble
- uniform pressure inside the bubble
- incipient fluidization far from the bubble (constant pressure gradient)

The equations of motion to be solved were:

The particle continuity:

$$\bar{\nabla}\cdot\varepsilon\,\bar{v} = \varepsilon\,\bar{\nabla}\cdot\bar{v} = 0 \tag{3.2}$$

The fluid phase continuity:

$$\bar{\nabla}\cdot\varepsilon\,\mathbf{u} = \varepsilon\,\bar{\nabla}\cdot\mathbf{u} = 0 \tag{3.3}$$

The fluid phase momentum:

$$\bar{\nabla}P + \beta_o(\varepsilon)[\bar{u} - \bar{v}] = 0 \tag{3.4}$$

Only the solution for the pressure distribution was needed to determine the force on a particle from eqn. (4.4). The solution of the pressure distribution P(r):

$$P = P_b - \beta_o(\varepsilon)u_o\cos\theta\left(r - \frac{r_b^3}{r^2}\right) \tag{3.5}$$

where β_o is the permeability constant as in a Darcy law type expression for the drag on a particle such that $\beta_o u_o$ is the pressure gradient $\partial p/\partial y$ far from the bubble in the vertical direction. p_b is the pressure inside the bubble, r_b is the radius of the bubble, and u_o is the relative fluid/particle interstitial fluid velocity far from the bubble. A contour plot of lines of

constant pressure gradient (magnitude) was shown in Fig. 3.1. Figure 3.1 was obtained using eqn. (3.5) and the definition of ∇P. The maximum pressure gradient was found to be three times greater than the pressure gradient in the far field of the bubble (see Fig. 3.2)

$$\left|\frac{dP}{dy}\right|_{max} = 3\left(\frac{\partial P}{\partial y}\right)_{o} \tag{3.6}$$

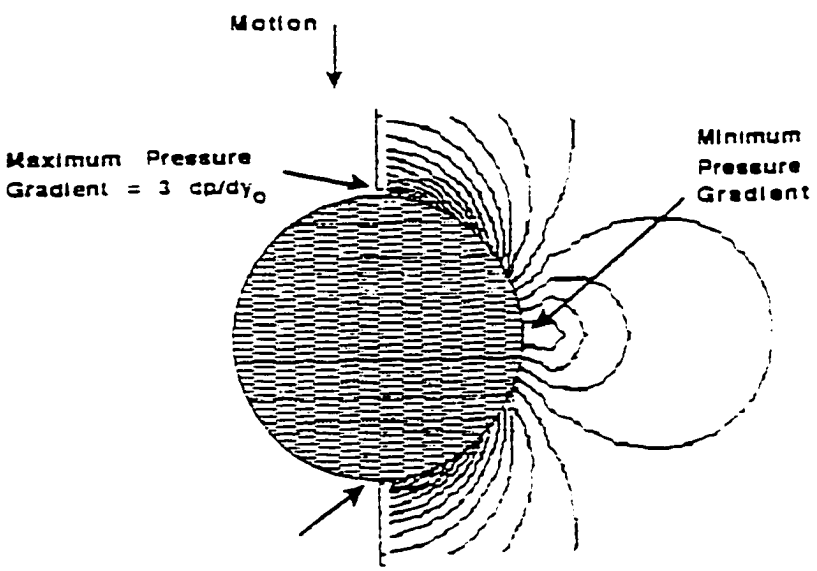

Figure 3.1: Contour plot of constant pressure gradient lines showing maximum pressure gradient on a spherical bubble of unit radius

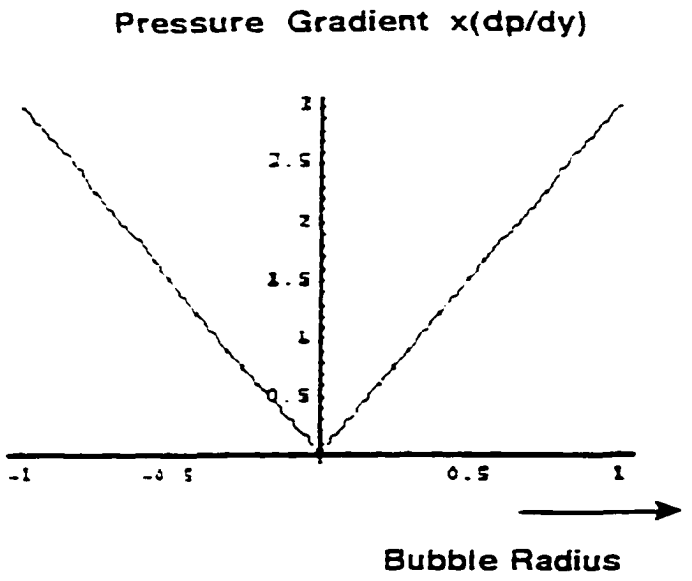

Figure 3.2: Pressure gradient on surface of bubble of unit radius (with the vertical z axis)

The following assumptions and equations are for the proposed bubble model with electrostatics.

Assumptions:

- spherical bubble with field axial symmetry
- uniform electrical conductivity throughout the particle phase (infinite resistivity in the bubble region)
- constant dc (horizontal) electric field far from the bubble
- no free charge
- negligible polarization forces
- negligible magnetic field effect from current in the bed

The equations of electricity are:

conservation of charge

$$\bar{\nabla} \cdot \bar{J} = 0 \tag{3.7}$$

Ohm's law

$$\bar{J} = \zeta \bar{E} \tag{3.8}$$

Definition of scalar potential

$$\bar{E} = -\bar{\nabla} \phi \tag{3.9}$$

Combining eqns. (3.7)-(3.9) lead to the Laplace equation for constant electrical conductivity ζ outside the bubble as follows (Nayfeh and Brussel, 1985):

$$\nabla^2 \phi = 0 \tag{3.10}$$

The boundary conditions are: $\bar{J}_n = 0$ and $\bar{E}_n = 0$ at bubble interface. Therefore, the solution for the field potential, ϕ, is

$$\phi = -E_o r \cos\theta [1 + \frac{r_b^3}{2r^3}] \tag{3.11}$$

The r and θ components of current around the bubble are

$$J_r = \zeta E_o \cos\theta \, [1 - \frac{r_b^3}{r^3}] \tag{3.12}$$

$$J_\theta = -\zeta E_o \sin\theta \, [1 + \frac{r_b^3}{2r^3}] \tag{3.13}$$

Figure 3.3 shows eqns. (3.12) and (3.13) as a vector field plot (length of arrow represents relative magnitude of current density or electric field strength).

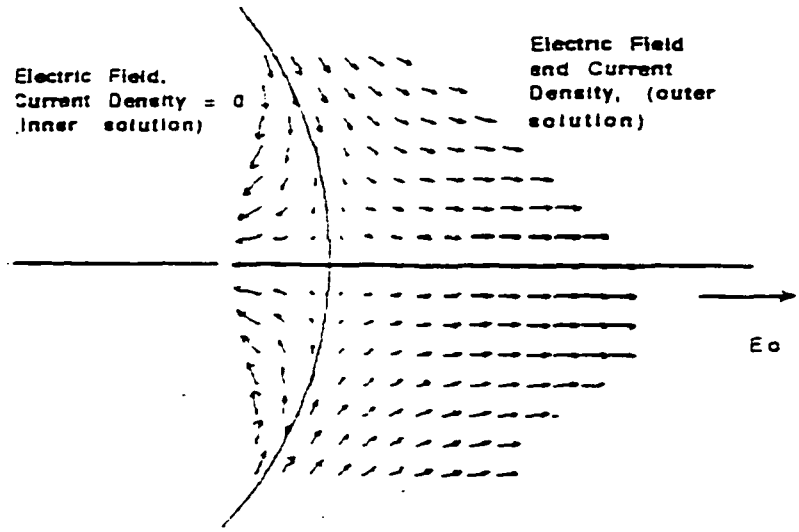

Figure 3.3 Vector field plot of current density magnitude and electricfield strength near bubble (θ =0), current density inside bubble =0

The current density is zero at the vertical surfaces of the bubble (θ=0.π). Inside the bubble the current is zero while the electric field strength is non-zero. The tangential component of the electric field must be continuous through the bubble interface since the free charge was zero. In the likely event of charged particles occurring at the bubble interface, the internal electric field would circulate these particles. Fig. 3.4 shows the flow direction of current around a bubble of unit radius.

The current density reaches its maximum value at the top and bottom of the bubble (θ=π/2, 3π/2) and was zero at the sides (θ=0.π). This means that the particle-particle forces due to the current would be greatest at the top and become zero at the sides of the bubble. From eqns. (3.12), (3.13) the maximum current at the interface is 3/2 times the far field current.

The resulting relations for current density and electric field strengths with the far field J_o and E_o are

$$J_{max} = \frac{3}{2} J_o \tag{3.14}$$

$$E_{max} = \frac{3}{2} E_o \tag{3.15}$$

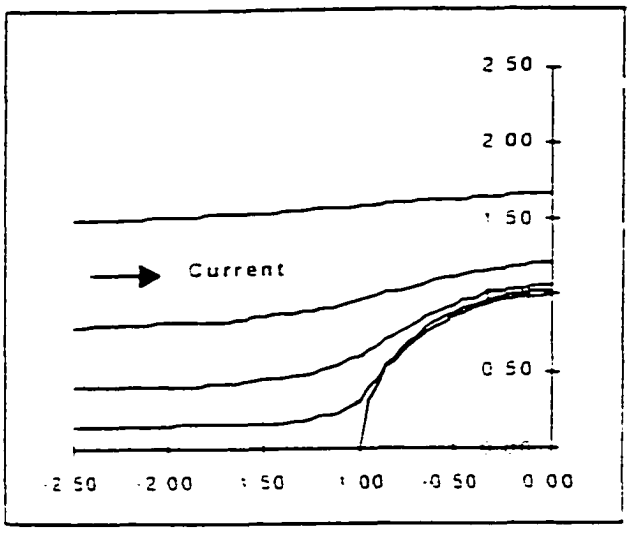

Figure 3.4 Lines of constant Ψ showing current path and direction of electric field past bubble of unit radius (largest current concentration at the top of the bubble)

The criteria for bubble control was that the ratio of the forces acting on the particles due to the electric field stresses and pressure gradient. This ratio is given as

$$\frac{F_{J\text{-}DC}}{F_{f\,max}} = \frac{\left(\frac{F_{J\text{-}DC}}{d^2}\right)}{\nabla P_{max}} \left[\frac{6(1-\varepsilon)}{\varepsilon \pi d}\right] \approx 1 \tag{3.16}$$

The following relationship for the pressure gradient can be obtained using eqns. (3.6), (3.8), (3.14), and (3.15), and the relationship for the far field pressure gradient as

$$\left(\frac{\partial P}{\partial y}\right) = \rho_p(1-\varepsilon)g \tag{3.17}$$

Substituting eqn. (3.17) into eqn. (3.16) gives the criteria for bubble control as (Colver and Wang, 1993)

$$\frac{F_{J\text{-}DC}}{F_f} = \frac{2K_aK_b}{\varepsilon(U)\rho_p\pi\, dg}\left(\frac{3}{2}K_cE_o\right)^{\beta} \approx 1 \tag{3.18}$$

where the voidage, $\varepsilon(U)$, can be found using the Richardson-Zaki equation given in eqn. (3.14). The n and u_s in eqn. (3.14) could be found from the experimental data.

As a numerical example, consider the Microbeads glass spheres which have the following values: $K_a=\varepsilon_{em.o}=8.85\text{x}10^{-12}$, $K_b=\varepsilon_{em}/\varepsilon_{em.o}=7.0$, $K_c=1$ (typically 1-20), $\beta=2$ (typically 1-2), $\rho_p=2500$ kg.m^{-3}, $g=9.81$ m.s^{-2}, and $d=62\mu$m. From the above equations, the far field strength is calculated to be $E_o=1.8\text{x}10^5$ V/m for bubble control in the fluidized bed. This value was typical of the field strength required for bubble control as measured in the experiment.

Assuming that only the current constriction force was important in dc electric field. Then the force equation is given by Dietz and Melcher (AIChE Symp., 1978b) is

$$F_{J\text{-}DC} = K4\pi\varepsilon_{em.o}d^2E_{max}^{\gamma}E^{2-\gamma} \tag{3.19}$$

where K and γ ($=0\rightarrow2$) were experimentally or theoretically derived constants, and $\varepsilon_{em.o}$, d, E_{max}, and E, were the permitivity of free space, the particle diameter, the breakdown electric field strength between particle contacts, and the average electric field strength in the bed, respectively. Dietz and Melcher (1980) found that K=0.1, γ=0.8 and E_{max}=30 kV/cm. From the results of scale-up parameters , a further relation can be written as

$$\gamma = 2 - \frac{1}{n} \tag{3.20}$$

where n was a constant of the Richardson-Zaki equation. By substituting eqn. (3.20) into eqn. (3.19), eqn. (3.18) is rewritten as

$$\frac{8K\varepsilon_{em,o}E_{max}^{2-\frac{1}{n}}\left(\frac{3}{2}E_o\right)^{\frac{1}{n}}}{\varepsilon(U)d\rho_p g} \geq O(1) \tag{3.21}$$

Equation (3.21) implies that increasing the superficial velocity, particle diameter, and particle density can lead to an increase in the required electric field strength in the far field (E_o) in order to suppress bubbles. These predictions are consistent with experimental results.

AC Electrical Field Model

A model describing the inter-particle forces with an ac field has been studied. Fig. 3.5 shows the two particle model. The capacitance (C_c) between the two particles was determined in large part from the close separation distance of the surfaces, as could be seen from the definition of capacitance (i.e., $C \approx \varepsilon_{em}A/x$, where x was the separation distance and A was some appropriate effective area). For ac fields, inter-particle forces exist between two particles even if the particles are separated and the contact resistance is infinitely large because of the mutual capacitance. This is in contrast to the usual dc current related electrostatic particle forces listed in Table 3.1 where electrical contact between the particles was assumed. Thus, particles need not be touching for induced electrostatic forces to exist with ac fields. The differential equation for the voltage across two particles can be obtained by applying Kirchhoff's law (Colver and Wang, 1993b)

$$\frac{dV_c}{dt} + \frac{V_c}{\tau_c} = \frac{V_o}{\tau_s} e^{(i\omega t)} \tag{3.22}$$

where the time constants for the particle contact (τ_C) and surface contact resistance (τ_S) are

$$\tau_c = \frac{R_s R_c}{R_s + R_c} C_c \tag{3.23}$$

$$\tau_s = R_s C_c \tag{3.24}$$

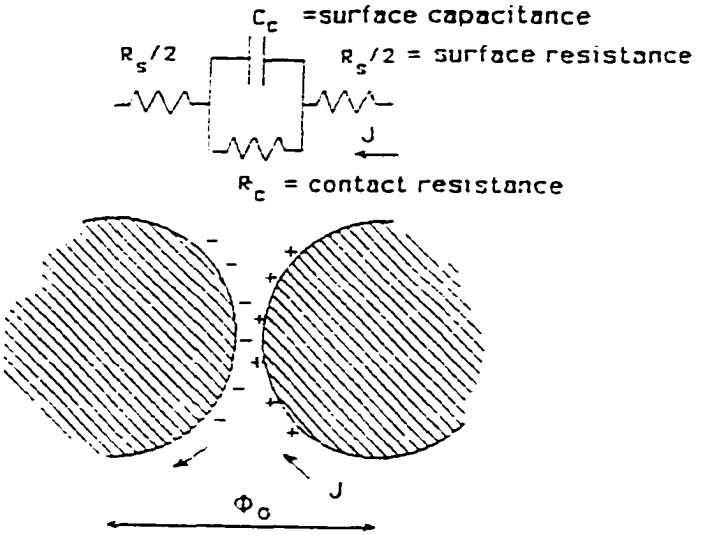

Figure 3.5 Equivalent circuit for particles with mutual capacitance, including contact resistance and surface conductivity

There are two limiting cases which depend on the relative position of the particles and the magnitudes of the surfaces and contact resistance.

(I) $R_s >> R_c$ (e.g. particles touching, DC/AC field)

(II) $R_s << R_c$ (e.g. particles not touching, AC field only)

The steady periodic solution for eqn. (3.22) is

$$V_c = \frac{V_o\left(\frac{\tau_c}{\tau_s}\right)}{\left[1+(\tau_c\omega)^2\right]^{\frac{1}{2}}} e^{(i\omega t-\delta)} \tag{3.25}$$

where $\tan\delta=\omega\tau_c$. The force magnitude per unit area between the plates of the capacitor is given by the relation

$$\frac{F_{J\text{-}AC}}{A} = \frac{\varepsilon_{em/o}E_c^2}{2} = \frac{\varepsilon_{em/o}\left(\frac{\tau_c}{\tau_s}\right)\left(\frac{V_o}{x}\right)^2}{2\left[1+(\tau_c\omega)^2\right]} \tag{3.26}$$

The value for τ_s could be calculated if the resistivity of the bulk bed was known (Colver, 1980). For the 44-74 μm glass spheres, τ_s=0.44 s when the bulk bed resistivity was 2×10^{10} Ω-m at 25°C. For the FCC (2-A), τ_s=0.12 sec when the bulk bed resistivity equaled 5.4×10^{9} Ω-m at 25°C. If it was assumed that $\tau_c=\tau_s$=0.44 sec and ignoring the variation in the particle separation distance (x) as the bed volume decreased, the experimental (Wang, 1995) results showed good agreement with the theoretical model. By comparing eqn. (3.26) with $F_{J\text{-}DC}$ eqn. (3.19), a possible expression for the ac electric force can be written as

$$F_{J\text{-}AC} = \frac{K\pi\varepsilon_{em.o}d^2E_{max}^{\gamma}\left(\frac{3}{2}E_o\right)^{2-\gamma}}{1+(\tau_c\omega)^2} \tag{3.27}$$

for which the zero frequency limit is satisfied.

Using eqn. (3.26) and assuming $\tau_c=\tau_s$, τ_c is found to be 0.25 sec. Comparing the calculated values with the result found previously of τ_c=0.12 sec, it can be seen that the

calculated value is of the same order. However, the dc limit is not well fitted to this model. This is possibly due to the different mechanism between dc and ac electric fields.

Stability Analysis

The perturbation method was applied to the governing equations of both fluid and dispersed phases giving the stability analysis of the bed expansion (Rietema, 1991). A bed modulus of elasticity (Y) was proposed to account for observations of cohesive behavior in a field-free bed such as bed expansion and tilting of beds which both resulted from interparticle forces. As the bed expanded with superficial velocity, particle contact remained but the number of contacts (k) was reduced as particles shifted into a less dense formation, retaining a chain-like structure.

The procedure for applying the perturbation method is as follows:

1. Added a disturbance to the basic equations.
2. Subtracted out steady solution from basic equations.
3. Linearized the disturbance equation (the eigenvalue should be homogenous with homogenous boundary conditions).
4. Assumed a form for disturbance such as traveling wave with attenuation/growth term.
5. Solved for certain values of parameters (eignvalues).
6. Examined eignvalues for growth, neutrality, or decay of disturbance (into bubbles).

The form of the modulus equation is

$$\frac{\partial \sigma_{s,xx}}{\partial x} = -Y\frac{\partial \varepsilon}{\partial x} \tag{3.28}$$

The purpose for extending this continuum concept was to include interparticle forces resulting from electric fields in Y so that Y=Y(E,k...). Such a bed structure, as shown in Fig.3.6, allowed for conducting paths of current along chains of contacting particles through the bed. Because Y_{mb} is a measure of the bed interparticle forces, the lower the Y_{mb}, the easier it is for bubbles to form.

The criteria for bubble control was obtained based on perturbation theory utilizing continuum equations for the conservation of mass and momentum of the solids and gas phases was obtained (Wang 1995). The Kozeny-Carman (K&C) (which was used to derive Ergun equation) and Richardson-Zaki (R&Z) relationships were used to derive the particle drag force.

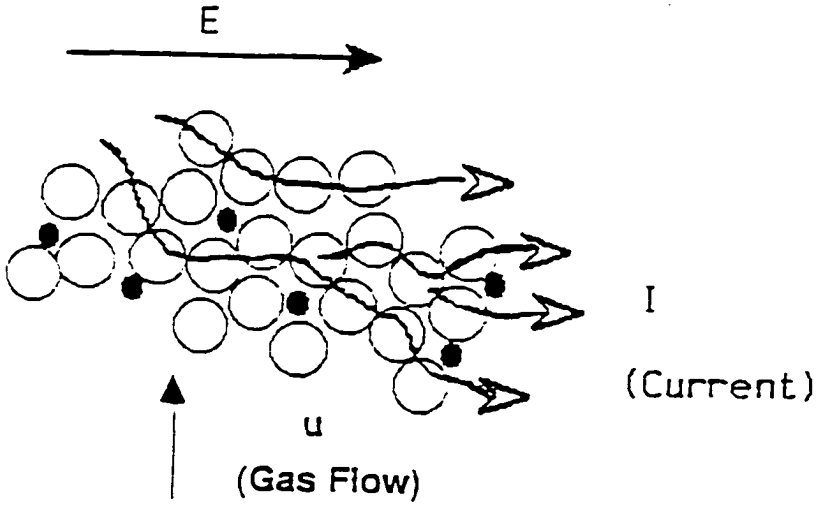

Figure 3.6 Conception of particle contacts during fluidizatio

Using the Kozeny-Carman relationship, $f(\varepsilon)=\varepsilon^2/k(1-\varepsilon)$ where k is a constant, the theoretical criteria for bubble control was given (Colver and Wang, 1993) as

$$\frac{\rho_p(\rho_p-\rho_f)^2 g^2(\phi_s d_p)^4}{\mu^2 Y_{mb}}=\left[\frac{150(1-\varepsilon_{mb})}{(3-2\varepsilon_{mb})\varepsilon_{mb}^2}\right]^2 \tag{3.29}$$

An experimental relationship for the bubble control criteria is given as

$$Y_{mb}=\rho_p\left[(3-2\varepsilon_{mb})\frac{U_{mb}}{\varepsilon_{mb}}\right]^2 \tag{3.30}$$

The Ergun constant, 150, and sphericity ϕ_s in eqn. (3.29) were chosen to fit the bed expansion data. The values also satisfied the momentum equations for the solids and gas phases. It should be noted that in the theoretical derivation of eqn. (3.29), a constant of 180 was obtained (Wang,1995). However, the value of 150 for the constant had also been used by Davidson (1985) and Levenspiel (1991). A way to check the validity of the assumed values for the constants was to compare the drag force to the hydrodynamic force from the momentum equation. The following ratio should yield a constant value of 1.

$$\frac{(\rho_p-\rho_f)g(\phi_s d_p)^2\varepsilon^3}{150(1-\varepsilon)\mu U}=1 \tag{3.31}$$

The effect of the electric field needed to be explicitly included in the theory. This could be accomplished by relating Y_{mb} to E_{mb} using either the empirical relationships or particle force theory. An empirical relationship from the experimental data is given as

$$Y_{mb}(N/m)=Y_{vdw,el}+cE_{mb}(kV/m) \tag{3.32}$$

where $Y_{vdw.el}$ is the Van der Waals and electronic contribution to the modulus and c is a constant. Equations (3.29)-(3.32) formed a complete set of relationships for the bed stability analysis. The value of constant c for modulus of elasticity for the 44.1 μm n.w.p. Microbeads glass particles in different electrical field with Ar and N_2, respectively has been reported by (Wang, 1995).

If the Richardson-Zaki type relationship is used for bed expansion,

$$f(\varepsilon) = k\varepsilon^n \tag{3.33}$$

the theoretical result is given as

$$\frac{\rho_p(\rho_p - \rho_f)^2 g^2 (\phi_s d_p)^4}{\mu^2 Y_{mb}} = \left[(1+n)(1-\varepsilon_{mb})\varepsilon_{mb}^n \frac{k}{18}\right]^{-2} \tag{3.34}$$

and the experimental result is given as

$$Y_{mb} = \rho_p \left[(1-\varepsilon_{mb})(1+n)\frac{U_{mb}}{\varepsilon_{mb}}\right]^2 \tag{3.35}$$

the values of k and n were derived from experimental data using superficial velocity and voidage at minimum bubbling and were chosen to fit the bed expansion data f(ε) and satisfy the momentum equation for the solids and gas phases. The constants k and n can be calculated from the plot of log(U) v.s. log(ε) (Wang, 1995), where the interception of the first order regression fit was coordinated to k and the value of the first order of the regression was coordinated to n. A method to check the validity of the assumed values for the constants is to compare the drag force to the hydrodynamic force from the momentum equation. The following ratio should yield a constant value of unity.

$$\frac{(\rho_p - \rho_f) g (\phi_s d_p)^2 \varepsilon f(\varepsilon)}{18 \mu U} = 1 \qquad (3.36)$$

The summary results for the bed modulus and the Richardson-Zaki fit for different materials used in the tests are listed in Table 3.2. In the numerical simulation second term of the bed modulus has been used along the modulus of elasticity which is a funtion of bed voidages.

Table 3.2: Summary results for bed modulus and Richardson-Zaki fit for different materials (Wang, 1995).

Material Fluidized in Argon (Waddle diameter)	Bed Modulus of elasticity $Y_{mb}=A+BxE_{mb}$ Y_{mb} (N/m^2) E_{mb}(kV/m)	n and k	Bulk Powder Resistivity ohm-m (Packed)	Comment on Particle Fluidization
Glass beads 44 μ m	A =0.177 B=$8.854x10^{-5}$	n=1.585 k=0.0101	$2.5x10^{10}$	Good Fluidized (spherical:) Large Expansion
FCC Kaolin (1-B) 45.5 μ m	A =0.262 B=$6.753x10^{-4}$	n=5.287 k=0.0272	$2.2x10^{8}$	Moderate Fluidized (irregular:) will channel:small expansion
FCC Zeolitic(spent) (1-A) 35 μ m	A =0.258 B=$2.89x10^{-4}$	n=4.304 k=0.0357	$1.1x10^{9}$	Moderate Fluidized (near spherical:) will channel: small expansion
FCC Zeolitic(fresh)(2-A) 58.8 μ m	A=0.250 B=$1.860x10^{-4}$	n=3.891 k=0.0099	$5.4x10^{9}$	Good Fluidized(near spherical:) moderate expansion
FCCAluminum oxide(3-A)66.7 μ m(Avg. Large size)	can not be calculated	can not be calculated	$7.5x10^{6}$	Poorly Fluidized, channeling, irregular(many fines)

From eqn (3.35) it is evident that Y_{mb} depends on air voidage, onset bubbling velocity and the constant n. In eqn (3.36), to maintain the ratio of drag force to hydrodynamic force as unity, again the parameters involved are gas voidage, particle diameter, and the viscosity of the fluidizing gas as controlling factors. In addition to these variables the most important parameter needed to keep the bed stable is electric field. The effect of all the abovementioned variables have experimentally verified and included in an empirical relationship (Wang, 1995). For numerical simulations of electrofluidized bed behavior, appropriate modulus of elasticity equations has been used.

4. MULTIPHASE HYDRODYNAMICS

From a macroscopic viewpoint. the solid phase in a fluidized bed behaves like a kind of fluid. Thus. most numerical simulations of fluidized beds are based on theories assuming that the solid phase is a continuum. Many such simulations have used a two-fluid model. which regards a solid fluid mixture as consisting of two kinds of fluids. For example. Prictchett et al (1978) simulated a fluidized bed using the two-fluid model and showed the formation of bubbles. It is necessary in the two fluid-model to assume constitutive equations for the solid phase. The problem of the method is that parameters included in the constitutive equations lack generality. If good agreement with experiment is required. some parameters in the constitutive equations should be determined empirically. some times even from experiments similar to the simulation to be done.

The Governing Equations

A multiphase system consists of particles and a gas. Separate sets of field equations govern the gas and liquid phase dynamics. The following differential equations are written in a form suggested by Soo (1967). The continuity and momentum equations are written for the gas phase and particulate phase. For an isothermal. two-dimensional transient two-phase flow bed there are six nonlinear coupled partial differential equations for six dependent variables. The variables to be computed are the void fraction. ε. the pressure P. the velocity components u_g. v_g. and the solid velocity components u_s, and v_s in the r and z directions respectively.

The sum of the solids and gas momentum equations gives the mixture momentum equations. These mixture momentum equations and the continuity equations in cylindrical

coordinates and for Cartesian coordinates r=1. dr=dx and dz=dy ,are generally accepted by the majority of the two phase flow investigators.

Continnuity Equations

Gas Phase

$$\frac{\partial}{\partial t}\left(\varepsilon_g \rho_g\right)+\frac{\partial}{r\partial r}\left(\varepsilon_g \rho_g u_g r\right)+\frac{\partial}{\partial z}\left(\varepsilon_g \rho_g v_g\right)=0 \tag{4.1}$$

Solid Phase

$$\frac{\partial}{\partial t}\left[\left(1-\varepsilon_g\right)\rho_s\right]+\frac{\partial}{r\partial r}\left[\left(1-\varepsilon_g\right)\rho_s u_s r\right]+\frac{\partial}{\partial z}\left[\left(1-\varepsilon_g\right)\rho_s v_s\right]=0 \tag{4.2}$$

Gas Momentum in r-direction

$$\begin{aligned}&\frac{\partial}{\partial t}\left(\varepsilon_g\rho_g u_g\right)+\frac{\partial}{r\partial r}\left(\varepsilon_g\rho_g u_g r u_g\right)+\frac{\partial}{\partial z}\left(\varepsilon_g\rho_g u_g v_g\right)=\\&-\varepsilon_g\frac{\partial p}{\partial r}+\beta_r\left(u_s-u_g\right)\end{aligned} \tag{4.3}$$

Solids Momentum in r-direction

$$\begin{aligned}&\frac{\partial}{\partial t}\left[\varepsilon_s\rho_s u_s\right]+\frac{\partial}{r\partial r}\left[\varepsilon_s\rho_s u_s r u_s\right]+\frac{\partial}{\partial z}\left[\varepsilon_s\rho_s u_s v_s\right]=\\&-\varepsilon_s\frac{\partial p}{\partial r}+\beta_r\left(u_g-u_s\right)-\frac{\partial \tau}{\partial r}\end{aligned} \tag{4.4}$$

Gas Momentum in z-direction

$$\begin{aligned}&\frac{\partial}{\partial t}\left(\varepsilon_g\rho_g v_g\right)+\frac{\partial}{r\partial r}\left(\varepsilon_g\rho_g v_g r u_g\right)+\frac{\partial}{\partial z}\left(\varepsilon_g\rho_g v_g v_g\right)=\\&-\varepsilon_g\frac{\partial p}{\partial z}+\beta_z\left(v_s-v_g\right)-\varepsilon_g\rho_g g\end{aligned} \tag{4.5}$$

Solids Momentum in z-direction

$$\frac{\partial}{\partial t}(\varepsilon_s \rho_s v_s) + \frac{\partial}{r\partial r}(\varepsilon_s \rho_s v_s r u_s) + \frac{\partial}{\partial z}(\varepsilon_s \rho_s v_s v_s) = -\varepsilon_s \frac{\partial p}{\partial z} + \beta_z (v_g - v_s) - \varepsilon_s \rho_s g - \frac{\partial \tau}{\partial z} \tag{4.6}$$

Fluid-Particle Friction Coefficient

The friction coefficients are obtained for different states of the fluidized bed from standard correlation with negligible acceleration. Neglecting gravity and with no acceleration the gas momentum balance is

$$\varepsilon_g \frac{\partial p}{\partial z} - \beta_z (v_g - v_s) = 0 \tag{4.7}$$

The coefficient β_z is now obtained by comparing eqn. (4.7) to the Ergun equation. as for example given in Kunii and Levenspiel's book (1991)

$$\frac{\Delta p}{\Delta z} = 150 \frac{\varepsilon_s^2}{\varepsilon_g^3} \frac{\mu_g U_0}{(\varphi_s d_p)^2} + 1.75 \frac{\varepsilon_s \rho_g U_0^2}{\varepsilon_g^3 \varphi_s d_p} \tag{4.8}$$

where U_0 is the superficial velocity $U_0 = \varepsilon_g (v_g - v_s)$

$$\varepsilon_g + \varepsilon_s = 1.0 \tag{4.9}$$

A comparison of eqns. (4.7) and (4.8) shows that

$$\beta_z = 150 \frac{(1-\varepsilon_g)^2 \mu_g}{\varepsilon_g (d_p \varphi_s)^2} + 1.75 \frac{\rho_g |v_g - v_s| (1-\varepsilon_g)}{(\varphi_s d_p)} \tag{4.10}$$

where $0.2 \le \varepsilon_g < 0.8$

$$\beta_z = \frac{3}{4} C_D \frac{\varepsilon_g |\vec{v}_g - \vec{v}_s| \rho_g \varepsilon_s}{(d_p \phi)} f(\varepsilon_g) \tag{4.11}$$

where $0.8 \geq \varepsilon_g \geq 1.0$

where $f(\varepsilon_g) = \varepsilon_g^{-2.65}$ (4.12)

$$C_D = \frac{24}{Re}\left(1 + 0.15\,Re^{0.687}\right) \qquad Re < 1000$$

$$= 0.44, \qquad Re \geq 1000 \tag{4.13}$$

and $$Re = \frac{d_p |\vec{v}_g - \vec{v}_s| \rho_g \varepsilon_g}{\mu} \tag{4.14}$$

Solid-Stress

The terms τ_{rr} and τ_{zz} are the normal components of the solid phase stress tensor. The solid stress terms are function of porosity, pressure and the displacement tensors of solids velocity, gas velocity and relative velocity. In the absence of such terms the local values of the void fraction in the fluidized bed become unrealistically low. Rietema and Musters (1973) have included such a term in their solid equation of motion. Kos (1977) has measured such a stress for settling and found it to be quite small compared with the hydrostatic pressure. In view of the previous theory and measurements, the constitutive equation for the normal component of the stress, τ is $\tau = \tau(\varepsilon_g)$.

Then by the chain rule,

$$\frac{\partial \tau}{\partial z} = \frac{\partial \tau}{\partial \varepsilon_g} \cdot \frac{\partial \varepsilon_g}{\partial z} \qquad (4.15)$$

Pritchett, et al. (1978) use the nomenclature, $G(\varepsilon)$ for the modulus of elasticity or particle-particle interaction coefficient, $\frac{\partial \tau}{\partial \varepsilon_g}$ i.e. $G(\varepsilon_g) = \frac{\partial \tau}{\partial \varepsilon_g}$

In this study , the modulus o f elasticity is fitted to the experimental data by Colver and Wang (1993). by the equation.

$$Y\ (N/m^2) = Y_{vdw.el} + c\ E\ (kV/m) \qquad (4.16)$$

where $Y_{vdw.el}$ is the Van der Waals and electronic contribution to the modulus and c is a constant.

The modulus of elasticity has been used by Syamlal (1985).

$$G(\varepsilon) = g_1 \exp[\, g_2\, (\varepsilon^*_g - \varepsilon_1)] \qquad (4.17)$$

where $g_1 = 1.5 \times 10^{-3}$ dynes/cm ^{2} and g_2 =500 and ε^* may be varied according to the void fraction at the maximum packing expected. A typical value would be 0.4. For the purpose of numerical simulation with electric field the following composite model is used which satisfies both conditions such as with and without electric field.

$$G(\varepsilon) = g_1 \exp[\, g_2\, (\varepsilon^*_g - \varepsilon_1)] + c\ E \qquad (4.18)$$

where c =8.845*10 $^{-5}$ N/m-kV (for d_p=49 micron). Addition of electric field to eqn. (4.17) not only enhance the bed stability but also enhance the existing numerically stable scheme more by converting the imaginary characteristics into real values.

Numerical Analysis

Separate sets of field equations govern the gas and liquid phase dynamics. The field equation sets are coupled through the condition of pressure equilibrium between phases and through exchange of mass and momentum. The set of nonlinear partial differential equations is solved for U_s, U_g, V_s, V_g, ε and P using the K-Fix program (Rivard and Torrey, 1977). Figure. 4.1 shows typical computational cell and the relative spatial locations of the variables that appear in the finite difference equations. Velocities of each phase are centered at the boundaries. Quantities such as density, porosity and pressure are centered at the center of the mesh. Flux terms in continuity and momentum equations are full donor-cell differenced. When we apply the momentum principle to a control volume, the momentum storage or depletion is evaluated within the control volume, but the pressure force, shear force, and momentum flows are evaluated at the control surface. If the control volume is selected to be the computational cell, the pressure force must be computed at the cell faces even though the pressure is a cell-centered quantity. Similarly, computation of the shear forces is based on conveniently located variables. Consider an alternative control volume for the x-momentum equation centered on the I-1, j face of the computational cell as shown in Fig 4.1. The net pressure force acting in the x-direction is readily expressed in terms of the variables associated with the staggered-grid convention Similarly the net pressure force acting in the y-direction can be expressed in terms of the variables associated with the same staggered grid convention. In this case control volume for the y-momentum equation centerded on the I, j-1 face of the computational cell.

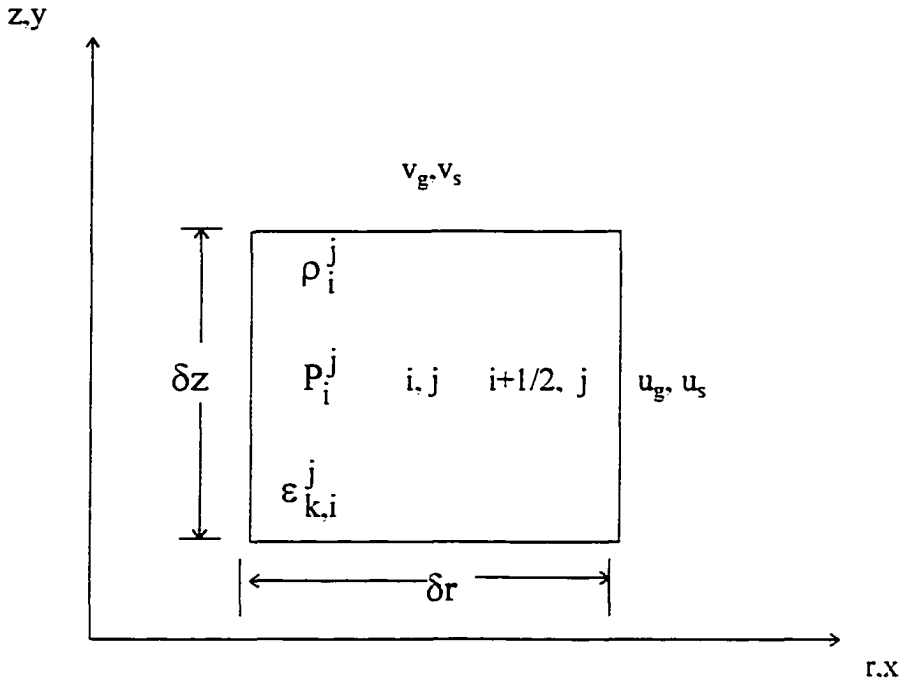

Figure 4.1: Locations of variables in the finite difference equations for a typical cell

The "shifted" control volume of Fig. 4.2 allowed accurate and convenient expressions for the stress, pressure, gravity, and momentum storage terms, but computation of the flow-of-momentum term requires variables at locations other than where they are defined. One idea is to use linear interpolation to obtain values at the desired locations, and there are sound mathematical arguments for doing so. Unfortunately, the algorithm produced by this idea is numerically unstable. To obtain a simple stable formulation, we use a technique called upwind differencing or donor-cell differencing. In this formulation, we assume that convection of momentum far outweighs viscous diffusion of momentum in the flow direction. We approximate the momentum-per-unit-mass at the control volume boundary by the nearest value "upwind" from the boundary.

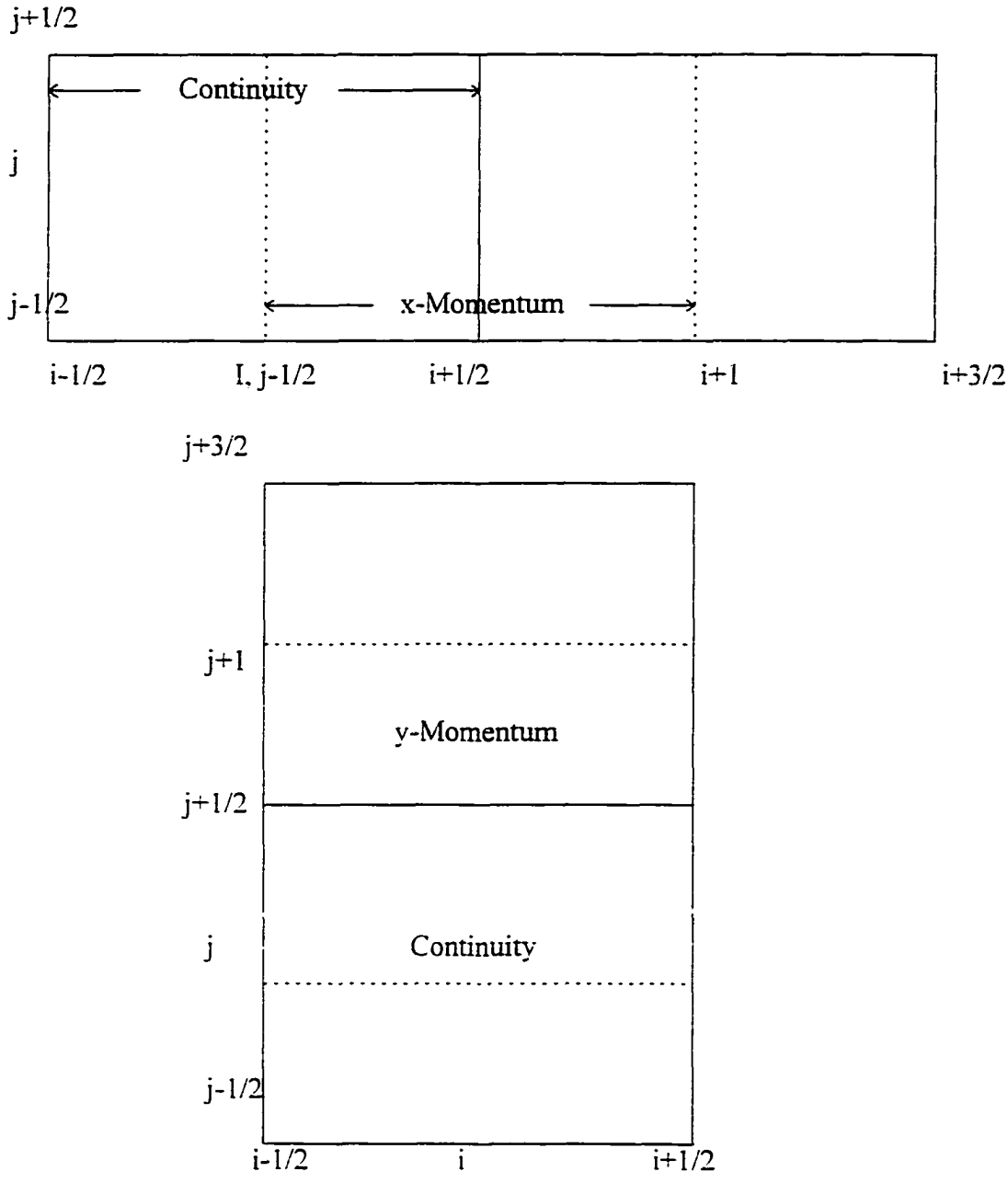

Figure 4.2: Shifted computation cells for momentum calculations

For instance, $u_{i,j}$ is approximated by $u_{i-1,j}$ if the flow is in the positive direction but by $u_{i+1,j}$ if the flow is in the negative direction. Although the velocity associated with the momentum is assigned an "upwind" value, the velocity associated with mass flow rate is still computed from a linear interpolation. The upwind formulation has two shortcomings: it burdens the computer code with the logic required to select the upwind values, and it introduces "artificial viscosity", which reduces the accuracy of the solution. The donor cell differencing (Rivard and Torrey, 1977) helps to prevent a cell from getting drained completely giving negative volume fractions and also aids computational stability. Convective terms in the momentum equations are advanced in time explicitly, where as all exchanges of mass, and momentum, when occur they, are treated implicitly.

The continuity equation is differenced fully implicitly as follows.

$$ {}^{n+1}(\varepsilon_k \rho_k)_i^j = {}^{n}(\varepsilon_k \rho_k)_i^j - \frac{\delta t}{r_i \delta r} {}^{n+1}\langle (\varepsilon_k \rho_k r) u_k \rangle_i^j - \frac{\delta t}{\delta z} {}^{n+1}\langle (\varepsilon_k \rho_k r) u_k \rangle_i^j \qquad (4.19) $$

The angular brackets represent a donor cell differencing as shown below.

$$ \langle (\varepsilon_k \rho_k r) u_k \rangle_i^j = (u_k)_{i+\frac{1}{2}} \begin{cases} (\varepsilon_k \rho_k r)_i' & \text{if } (u_k)_{i-\frac{1}{2}}' > 0 \\ (\varepsilon_k \rho_k r)_{i+1}' & \text{if } (u_k)_{i-\frac{1}{2}}' < 0 \end{cases} $$

$$ - (u_k)_{i-\frac{1}{2}}^j \begin{cases} (\varepsilon_k \rho_k r)_{i-1}' & \text{if } (u_k)_{i-\frac{1}{2}} > 0 \\ (\varepsilon_k \rho_k r)_i' & \text{if } (u_k)_{i-\frac{1}{2}} < 0 \end{cases} $$

and

$$\left\langle (\varepsilon_k \rho_k) v_k \right\rangle_i^j = (v_k)_i^{j+\frac{1}{2}} \begin{cases} (\varepsilon_k \rho_k)_i^j & \text{if } (v_k)_i^{j+\frac{1}{2}} > 0 \\ (\varepsilon_k \rho_k)_i^{j+\frac{1}{2}} & \text{if } (v_k)_i^{j+\frac{1}{2}} < 0 \end{cases}$$

$$- (v_k)_i^{j-\frac{1}{2}} \begin{cases} (\varepsilon_k \rho_k)_i^{j-1} & \text{if } (v_k)_i^{j-\frac{1}{2}} > 0 \\ (\varepsilon_k \rho_k)_i^j & \text{if } (v_k)_i^{j-\frac{1}{2}} < 0 \end{cases}$$

The momentum differenced equations are given below:

$$^{n+1}(\varepsilon_k \rho_k u_k)_{i+\frac{1}{2}}^j = {}^n\overline{(\varepsilon_k \rho_k u_k)}_{i+\frac{1}{2}}^j - \frac{\delta t}{\delta r}\, {}^{n+1}(\varepsilon_k)_{i+\frac{1}{2}}^j\, {}^{n+1}(p_{i+1} - p_i)_{i+\frac{1}{2}} +$$

$$\delta t \sum_{l=1}^{N} {}^n K_{kl}^j{}_{i+\frac{1}{2}}^{n+1} (u_l - u_k)_{i+\frac{1}{2}}^j + \frac{\delta t}{\delta r}\, {}^{n+1}(G_k)_{i+\frac{1}{2}}^{n+1} \left((\varepsilon_l)_{i+1}^j - (\varepsilon_l)_i^j \right) \tag{4.20}$$

$$^{n+1}(\varepsilon_k \rho_k v_k)_i^{j+\frac{1}{2}} = \overline{(\varepsilon_k \rho_k v_k)}_i^{j+\frac{1}{2}} - \frac{\delta t}{\delta z}\, {}^{n+1}(\varepsilon_k)_i^{j+\frac{1}{2}} \left(p^{j+1} - p^j \right)_i +$$

$$\delta t \sum_{l=1}^{N} {}^n K_{kl}^{j+\frac{1}{2}}{}^{n+1} (v_l - v_k)_i^{j+\frac{1}{2}} + \frac{\delta t}{\delta z}\, {}^{n+1}(G_k)_i^{j+\frac{1}{2}}{}^{n+1} \left((\varepsilon_l)^{j+1} - (\varepsilon_l)^j \right)_i \tag{4.21}$$

All the explicit terms have been lumped into the tilde quantities as shown below:

$$\overline{(\varepsilon_k \rho_k u_k)}_{i+\frac{1}{2}}^j = {}^n(\varepsilon_k \rho_k u_k)_{i+\frac{1}{2}}^j - \frac{\delta t}{r_i \delta r}\, {}^n\left\langle (\varepsilon_k \rho_k u_k r) u_k \right\rangle_{i+\frac{1}{2}}^j - \frac{\delta t}{\delta z}\, {}^n\left\langle (\varepsilon_k \rho_k u_k) v_k \right\rangle_{i+\frac{1}{2}}^j \tag{4.22}$$

$$\overline{(\varepsilon_k \rho_k v_k)} = {}^n(\varepsilon_k \rho_k v_k)_i^{j+\frac{1}{2}} - \frac{\delta t}{r_i \delta r}\, {}^n\left\langle (\varepsilon_k \rho_k v_k r) u_k \right\rangle_i^{j+\frac{1}{2}} -$$

$$\frac{\delta t}{\delta z}\, {}^n\left\langle (\varepsilon_k \rho_k v_k) v_k \right\rangle_i^{j+\frac{1}{2}} - \varepsilon_k \rho_k g \tag{4.23}$$

As explained before the angular brackets represent the donor cell differenced quantities.

$$\left\langle (\varepsilon_k \rho_k u_k) v_k \right\rangle^{j}_{i+\frac{1}{2}} = (v_k)^{j+\frac{1}{2}}_{i+\frac{1}{2}} \begin{cases} (\varepsilon_k \rho_k u_k)^{j}_{i-\frac{1}{2}} & \text{if } (v_k)^{j+\frac{1}{2}}_{i+\frac{1}{2}} > 0 \\ (\varepsilon_k \rho_k u_k)^{j}_{i+\frac{1}{2}} & \text{if } (v_k)^{j+\frac{1}{2}}_{i+\frac{1}{2}} < 0 \end{cases}$$

$$- (v_k)^{j-\frac{1}{2}}_{i+\frac{1}{2}} \begin{cases} (\varepsilon_k \rho_k u_k)^{j-1}_{i-\frac{1}{2}} & \text{if } (v_k)^{j-\frac{1}{2}}_{i+\frac{1}{2}} > 0 \\ (\varepsilon_k \rho_k u_k)^{j-1}_{i+\frac{1}{2}} & \text{if } (v_k)^{j-\frac{1}{2}}_{i+\frac{1}{2}} < 0 \end{cases}$$

$$^{n}\left\langle (\varepsilon_k \rho_k v_k) v_k \right\rangle^{j+\frac{1}{2}}_{i} = (v_k)^{j+1}_{i} \begin{cases} (\varepsilon_k \rho_k v_k)^{j+\frac{1}{2}}_{i-\frac{1}{2}} & \text{if } (v_k)^{j+1}_{i} > 0 \\ (\varepsilon_k \rho_k v_k)^{j+\frac{1}{2}}_{i+\frac{1}{2}} & \text{if } (v_k)^{j+1}_{i} < 0 \end{cases}$$

$$- (v_k)^{j}_{i} \begin{cases} (\varepsilon_k \rho_k v_k)^{j-\frac{1}{2}}_{i-\frac{1}{2}} & \text{if } (v_k)^{j-\frac{1}{2}}_{i} > 0 \\ (\varepsilon_k \rho_k v_k)^{j-\frac{1}{2}}_{i+\frac{1}{2}} & \text{if } (v_k)^{j-\frac{1}{2}}_{i} < 0 \end{cases}$$

x-Component:

$$\left\langle (\varepsilon_k \rho_k u_k r) u_k \right\rangle^{j}_{i+\frac{1}{2}} = (u_k)^{j}_{i+1} \begin{cases} (\varepsilon_k \rho_k u_k r)^{j}_{i+\frac{1}{2}} & \text{if } (u_k)^{j}_{i+1} > 0 \\ (\varepsilon_k \rho_k u_k r)^{j}_{i-\frac{1}{2}} & \text{if } (u_k)^{j}_{i+1} < 0 \end{cases}$$

$$- (u_k)^{j}_{i} \begin{cases} (\varepsilon_k \rho_k u_k r)^{j}_{i-\frac{1}{2}} & \text{if } (u_k)^{j}_{i} > 0 \\ (\varepsilon_k \rho_k u_k r)^{j}_{i+\frac{1}{2}} & \text{if } (u_k)^{j}_{i} < 0 \end{cases}$$

y-component:

$$\left\langle (\varepsilon_k \rho_k v_k r) u_k \right\rangle_i^{j+\frac{1}{2}} = (u_k)_{i+\frac{1}{2}}^{j+\frac{1}{2}} \begin{cases} (\varepsilon_k \rho_k v_k r)_i^{j+\frac{1}{2}} & \text{if } \begin{cases} (u_k)_{i-\frac{1}{2}}^{j+\frac{1}{2}} > 0 \\ (u_k)_{i-\frac{1}{2}}^{j+\frac{1}{2}} < 0 \end{cases} \\ (\varepsilon_k \rho_k v_k r)_{i+1}^{j+\frac{1}{2}} \end{cases}$$

$$-(u_k)_{i-\frac{1}{2}}^{j+\frac{1}{2}} \begin{cases} (\varepsilon_k \rho_k v_k r)_{i-1}^{j+\frac{1}{2}} & \text{if } \begin{cases} (u_k)_{i-\frac{1}{2}}^{j+\frac{1}{2}} > 0 \\ (u_k)_{i-\frac{1}{2}}^{j+\frac{1}{2}} < 0 \end{cases} \\ (\varepsilon_k \rho_k v_k r)_i^{j+\frac{1}{2}} \end{cases}$$

The resulting finite difference equations are solved by a combination of point relaxation, Newton's and secant iteration method, without any linearization. The entire problem is complicated by the fact that pressure does not appear as a variable in the continuity equation. Although this lack may not seem troubling at first as only a few unknowns typically appear in each equation of any system of equations. It is a significant feature that severely restricts the numerical tools that can be used successfully to solve this particular problem. To find the velocities at current time level we have to assume some pressure values, and the solved velocities to be checked whether it satisfies continuity equations or not. Pressure does not appear as a variable in the continuity equations, and apparently we do not have anyway to compute P^{n+1} . The heart of a solution procedure based on a pressure correction algorithm is to recast the continuity equation so that the pressure does appear as a variable in the equation that represents conservation of mass. In the momentum equations the pressure, the drag and the solid stress terms are implicitly differenced. Also note that the drag terms are linearly implicit which is necessary for the particular method of solution adopted here in matrix form. There are no other restrictions on

the form of the drag relations. In calculations involving dense beds it is necessary to have the solids stress term may be differenced explicitly to save computational time.

The Solution Technique

A Gauss-Jordan iterative technique is used to solve the finite difference equations given in previous section. To facilitate the particular method of solution the equations are recast in the following form. The momentum equation could be collected together in matrix form.

Thus eqn. (4.20) gives

$$\begin{bmatrix} \beta_r \delta t + \varepsilon_g \rho_g & -\beta_r \delta t \\ -\beta_r \delta t & \beta_r \delta t + \varepsilon_s \rho_s \end{bmatrix} \begin{bmatrix} u_g \\ u_s \end{bmatrix} =$$

$$\begin{bmatrix} \overline{(\varepsilon_g \rho_g u_g)} - \dfrac{\delta t}{\delta r} \varepsilon_g{}^{n+1} (p_{i+1} - p_i)^j + \dfrac{\delta t}{\delta r} G_g \left((\varepsilon_g)_{i+1} - (\varepsilon_g)_i \right) \\ \overline{(\varepsilon_s \rho_s u_s)} - \dfrac{\delta t}{\delta r} \varepsilon_s{}^{n+1} (p_{i+1} - p_i)^j + \dfrac{\delta t}{\delta r} G_s \left((\varepsilon_g)_{i+1} - (\varepsilon_g)_i \right) \end{bmatrix} \quad (4.24)$$

and eqn. (4.21) gives

$$\begin{bmatrix} \beta_z \delta t + \varepsilon_g \rho_g & -\beta_r \delta t \\ -\beta_r \delta t & -\beta_r \delta t + \varepsilon_s \rho_s \end{bmatrix} \begin{bmatrix} v_g \\ v_s \end{bmatrix} =$$

$$\begin{bmatrix} \overline{(\varepsilon_g \rho_g v_g)} - \dfrac{\delta t}{\delta z} \varepsilon_g{}^{n+1} \left(p^{j+1} - p^j \right)^j + \dfrac{\delta t}{\delta z} G_g \left((\varepsilon_g)^{j+1} - (\varepsilon_g)^j \right) \\ \overline{(\varepsilon_s \rho_s v_s)} - \dfrac{\delta t}{\delta z} \varepsilon_s{}^{n+1} \left(p^{j+1} - p^j \right)^j + \dfrac{\delta t}{\delta z} G_s \left((\varepsilon_g)^{j+1} - (\varepsilon_g)^j \right) \end{bmatrix} \quad (4.25)$$

The gas continuity equation can be written as

$$D_i^j = -^{n+1}\left(\varepsilon_g \rho_g\right)_i^j + {}^{n}\left(\varepsilon_g \rho_g\right)_i^j - \frac{\delta t}{r_i \delta r}\left\langle\left(\varepsilon_g \rho_g r\right) u_g\right\rangle_i^j - \frac{\delta t}{\delta z}{}^{n+1}\left\langle\left(\varepsilon_g \rho_g\right) v_g\right\rangle_i^j \tag{4.26}$$

where D_i^j is the residue of the gas continuity equation , which should be equal to zero for absolute convergence. To solve the finite difference equations the pressure in each cell is corrected iteratively such that D_i^j , meets the convergence criterion. The iterations are continued till the convergence criterion is met in all the computational cells simultaneously. The details of this iterative procedure are given below.

1. Calculate the tilde quantities using eqns. (4.22) and (4.23).

2. Calculate the drag coefficients using eqns (4.10) through (4.14).

3. Estimate the new time level velocities solving eqns. (4.24) and (4.25).

4. Calculate β_i^j , approximately given (Rivard and Torrey, 1977) by

$$\frac{1}{\beta_i^j} = \frac{\partial D_i^j}{\partial P_i^j} = \frac{\varepsilon_g}{\left(C_i^j\right)^2} + \frac{(\delta t)^2}{r_i (\delta r)^2}\left(r_{i+\frac{1}{2}}\left(\varepsilon_g\right)_{i+\frac{1}{2}}^j + r_{i-\frac{1}{2}}\left(\varepsilon_g\right)_{i-\frac{1}{2}}^j\right) + \frac{(\delta t)^2}{(\delta z)^2}\left(\left(\varepsilon_g\right)_i^{j+\frac{1}{2}} + \left(\varepsilon_g\right)_i^{j-\frac{1}{2}}\right) \tag{4.27}$$

5. Correct the pressure iteratively. Refer to Fig. D.1 which gives the details of this procedure in terms of FORTRAN variables. The computations start with the left-bottom corner fluid cell. Pressure corrections are carried out in a cell till convergence is obtained or

the number of iterations exceed an inner iterations limit. Then the computations proceed from left to right and from bottom to top till the entire computational regime is covered. At the end of such a computational sweep, if convergence was not obtained in any of the cells, the sweeps are repeated. The number of such sweeps are restricted by an outer iterations limit. The iterative procedure for a single cell involves the following steps.

a. Calculate D_i' eqn. (4.26), using the velocities from eqns. (4.24) and (4.25). If $|D_i'| < \delta_g$ go to step e

b. If $|D_i'| > \delta_g$ the pressure in the cell needs to be adjusted. Initial adjustments are done using Newton's method.

$$^{m+1}P_i' = {}^{m}P_i' - \omega\beta_i' D_i' \qquad (4.28)$$

where ω is a relaxation parameter near unity. Newton's method is continued till D_i' changes sign. After D_i' changes sign the next pressure correction is done using a secant method (Appendix B), where

$$\beta = \frac{P_1 - P_2}{D_1 - D_2} \qquad (4.29)$$

There after the pressure corrections are done using a constrained two sided secant method as illustrated in Fig. D.1. Given the three points 1, 2, 3 of which 1 and 2 bracket the desired pressure and 3 lies between them, the presser P_A and P_B are determined by straight line extrapolation and interpolation, respectively. The new estimate of the advanced time pressure is then computed as $^{n+1}P_i' = \frac{1}{2}(P_A + P_B)$. If the presser P_A should lie outside the

interval P_1 to P_3 , it is given the value $\frac{1}{2}(P_1 + P_2)$. After ${}^{n+1}P_i^j$ is estimated , point 2 is discarded and points 1 and 3 are retained as improved bounds for the next pressure estimate.

c. Calculate the velocities using eqns. (4.24) and (4.25).

d. Calculate the gas mass fluxes.

e. Solve the solids continuity equations for ε_s .

f. Using eqn. (4.9) find the new value of ε_g .

g. If $|D_i^j| \rangle \delta_g$ go to step a.

Mathematical Classifications of Governing Equations

With r=1. replacing dr by dx and dz by dy the governing equations with one dimension could be written in the following manner.

In the (t. x) plane

$$\bar{A}\frac{\partial \bar{U}}{\partial t} + \bar{B}\frac{\partial \bar{U}}{\partial x} = \bar{D} \qquad (4.30)$$

where

$$\bar{A} = \begin{bmatrix} \rho_g & \frac{\varepsilon_g}{c^2} & 0 & 0 \\ -\rho_s & 0 & 0 & 0 \\ 0 & 0 & \rho_g \varepsilon_g & 0 \\ 0 & 0 & 0 & \rho_s \varepsilon_s \end{bmatrix} \quad . \quad \bar{U} = \begin{bmatrix} \varepsilon_g \\ P \\ u_g \\ u_s \end{bmatrix}$$

$$\bar{B} = \begin{bmatrix} \rho_g u_g & \frac{\varepsilon_g u_g}{c^2} & \varepsilon_g \rho_g & 0 \\ -\rho_s u_s & 0 & 0 & \rho_s \varepsilon_s \\ 0 & \varepsilon_g & \rho_g \varepsilon_g u_g & 0 \\ (G_x + E_x) & \varepsilon_s & 0 & \rho_s u_s \varepsilon_s \end{bmatrix} \quad \text{and} \quad \bar{D} = \begin{bmatrix} 0 \\ 0 \\ \beta_A (u_s - u_g) \\ \beta_A (u_g - u_s) \end{bmatrix}$$

In (t. y) plane . equations are followings

$$\bar{A}\frac{\partial \bar{U}}{\partial t}+\bar{C}\frac{\partial \bar{U}}{\partial y}=\bar{E} \tag{4.31}$$

where

$$\bar{A}\text{ and }\bar{U}\ \bar{C}=\begin{bmatrix} \rho_g v_g & \frac{\varepsilon_g v_g}{c^2} & \varepsilon_g \rho_g & 0 \\ -\rho_s v_s & 0 & 0 & \varepsilon_s \rho_s \\ 0 & \varepsilon_g & \rho_g \varepsilon_g v_g & 0 \\ -(G_y+E_y) & \varepsilon_s & 0 & \rho_s \varepsilon_s v_s \end{bmatrix}$$

$$\bar{E}=\begin{bmatrix} 0 \\ 0 \\ \beta(v_s-v_g)-\rho_g g \\ -\beta(v_s-v_g)-\varepsilon_s \Delta\rho_s g \end{bmatrix}$$

$$[C-\lambda A]=0 \tag{4.32}$$

After simplification

$$\frac{\rho_s \varepsilon_g}{c^2}(v_s-\lambda)^2(v_g-\lambda)^2-\rho_s\varepsilon_g(v_s-\lambda)^2-\rho_g\varepsilon_s(v_g-\lambda)^2$$

$$-(G_y+E_y)\varepsilon_g\left[\frac{(v_g-\lambda)^2}{c^2}-1\right]=0$$

For the fluidized bed at the inflow and outflow boundaries

$$\varepsilon_g \rightarrow 1.0:\ \varepsilon_2 \rightarrow 0.0\ :\ G \rightarrow 0.0 \text{ and } E \rightarrow 0.0$$

Hence the eigenvalues are

$$\lambda_{1,2} = v_g \pm c \text{ and } \lambda_{3,4} = v_s$$

Again with all the pressure drop in fluid phase (Gidaspow, 1994)

$$\bar{C}' = \begin{bmatrix} \rho_g v_g & \frac{\varepsilon_g v_g}{c^2} & \varepsilon_g \rho_g & 0 \\ -\rho_s v_s & 0 & 0 & \varepsilon_s \rho_s \\ 0 & 1 & \rho_g \varepsilon_g v_g & 0 \\ -(G_y + E_y) & 0 & 0 & \rho_s \varepsilon_s v_s \end{bmatrix}$$

with this matrix $\bar{C}'$ $\left[\bar{C}' - \lambda A\right] = 0$ (4.33)

$$\left\{\frac{\varepsilon_g^2 \rho_g}{c^2}(v_g - \lambda)^2 - \varepsilon_g \rho_g\right\}\left\{-(G_y + E_y)\varepsilon_s \rho_s + \rho_s^2 \varepsilon_s (v_s - \lambda)^2\right\} = 0$$

$$\frac{\varepsilon_g^2 \rho_g}{c^2}(v_g - \lambda)^2 - \varepsilon_g \rho_g = 0$$

$$\lambda_{1,2} = v_g \pm \sqrt{\frac{c^2}{\varepsilon_g}}$$

and $\lambda_{3,4} = v_s \pm \sqrt{\frac{(G_y + E_y)}{\rho_s}}$

Since all eigenvalues are real the system of governing equations are hyperbolic in (t, x) and (t, y) plane.

Stability Analysis

We can rewrite the system of equations (Anderson, Pletcher, and Tannehill, 1984)

$$U_j^{n+1} = \frac{1}{2}\left([I] + \frac{\Delta t}{\Delta x}[A]^n\right)U_{j-1}^n + \frac{1}{2}\left([I] - \frac{\Delta t}{\Delta x}[A]^n\right)U_{j+1}^n \quad (4.34)$$

Where $[I]$ is the identity matrix. The stability of the difference equation can be evaluated by applying the Fourier or von Neumann method. If a typical term of a Fourier series is substituted into above equation, an expression is obtained

$$e^{n+1}(k) = [G(\Delta t, k)]e^{k}(k) \tag{4.35}$$

where $$[G] = [I]\cos\beta - i\frac{\Delta t}{\Delta x}[A]\sin\beta$$

and e^n represents the Fourier coefficients of the typical term. The $[G]$ matrix is called the amplification matrix. This matrix is now dependent upon step size and frequency or wave number, i.e., $[G] = [G(\Delta t, k)]$. For a stable finite-difference calculation, the largest eigenvalue of $[G]$, σ_{max}, must obey

$$|\sigma_{max}| \leq 1 \tag{4.36}$$

This leads to the requirement that

$$\left|\lambda_{max}\frac{\Delta t}{\Delta x}\right| \leq 1 \tag{4.37}$$

where λ_{max} is the largest eigenvalue of the $[A]$ matrix.

$\lambda max = \max(\lambda_1, \lambda_2, \lambda_3, \lambda_4)$

Considering both the coordinates in x and y direction the time step constraint could be found $$\delta t < \frac{\min(\delta x, \delta y)}{\lambda_{max}}$$

5. RESULTS AND DISCUSSION

The two-dimensional two-phase flow numerical calculations based on the formulation of Harlow and Amsden (1975) was subsequently used in the K-Fix program (Rivard and Torrey, 1977). This led to significant details of development during the transient period. The calculated flow variables for the phases are the components of the velocities, pressure, and the void distributions in the fluidized bed. The coordinate system for the numerical simulation of the fluidized bed is rectangular with the cell flags designated in such a way that it approximately simulates two-dimensional (typically 21x45 grid cells) fluidized experimental bed shown in Fig. C.2. The finite difference governing equations are solved for an appropriate number of computational cells comprising the region of interest. The computing mesh is subdivided as shown in Fig. C.2 into a number of cells by a grid system. The coordinates of the center of the cells are denoted by the indices i and j. The center of the grid lines are denoted by half indices i+1/2 or j+1/2. The distributor plate is the boundary between cell I, 1 and I, 2 where I=2, IB1. The gas velocity and the pressure of the incoming flow are assigned to this cell row and never re-calculated or altered during the course of computation. Mass fluxes of gas into the bed are fixed. In the K-Fix code these type of cells are referred to as, "specified flux" inflow cells and are given cell type flag number 5. The pressure drop is shown to be very close to that at minimum fluidization. A solid wall is assigned by cell flag number 3. There are no fluxes of mass or momentum through a wall. This type of boundary condition is achieved by setting the normal components of the velocities are equal to zero. For solid walls the tangential velocities in the fictitious cells are

set by reflection for a free-slip wall, and by reflection with a change in sign for no slip walls. The bed is assumed to be open to atmosphere. Thus the pressure at center of cells I, JB2 (I=2, IB1) is one atmosphere and normal solid velocity at locations i, JB1+1/2 (I=2, IB1) is set to zero. For all cases the overall dimension of the bed is constant. The grid size for a single donor cell of the bed is taken as 0.5 cm x 0.7 cm. The electric field is incorporated into the program through the solids stress term using previous results from an perturbation theory, eqn. (4.16).

Bubble Free Bed

Figures 5.1 and 5.2 show the time sequences of bubble-free fluidization following the startup of a packed bed of 49 μm glass particles. Differences in circulation and voidage patterns are apparent with (E = 100 kV/m) and without (E=0) the applied electric field . Figures 5.1 and 5.2 show that the bed expansion, i.e., the bed from an initial height 28 cm to over 30 cm.

Bed with a Single Bubble

In a 21 x 45 grid cells (0.5 cm x 0.7 cm), the middle three cells of the second, third, and the fourth rows are initially set with the unity air void fraction at the minimum fluidization velocity , U_{mf} =0.49 cm/s. Figure 5.3-5.44 are the shading, contour, and vector plots with an inserted bubble at t=0 s with and without an electric field, followed by different time levels. These figures show the propagation, growth, and diffusion of the bubble in a two-dimensional fluidized bed. The inserted bubble retains its shape until the time t=0.6 s since its inception. The shape of the bubble voids are elliptical in shape immediately after

switching on the fluid velocity into the bed. All hydrodynamic phenomena occurring are shown in Fig. 5.3-5.4 in the absence of external applied electric field.

To observe the effect of electric field on hydrodynamic behavior of the fluidized bed with an inserted bubble, a strong electric field is applied across the bed. The strength of the electric field is taken as 100 kV (i.e., an electric field strength of 100 kV/m). The electric field and the initial voidage in the fluidized bed begin at t=0 s. Figures 5.4, 5.6, 5.8, 5.10, and 5.12 show the effect of the electric field on the bubble propagation, growth, and lateral diffusion in the bed. It is evident from the computation as well as from the experimental evidence that to control the bed stability the electric field plays a definite controlling mechanism since hydrodynamic actions of the bubble are the main cause of instability.

The contour plots of Fig. 5.19-5.34 at different time levels reveals that the spreading tendency of the bubble is elliptical, which is a consequence of the application of the electric field in x-direction. As a bubble propagates toward the upper part of the bed, it spreads out more towards the boundaries and eventually looses its previous shape and is dispersed in the bed. It follows from Fig. 5.34 that there is a bed expansion from 19.6 cm static bed height to 22 cm. From Figs. 5.34 and 5.35 it is also evident by observing the void distributions that the electric field does have a definite influence on bed hydrodynamics. The concentration of solid particles are relatively high towards the bottom part of the bed. In the middle sections of the bed, the distribution of concentration of both solid and air is more or less even. Figures 5.34 and 5.35 show that the computed results are in good agreement with the experimental results. It is noticeable form these figures that the top surface of the bed has a small bulging

effect without an electric field and a small depressing effect with an electric field. Figures 5.36-5.40 are vector plots of air with a single inserted bubble, which creates circulation that spread out with time in the bed as well as propagates toward the top surface.

Bed with a Jet

To simulate the effect of jet in a fluidized bed, at time zero a central jet is turned on. The shading, contour, and void plots of the bed with and without an electric field show that the nature of jet penetration at different stages in the bed. In Fig. 5.45 (without an electric field) the distribution of the contour more or less is mushroom in shape, but in Fig. 5.46 the effect of electric field effect is hardly noticeable. The field strength is 100 kV/m. Within 0.4 s of startup of the jet, the middle part of the free surface of the bed swells in the direction of the jet, Figs. 5.58 and 5.59. These two figures show the bed expansion and the effect of electric field. In Fig. 5.59, because of the application of the electric field the outward protrusion is suppressed and the contour lines are more smooth and spread in the direction of field. Figures 5.60 and 5.61 show that the bed expansion exceeds the computational free board region and thereby some of solid particles carried out by the air. Figures 5.60- 5.65 show that near the jet origin the concentration of the solid particles are higher than those of air. Figures 5.66-5.70 show the vector plots of an air jet in a gas solid fluidized bed. The jet creates some circulation around its origin and causes the bed to expand in its own direction.

Bed with Two Bubbles

In an another attempt to investigate the capability of the code, two bubbles are incorporated at the bottom and upper layer. The time history plot is given in Figs. 5.71 - 5.75.

They are equal in size, having 9 cells (3x3) each, and square in shape with a 10 cells apart vertically. From Figs. 5.72 and 5.73 it is observed that in the middle of the top most layer has an outward protrusion. Figure 5.75 at t=0.3 s shows that the upper bubble erupts into the free board zone. The top most surface of the bed gets depressed. Comparing Fig. 5.26 with a single bubble without an electric field at t=0.4 s with that of Fig. 5.75 it is observed that the presence of more bubbles in a fluidized bed alter the hydrodynamics of a bed. The conditions used for numerical simulation for a bed for all three cases are summarized in Table 5.1.

Table 5.1 Fluidization of glass beads (input data for K-Fix Code)

Width of bed	= 19.5 cm
Static bed height	= 19.6 cm
Superficial velocity	= 0.49 cm/s
Grid size in x direction	= 0.5 cm
Grid size in y direction	= 0.7 cm
Bubble size	= 0.5*0.7*9 = 3.15 cm^2
Jet opening	= 3*.5 = 1.5 cm
Jet velocity	= 49.49 cm/s
Electric field	= 100 kV/m
Particle diameter	= 49 μm
Time step	= 1.0 x 10^{-4} sec
Number of cells	= 21x 45
Initial voidage (Packed bed)	= 0.47
Constant g_1 (Page 33)	= 1.5x10^{-3} dynes/cm^2
Constant g_2 (Page 33)	=500
Constant c (for d_p = 49 μ m	= 8.845x10^{-5} N/m-kV
Stress electric field (Colver and Wang, 1993)	= cE N/m^2
Stress (Sayamlal, 1985) $G(\varepsilon_g)$	= $g_1 \exp[g_2 (\varepsilon_g^* - \varepsilon_g)]$ N/m^2

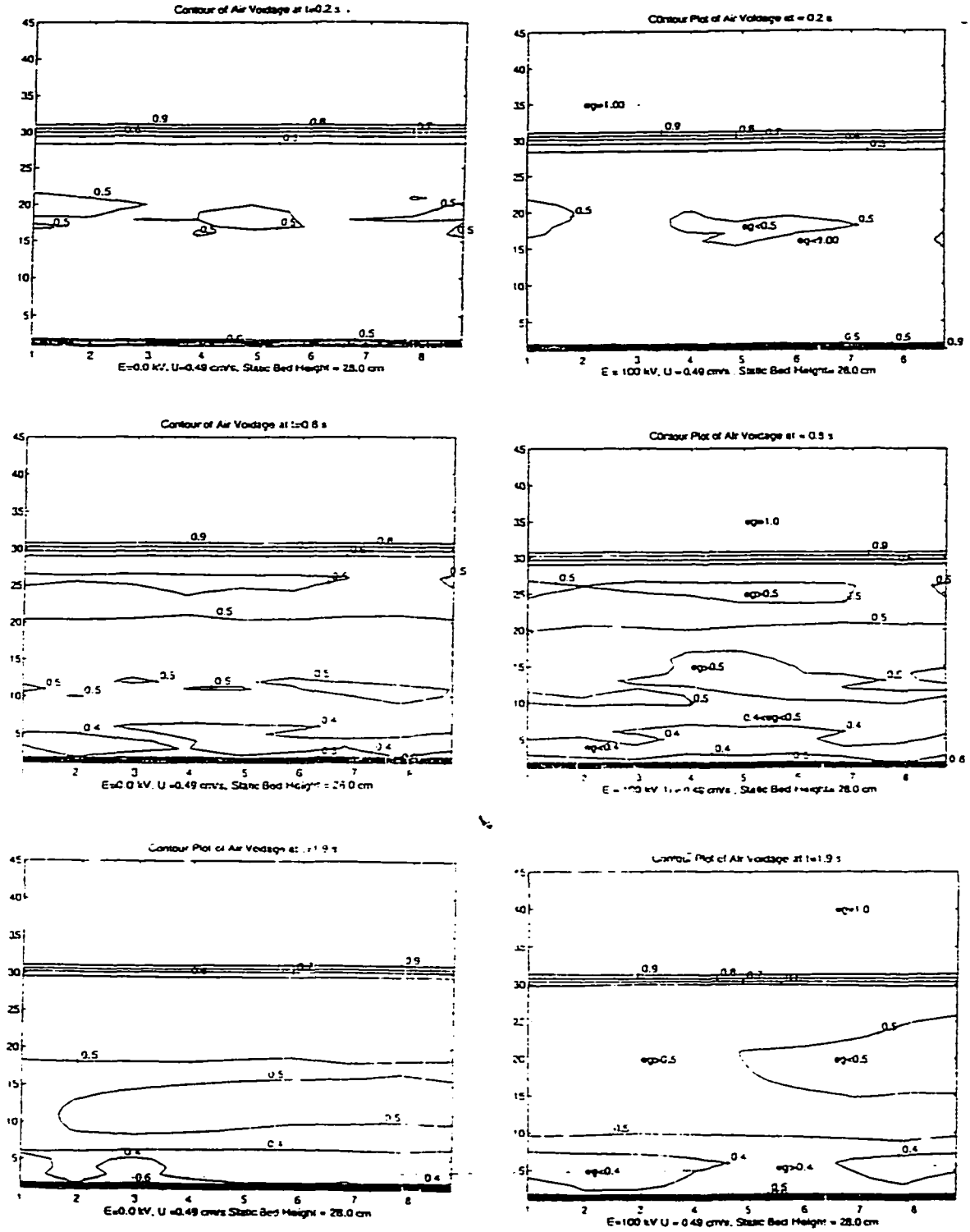

Figure 5.1: Contour Plots of Air Void Fraction in Gas-solid Fluidized Bed with and without electricfield (E=100 kV/m , E=0, U=Umf=0.49 cm/s, dp= 49 micron, bed static height 28 cm , bed width 9.5 cm)

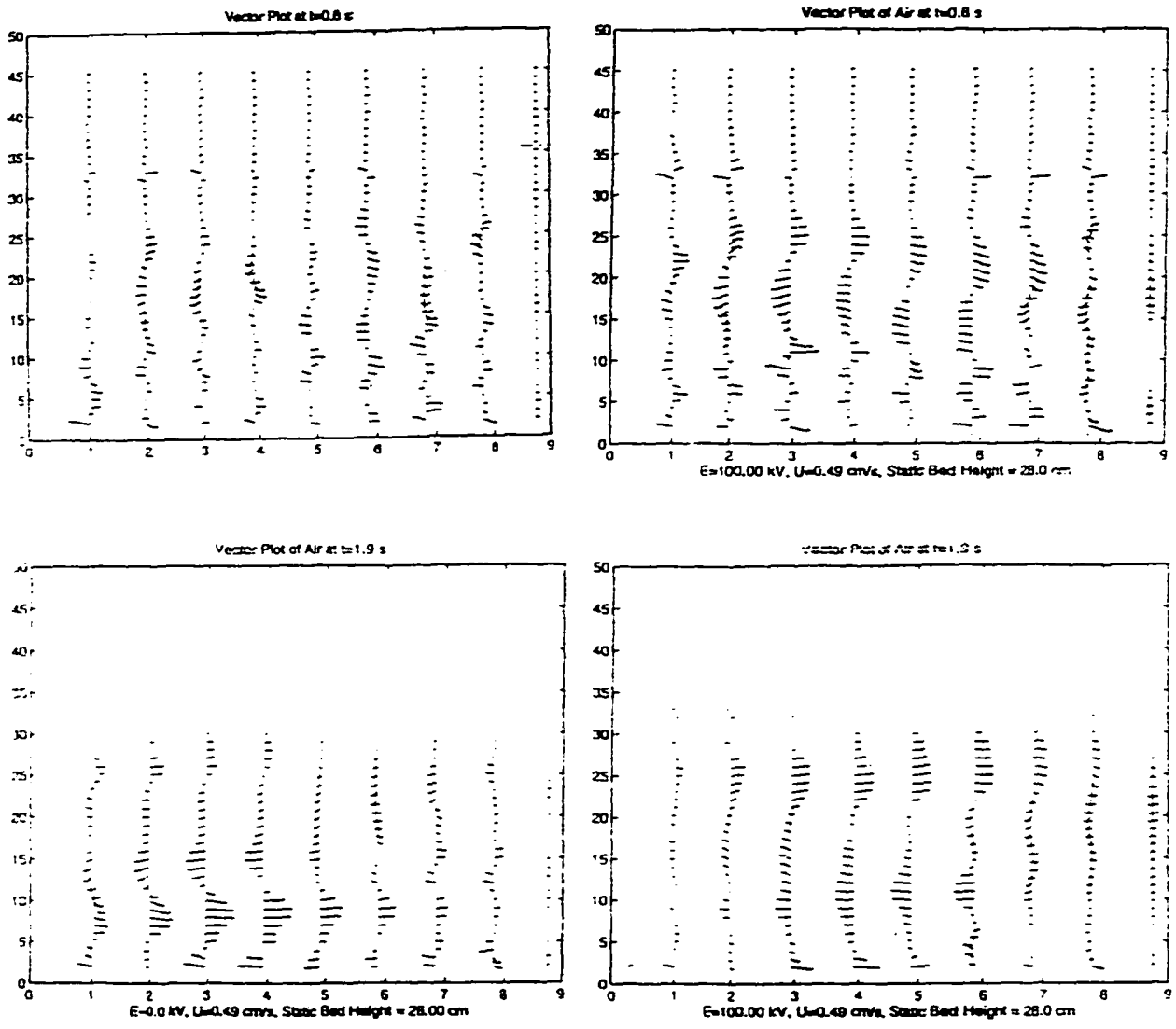

Figure 5.2: Vector plots of Air in a Gas-Solid Fluidized Bed with and without electricfield (E= 100 kV/m, E=0, U=Umf=0.49 cm/s, dp=49 micron. bed static height=28 cm, bed width 9.5 cm)

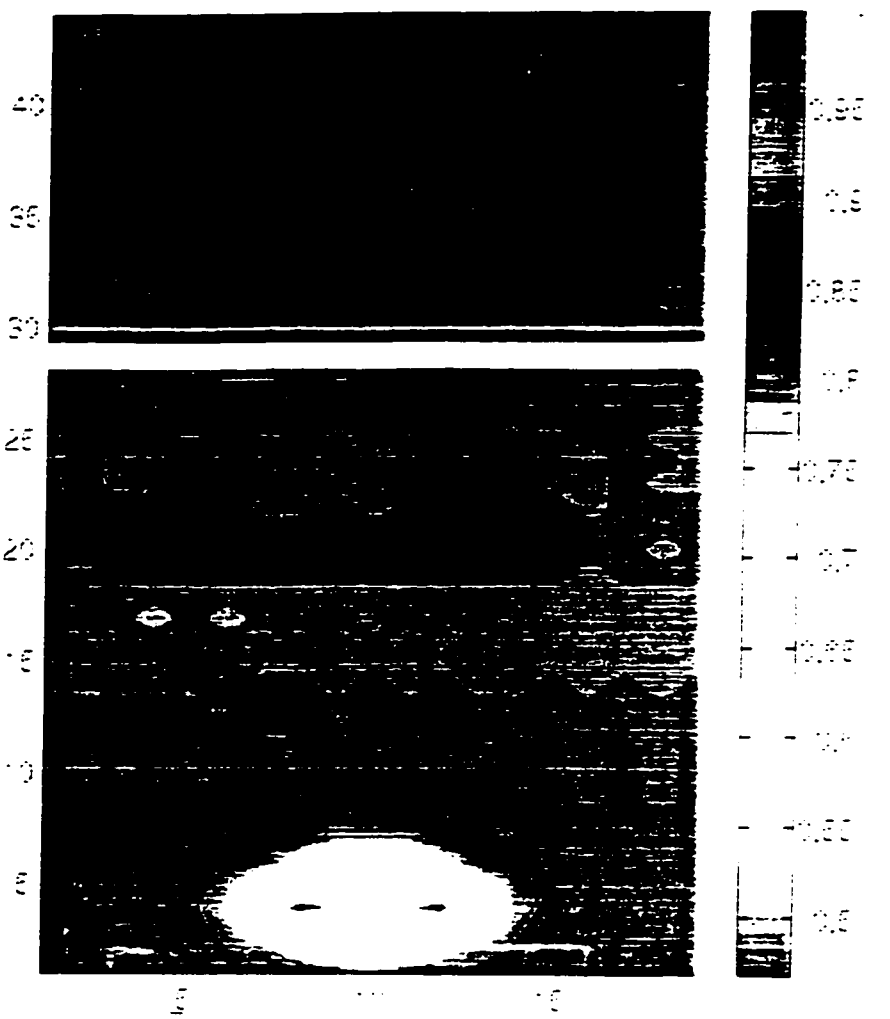

Figure 5.3: Shading plot of Air Void fraction of an iserted single bubble in Gas-Solid Fluidized bed with E=0 kV. at t=0.1 s
(Grid size 0.5X0.7 cm. U=Umf=0.49 cm/s. dp=49 micron. static bed height 19.6 cm. bed width 9.5 cm)

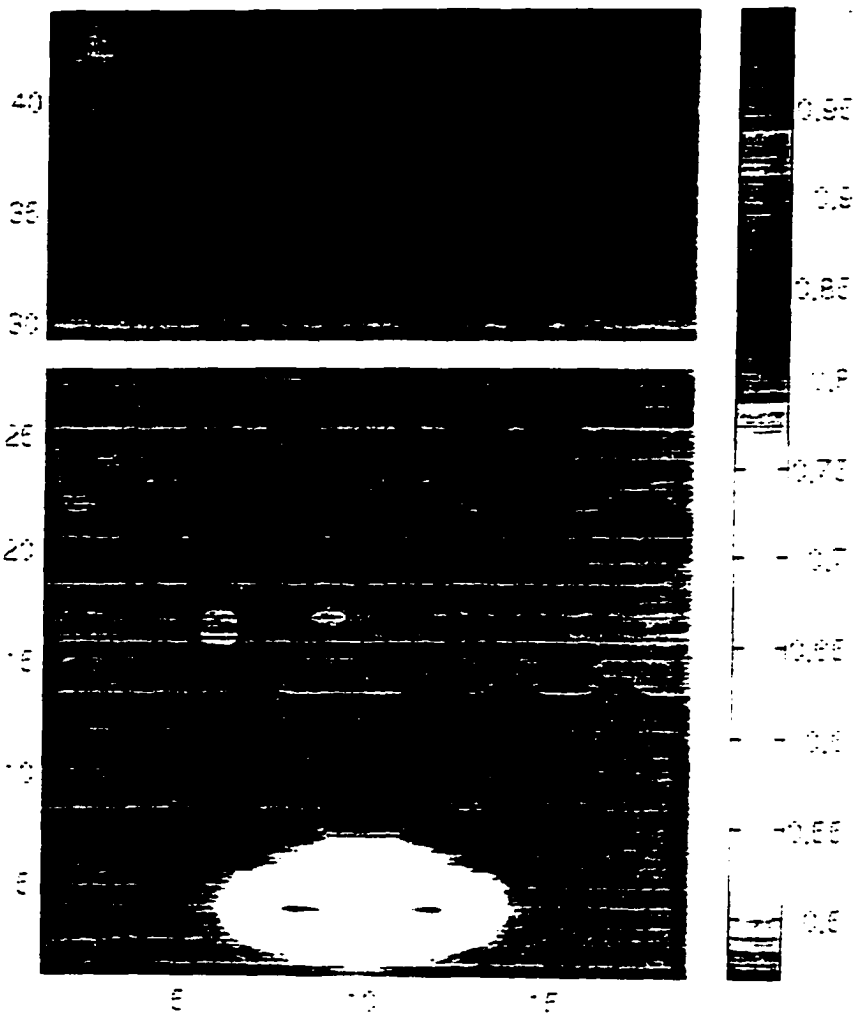

Figure 5.4: Shading plot of Air Void fraction of an iserted single bubble in Gas-Solid Fluidized bed with E=100 kV. at t=0.1 s
(Grid size 0.5X0.7 cm. U=Umf=0.49 cm/s. dp=49 micron. static bed height 19.6 cm. bed width 9.5 cm)

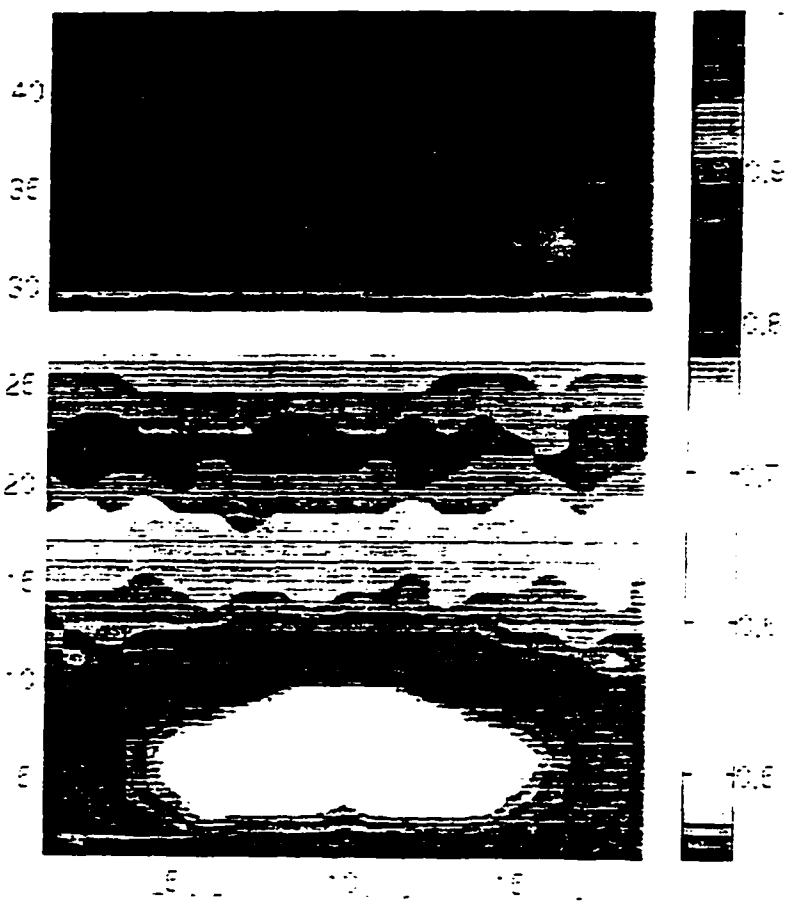

Figure 5.5: Shading plot of Air Void fraction of an iserted single bubble in Gas-Solid Fluidized bed with E=0 kV. at t=0.2 s
(Grid size 0.5X0.7 cm. U=Umf=0.49 cm/s. dp=49 micron. static bed height 19.6 cm. bed width 9.5 cm)

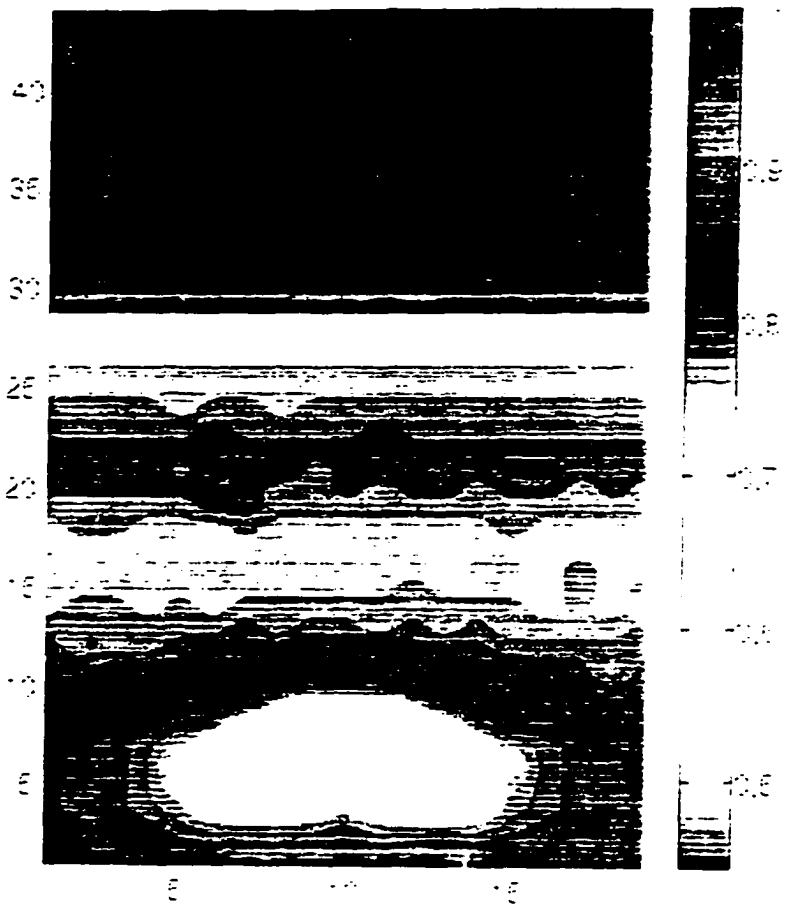

Figure 5.6: Shading plot of Air Void fraction of an iserted single bubble in Gas-Solid Fluidized bed with E=100 kV, at t=0.2 s
(Grid size 0.5X0.7 cm, U=Umf=0.49 cm/s, dp=49 micron, static bed height 19.6 cm, bed width 9.5 cm)

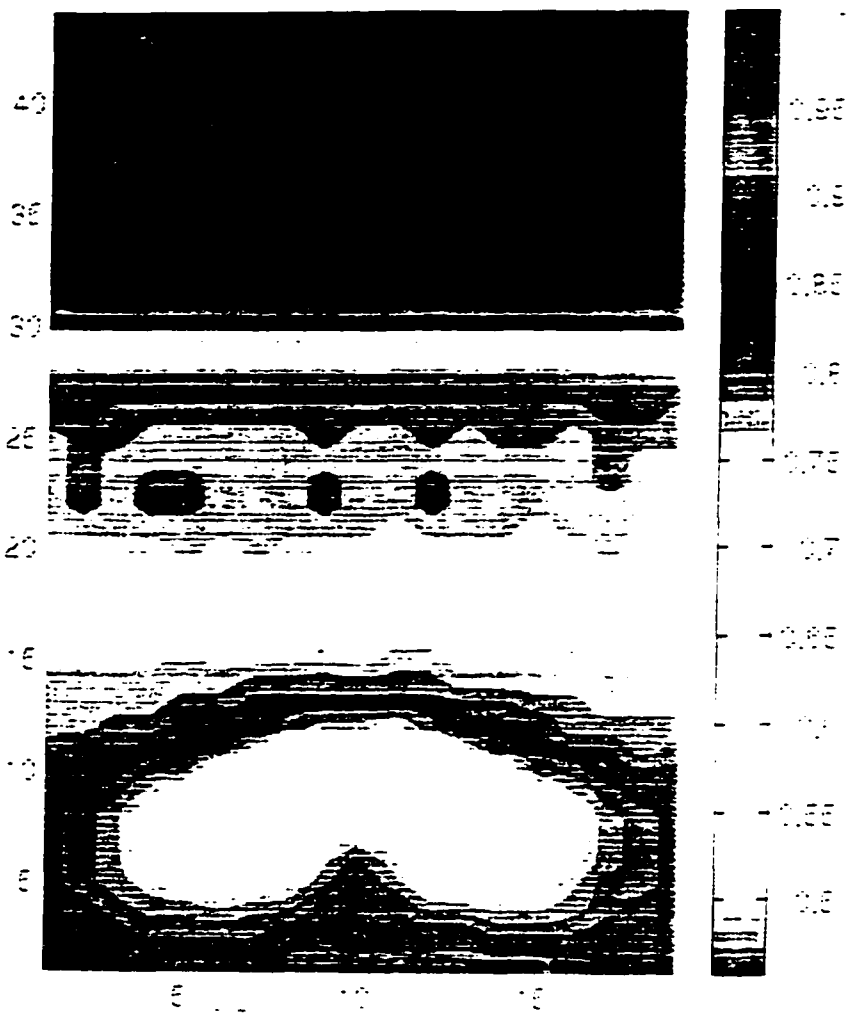

Figure 5.7: Shading plot of Air Void fraction of an iserted single bubble in Gas-Solid Fluidized bed with E=0 kV. at t=0.3 s
(Grid size 0.5X0.7 cm. U=Umf=0.49 cm/s. dp=49 micron. static bed height 19.6 cm. bed width 9.5 cm)

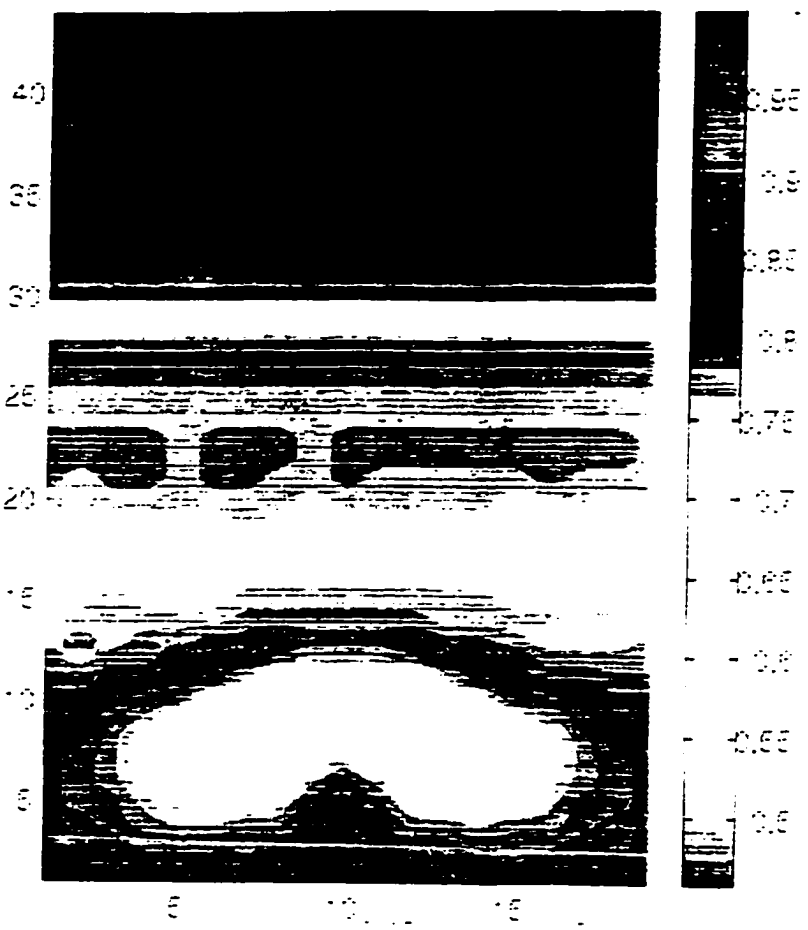

Figure 5.8: Shading plot of Air Void fraction of an iserted single bubble in Gas-Solid Fluidized bed with E=100 kV, at t=0.3 s
(Grid size 0.5X0.7 cm, U=Umf=0.49 cm/s, dp=49 micron, static bed height 19.6 cm, bed width 9.5 cm)

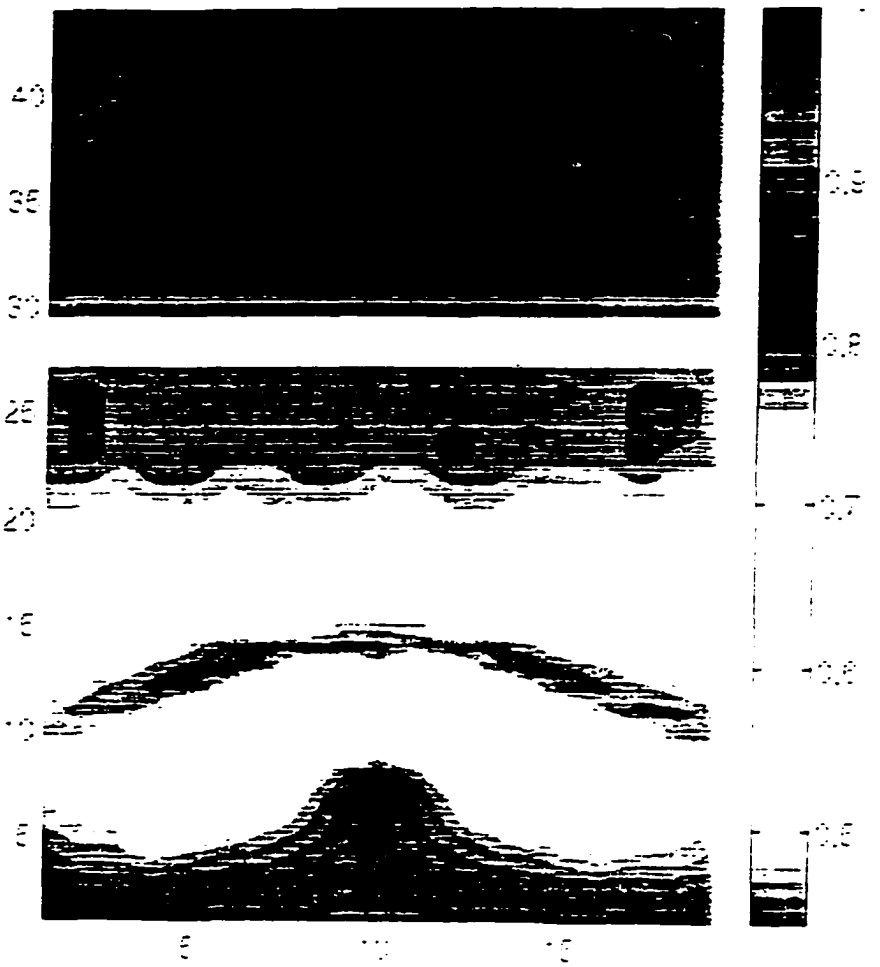

Figure 5.9: Shading plot of Air Void fraction of an iserted single bubble in Gas-Solid Fluidized bed with E=0 kV, at t=0.4 s
(Grid size 0.5X0.7 cm, U=Umf=0.49 cm/s, dp=49 micron, static bed height 19.6 cm, bed width 9.5 cm)

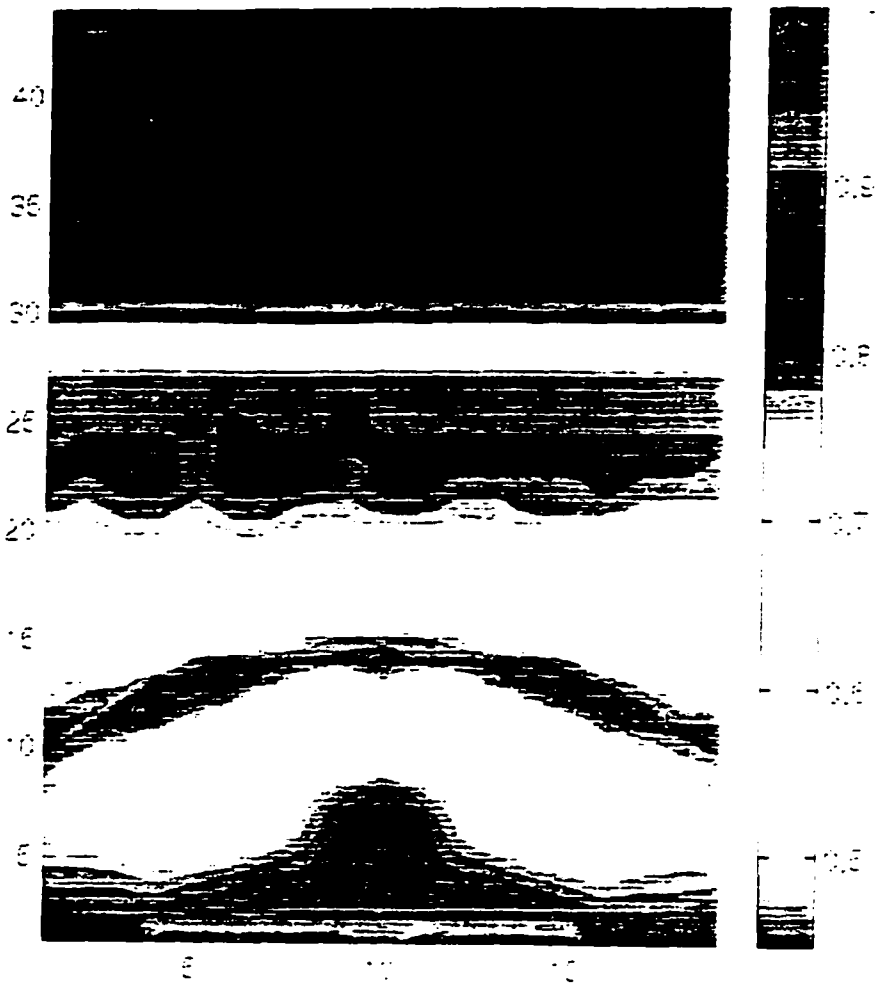

Figure 5.10: Shading plot of Air Void fraction of an iserted single bubble in Gas-Solid Fluidized bed with E=100 kV. at t=0.4s
(Grid size 0.5X0.7 cm. U=Umf=0.49 cm/s. dp=49 micron. static bed height 19.6 cm. bed width 9.5 cm)

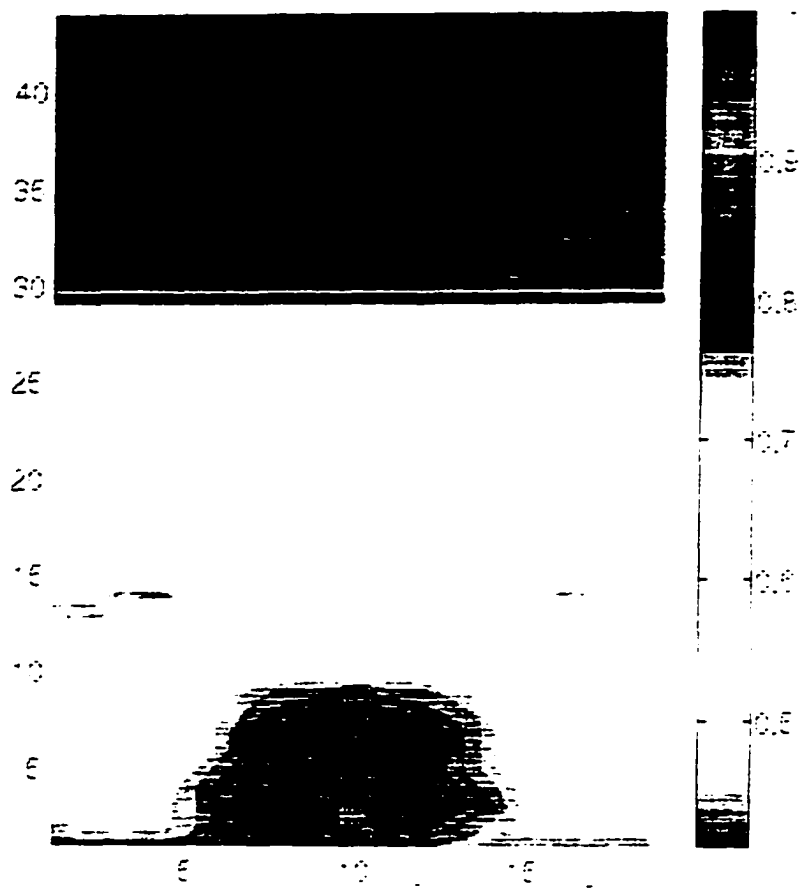

Figure 5.11: Shading plot of Air Void fraction of an iserted single bubble in Gas-Solid Fluidized bed with E=0 kV. at t=0.6 s
(Grid size 0.5X0.7 cm. U=Umf=0.49 cm/s. dp=49 micron. static bed height 19.6 cm. bed width 9.5 cm)

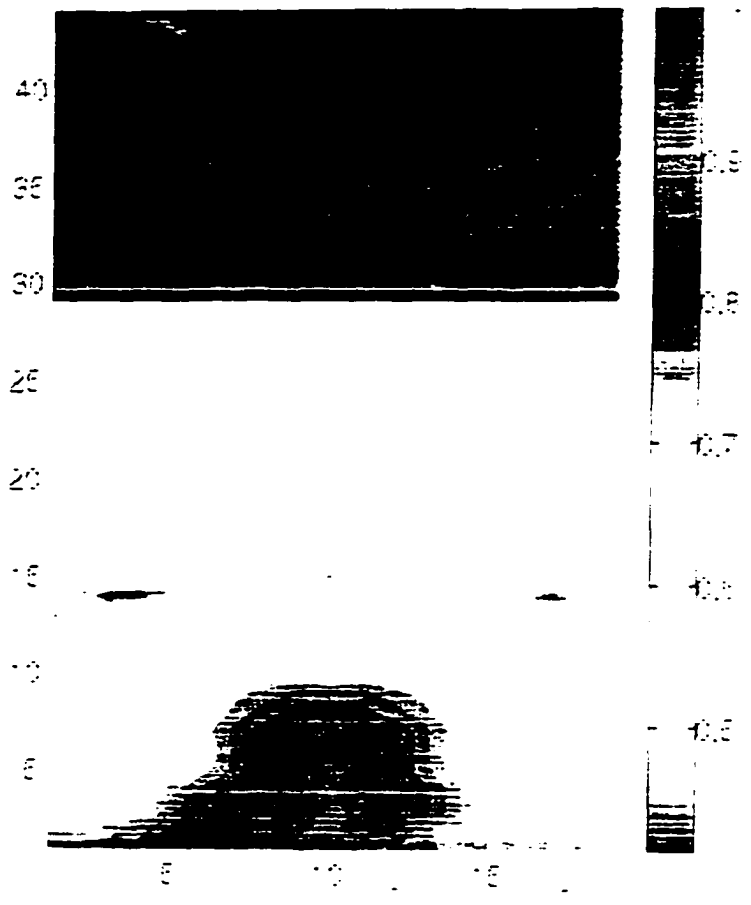

Figure 5.12: Shading plot of Air Void fraction of an iserted single bubble in Gas-Solid Fluidized bed with E=100 kV, at t=0.4 s
(Grid size 0.5X0.7 cm, U=Umf=0.49 cm/s, dp=49 micron, static bed height 19.6 cm, bed width 9.5 cm)

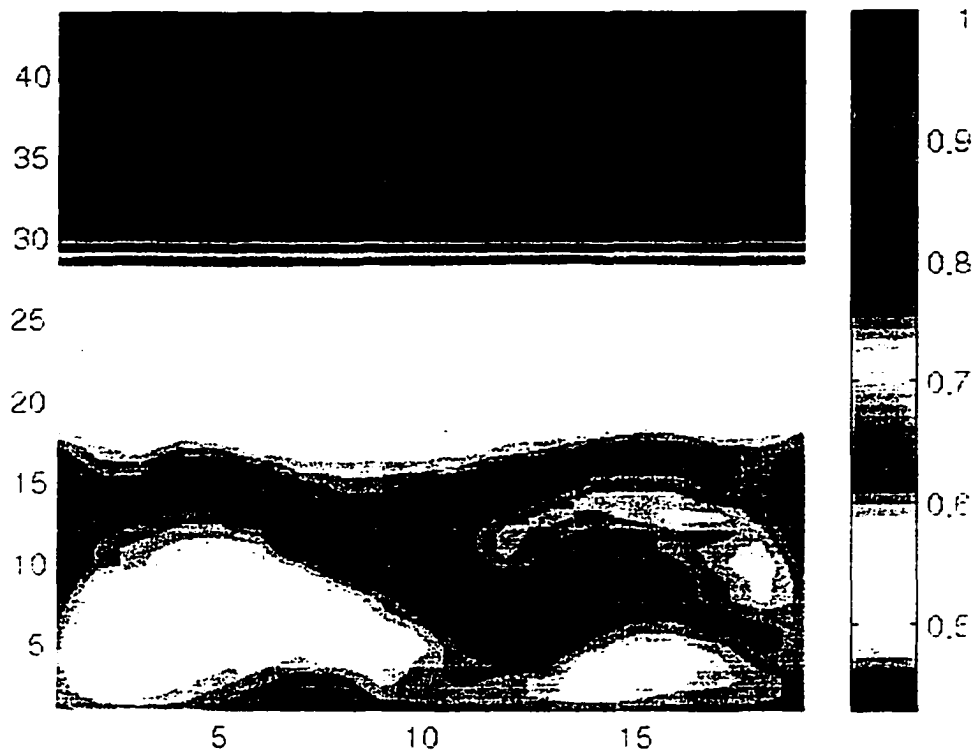

Figure 5.13: Shading plot of air void fraction of an inserted single bubble in gas-solid fluidized bed with E=0 kV. at t=1.5 s
(grid size 0.5X0.7 cm. U=Umf=0.49 cm/s. dp=49 micron, static bed height 19.6 cm. bed width 9.5 cm)

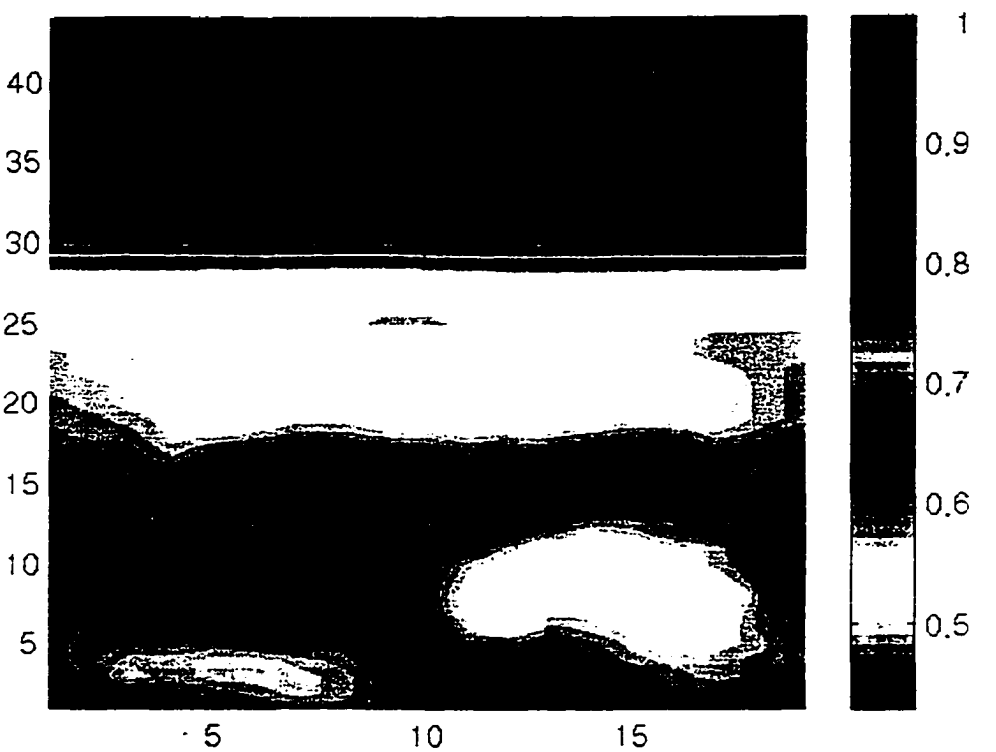

Figure 5.14: Shading plot of air void fraction of an inserted single bubble in gas-solid fluidized bed with E=100 kV, at t=1.5 s
(grid size 0.5X0.7 cm, U=Umf=0.49 cm/s, dp=49 micron, static bed height 19.6 cm, bed width 9.5 cm)

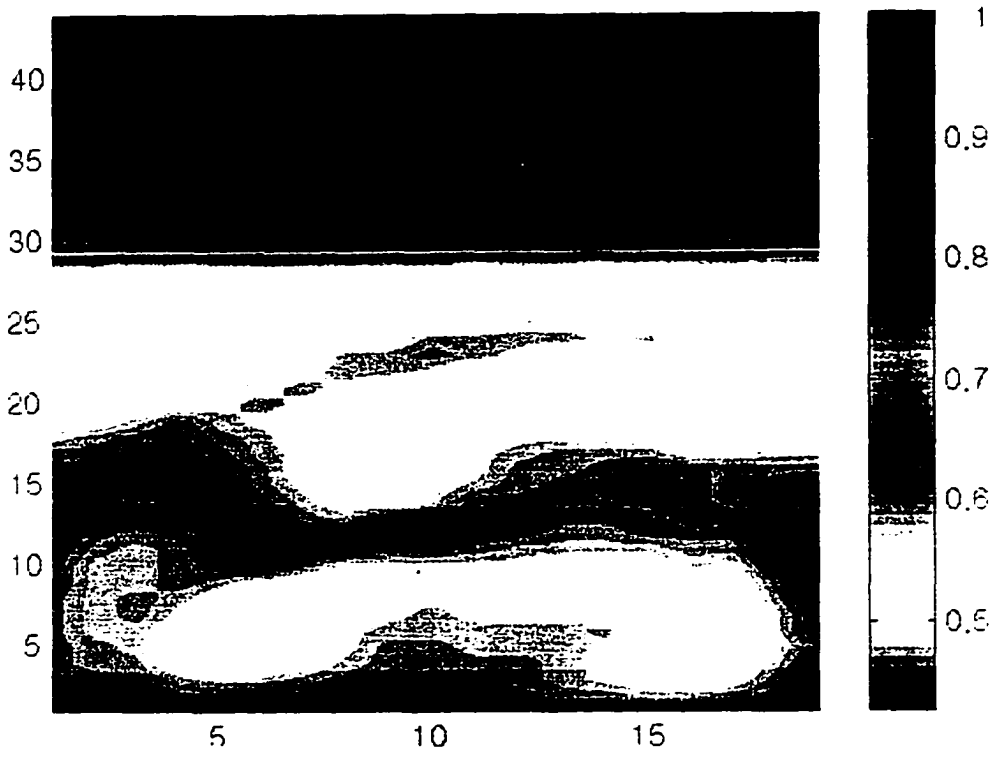

Figure 5.15: Shading plot of air void fraction of an inserted single bubble in gas-solid fluidized bed with E=0 kV, at t=2.0 s
(grid size 0.5X0.7 cm, U=Umf=0.49 cm/s, dp=49 micron, static bed height 19.6 cm, bed width 9.5 cm)

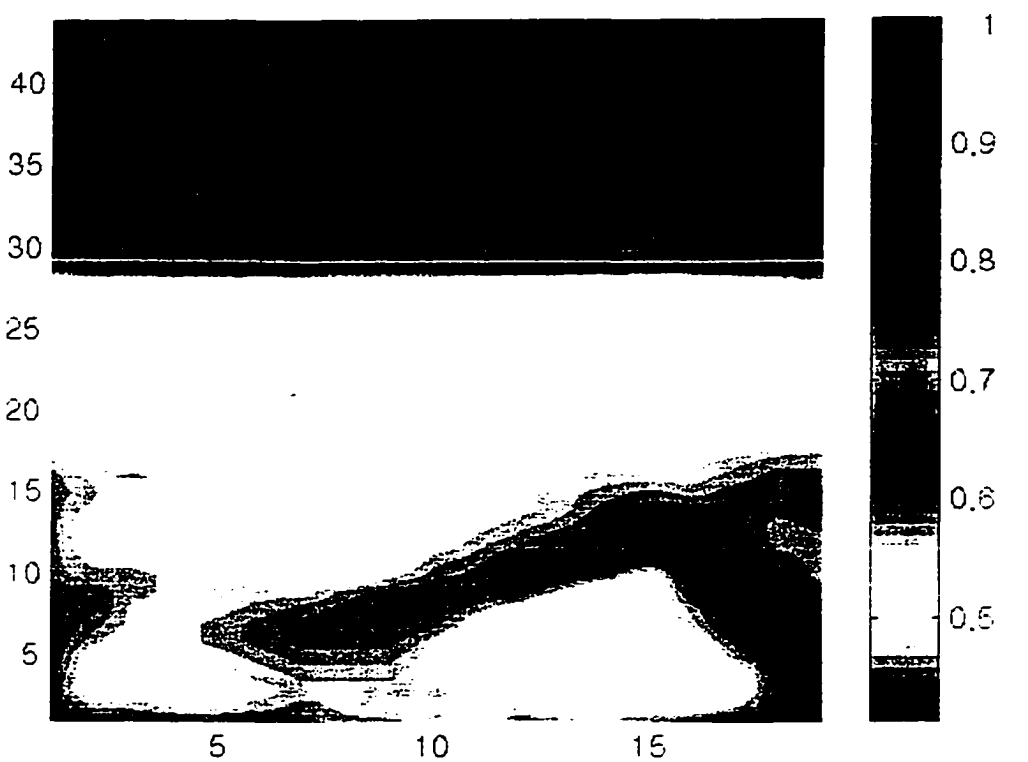

Figure 5.16: Shading plot of air void fraction of an inserted single bubble in gas-solid fluidized bed with E=100 kV, at t=2.0 s
(grid size 0.5X0.7 cm, U=Umf=0.49 cm/s, dp=49 micron, static bed height 19.6 cm, bed width 9.5 cm)

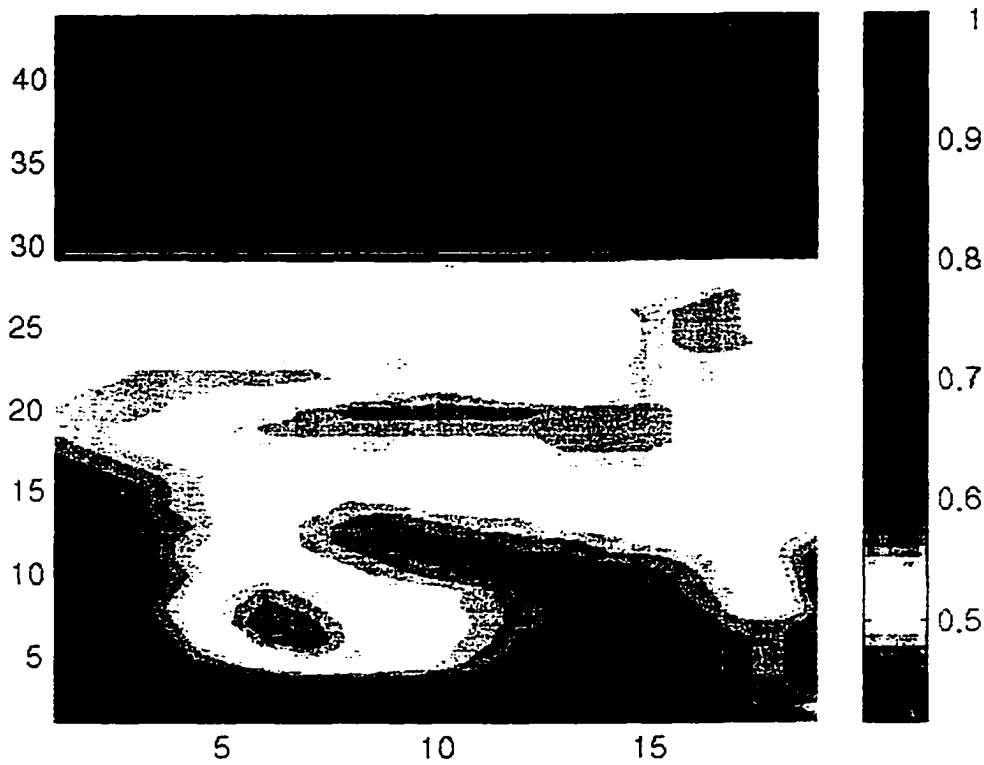

Figure 5.17: Shading plot of air void fraction of an inserted single bubble in gas-solid fluidized bed with E=0 kV, at t=3.0 s
(grid size 0.5X0.7 cm, U=Umf=0.49 cm/s, dp=49 micron, static bed height 19.6 cm, bed width 9.5 cm)

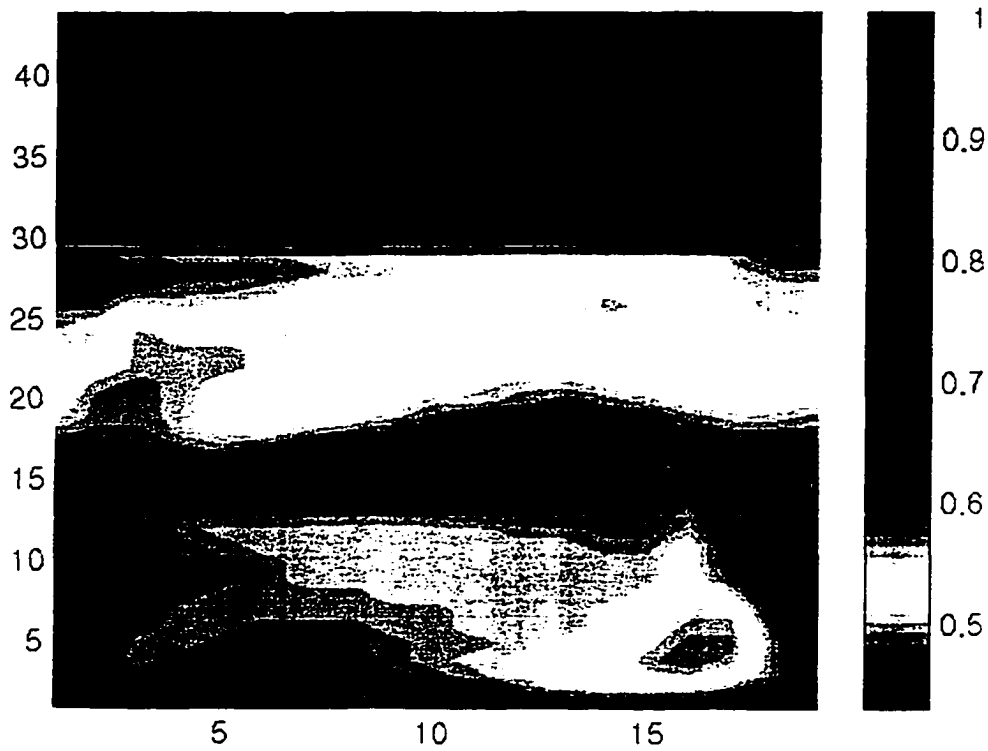

Figure 5.18: Shading plot of air void fraction of an inserted single bubble in gas-solid fluidized bed with E=100 kV, at t=3.0 s
(grid size 0.5X0.7 cm, U=Umf=0.49 cm/s, dp=49 micron, static bed height 19.6 cm, bed width 9.5 cm)

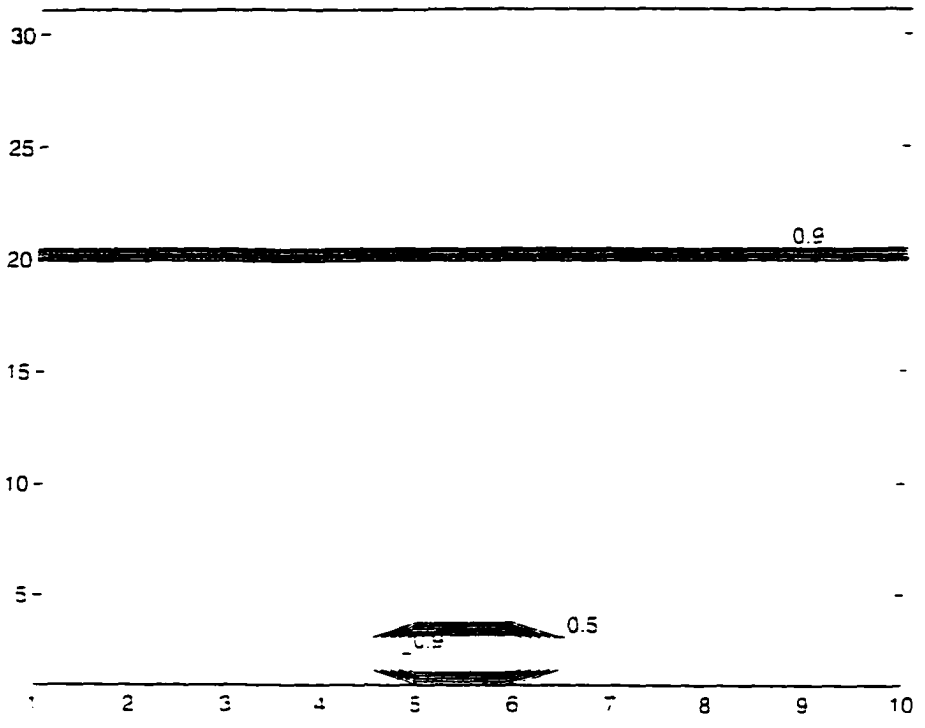

Figure 5.19: Contour plot of Air Void fraction of an iserted single bubble in Gas-Solid Fluidized bed with E=0 kV. at t=0.0 s
(Grid size 0.5X0.7 cm. U=Umf=0.49 cm/s. dp=49 micron. static bed height 19.6 cm. bed width 9.5 cm)

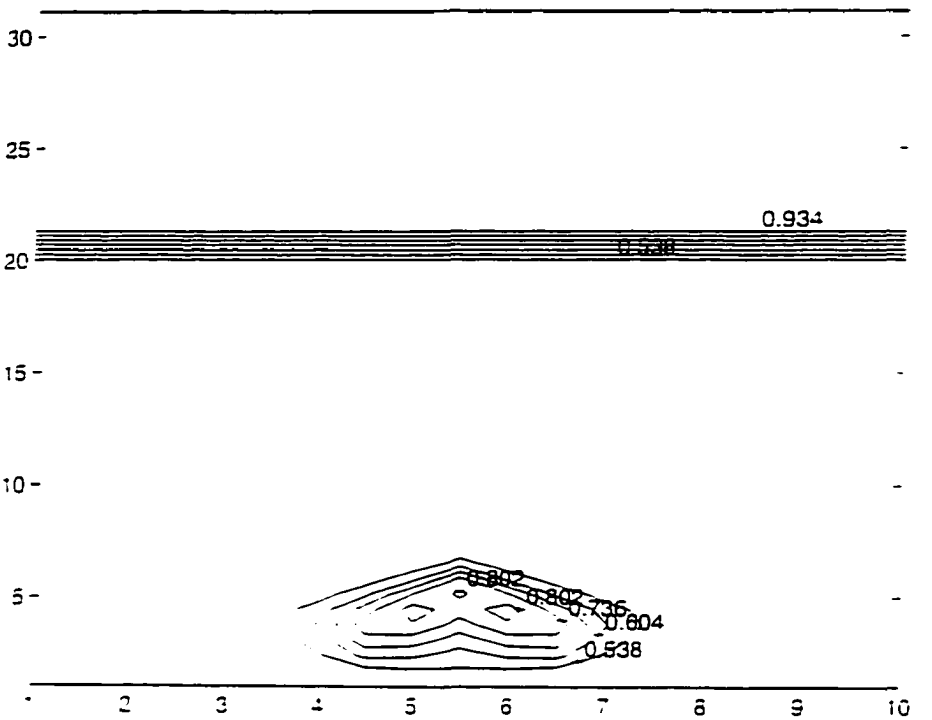

Figure 5.20: Contour plot of Air Void fraction of an iserted single bubble in Gas-Solid Fluidized bed with E=0 kV. at t=0.1 s
(Grid size 0.5X0.7 cm. U=Umf=0.49 cm/s. dp=49 micron. static bed height 19.6 cm. bed width 9.5 cm)

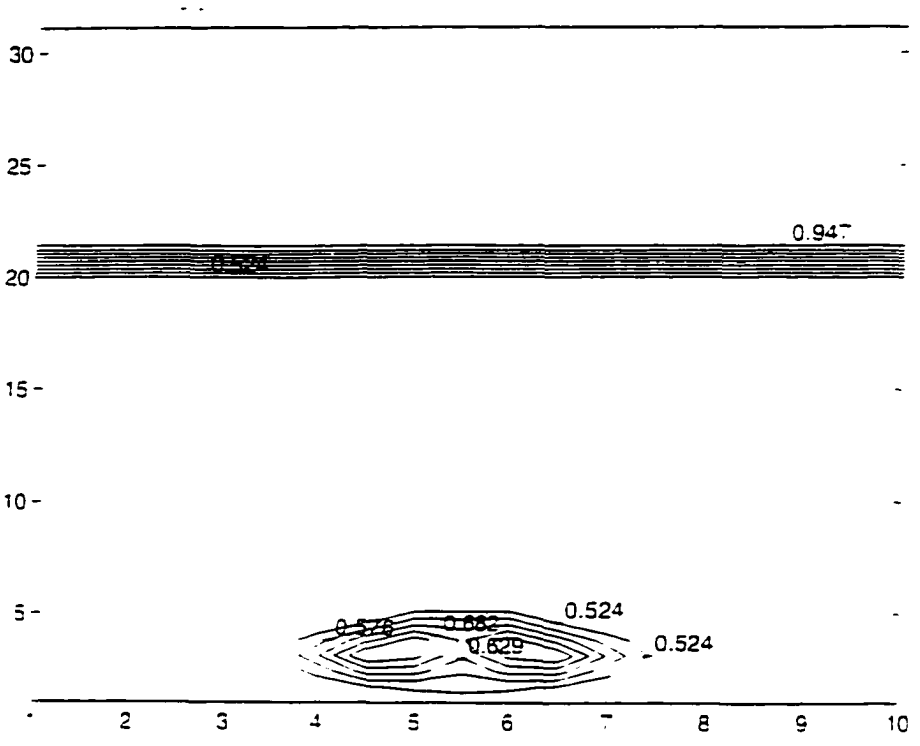

Figure 5.21: Contour plot of Air Void fraction of an iserted single bubble in Gas-Solid Fluidized bed with E=100 kV. at t=0.1 s
(Grid size 0.5X0.7 cm. U=Umf=0.49 cm/s. dp=49 micron. static bed height 19.6 cm. bed width 9.5 cm)

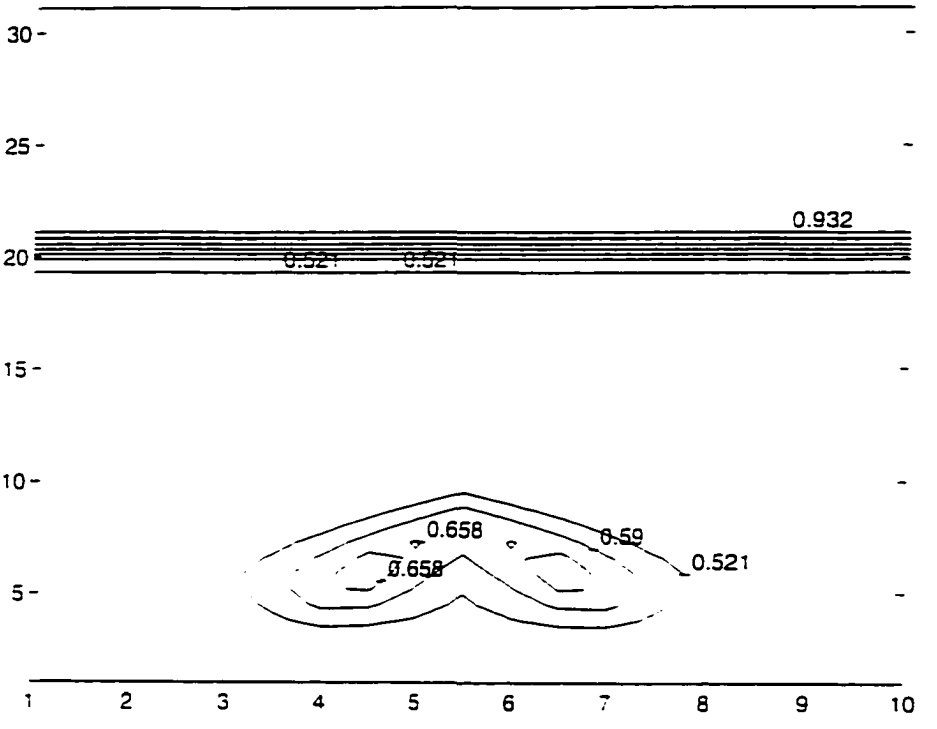

Figure 5.22: Contour plot of Air Void fraction of an iserted single bubble in Gas-Solid Fluidized bed with E=0 kV. at t=0.2 s
(Grid size 0.5X0.7 cm. U=Umf=0.49 cm/s. dp=49 micron. static bed height 19.6 cm. bed width 9.5 cm)

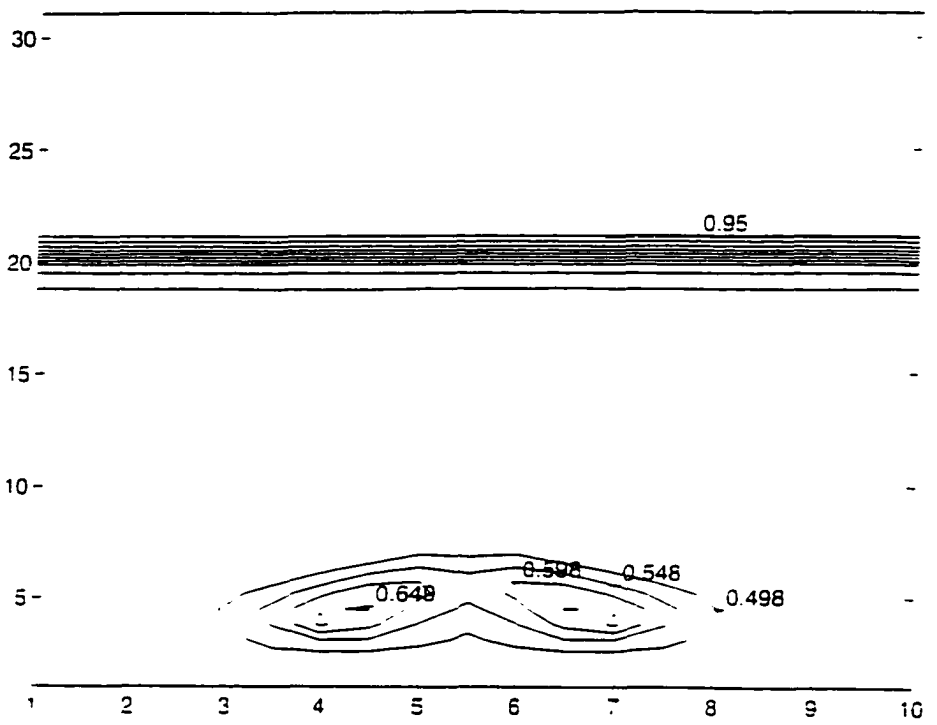

Figure 5.23: Contour plot of Air Void fraction of an iserted single bubble in Gas-Solid Fluidized bed with E=0 kV. at t=0.2 s
(Grid size 0.5X0.7 cm. U=Umf=0.49 cm/s. dp=49 micron. static bed height 19.6 cm. bed width 9.5 cm)

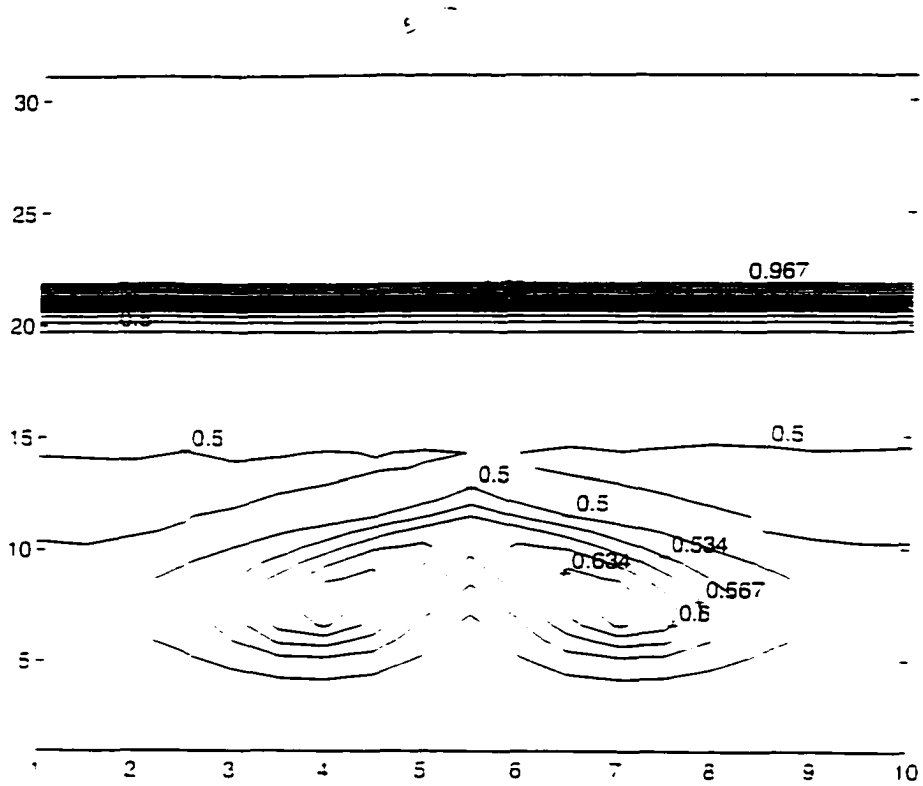

Figure 5.24: Contour plot of Air Void fraction of an iserted single bubble in Gas-Solid Fluidized bed with E=0 kV, at t=0.3 s
(Grid size 0.5X0.7 cm, U=Umf=0.49 cm/s, dp=49 micron, static bed height 19.6 cm, bed width 9.5 cm)

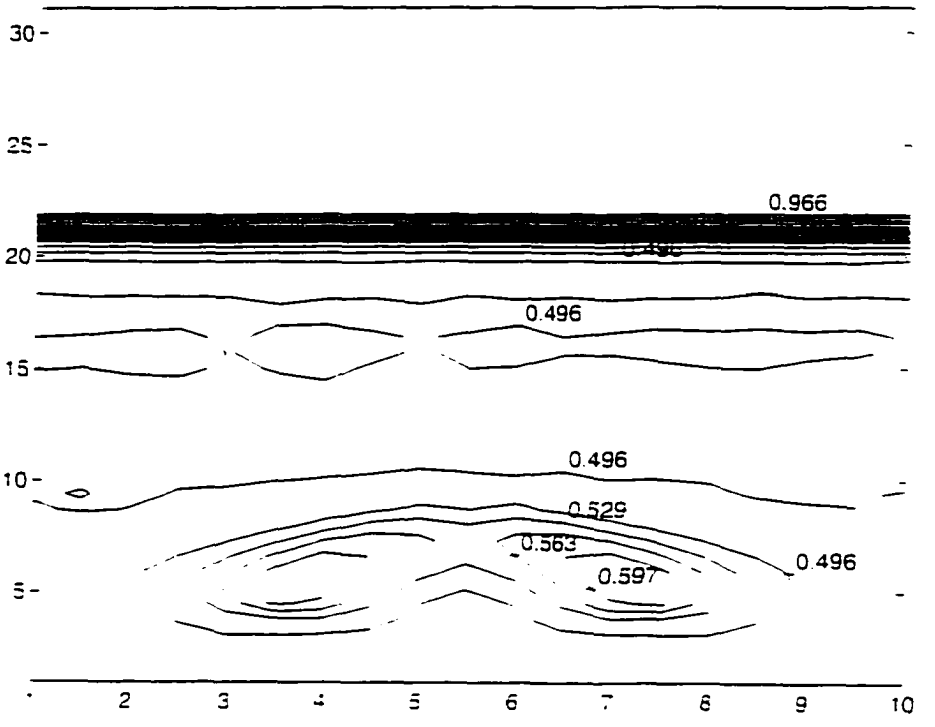

Figure 5.25: Contour plot of Air Void fraction of an iserted single bubble in Gas-Solid Fluidized bed with E=100 kV, at t=0.3 s
(Grid size 0.5X0.7 cm, U=Umf=0.49 cm/s, dp=49 micron, static bed height 19.6 cm, bed width 9.5 cm)

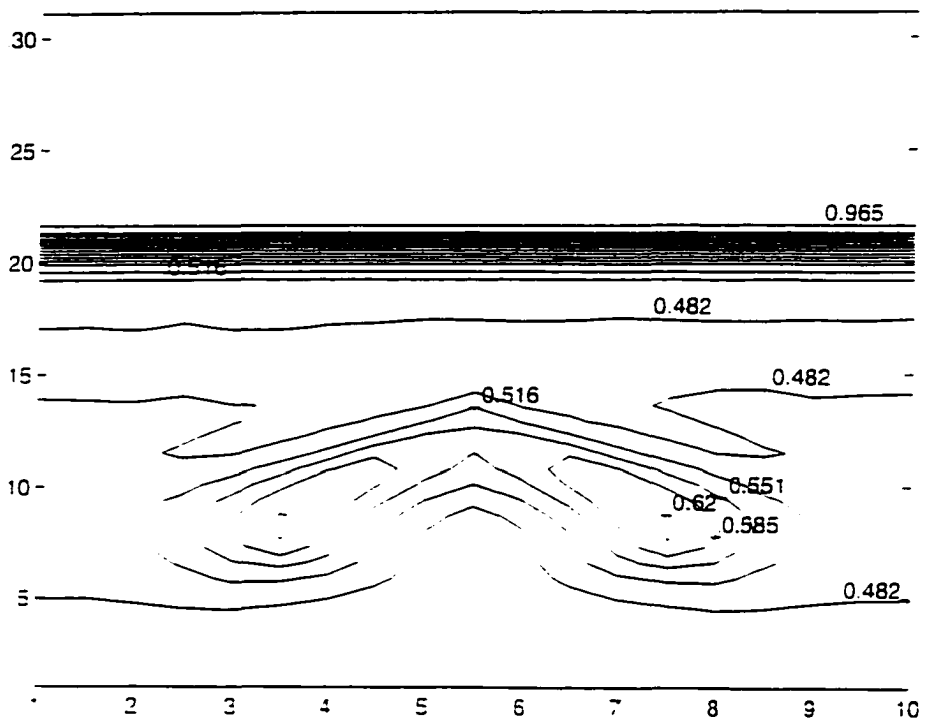

Figure 5.26: Contour plot of Air Void fraction of an iserted single bubble in Gas-Solid Fluidized bed with E=0 kV, at t=0.4 s
(Grid size 0.5X0.7 cm, U=Umf=0.49 cm/s, dp=49 micron, static bed height 19.6 cm, bed width 9.5 cm)

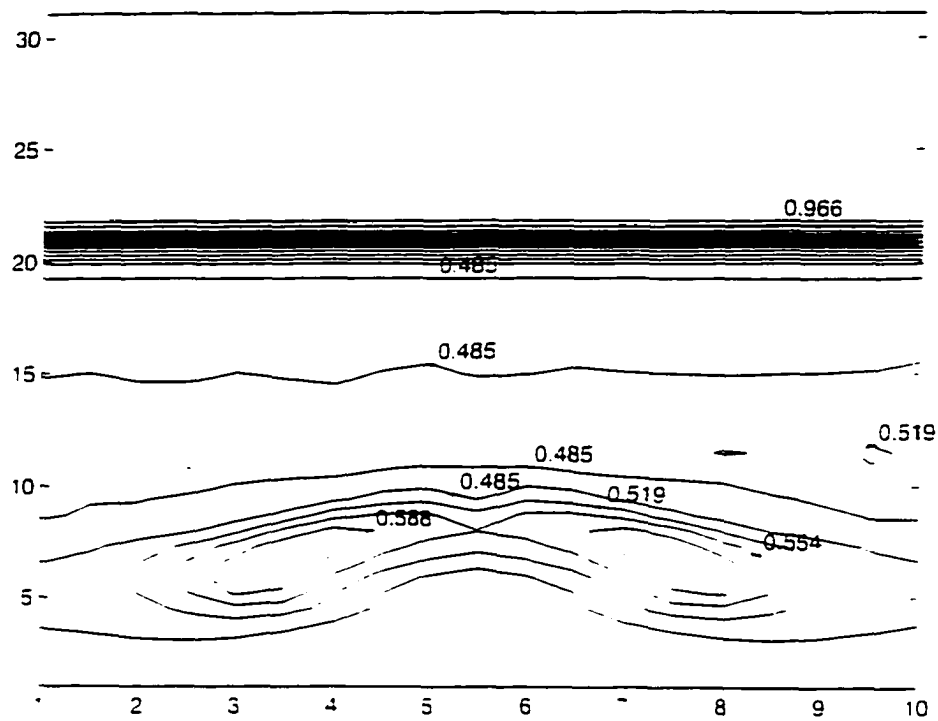

Figure 5.27: Contour plot of Air Void fraction of an iserted single bubble in Gas-Solid Fluidized bed with E=100 kV. at t=0.4 s
(Grid size 0.5X0.7 cm. U=Umf=0.49 cm/s. dp=49 micron. static bed height 19.6 cm. bed width 9.5 cm)

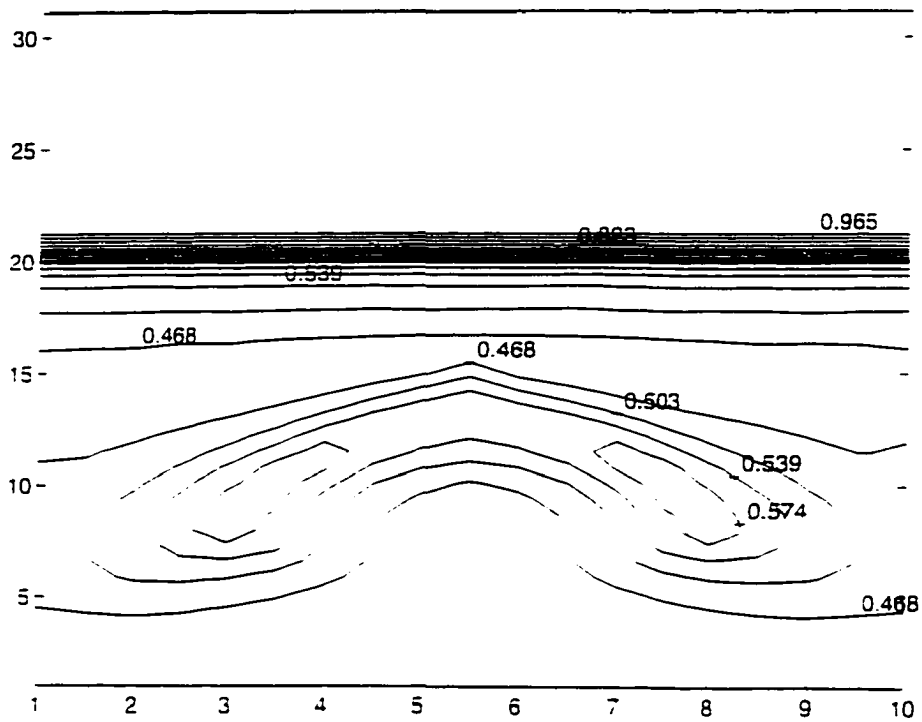

Figure 5.28: Contour plot of Air Void fraction of an iserted single bubble in Gas-Solid Fluidized bed with E=0 kV. at t=0.5 s
(Grid size 0.5X0.7 cm. U=Umf=0.49 cm/s. dp=49 micron. static bed height 19.6 cm. bed width 9.5 cm)

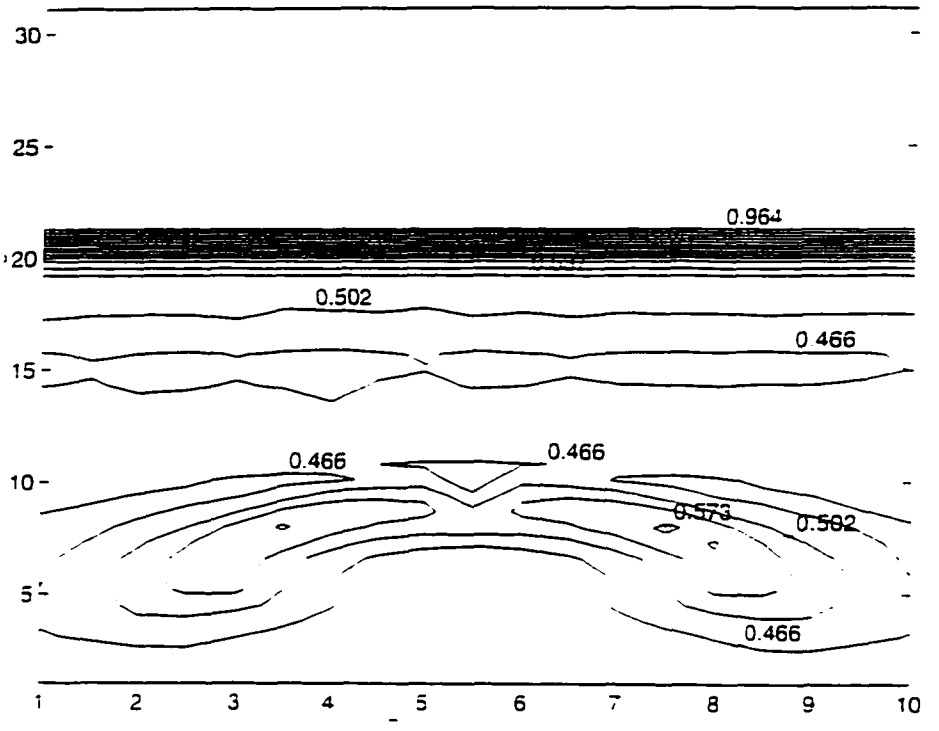

Figure 5.29: Contour plot of Air Void fraction of an iserted single bubble in Gas-Solid Fluidized bed with E=100 kV. at t=0.5 s
(Grid size 0.5X0.7 cm. U=Umf=0.49 cm/s. dp=49 micron. static bed height 19.6 cm. bed width 9.5 cm)

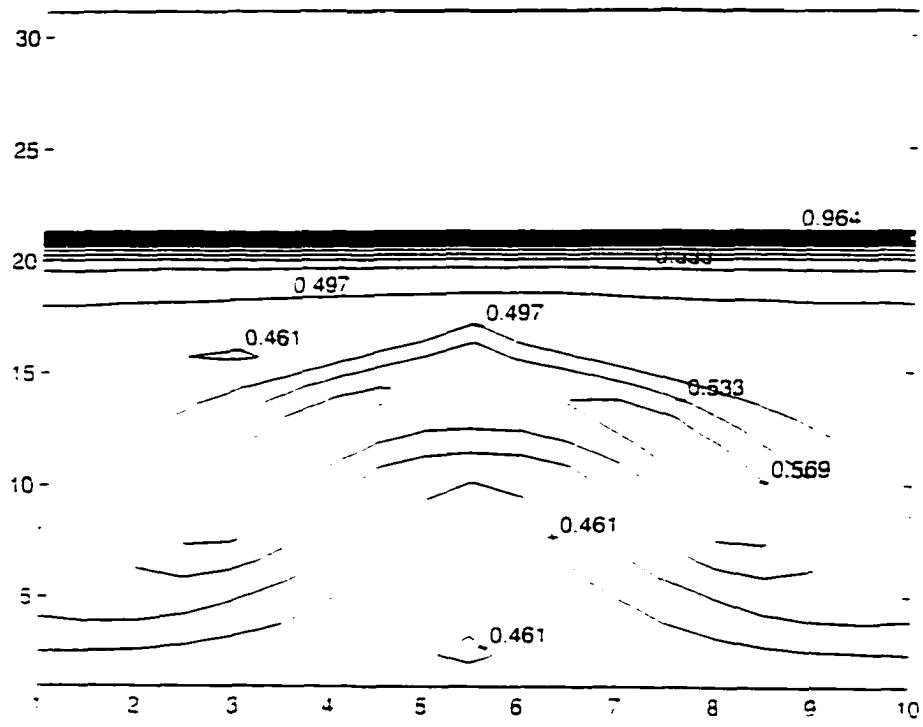

Figure 5.30: Contour plot of Air Void fraction of an iserted single bubble in Gas-Solid Fluidized bed with E=0 kV, at t=0.6 s
(Grid size 0.5X0.7 cm, U=Umf=0.49 cm/s, dp=49 micron, static bed height 19.6 cm, bed width 9.5 cm)

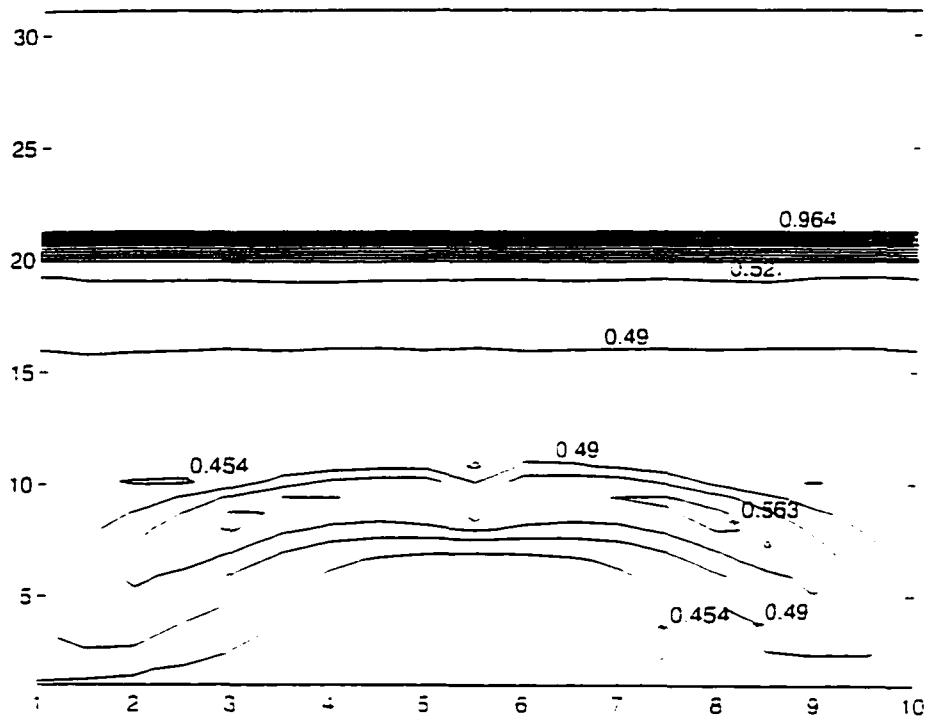

Figure 5.31: Contour plot of Air Void fraction of an iserted single bubble in Gas-Solid Fluidized bed with E=100 kV. at t=0.6 s
(Grid size 0.5X0.7 cm. U=Umf=0.49 cm/s. dp=49 micron. static bed height 19.6 cm. bed width 9.5 cm)

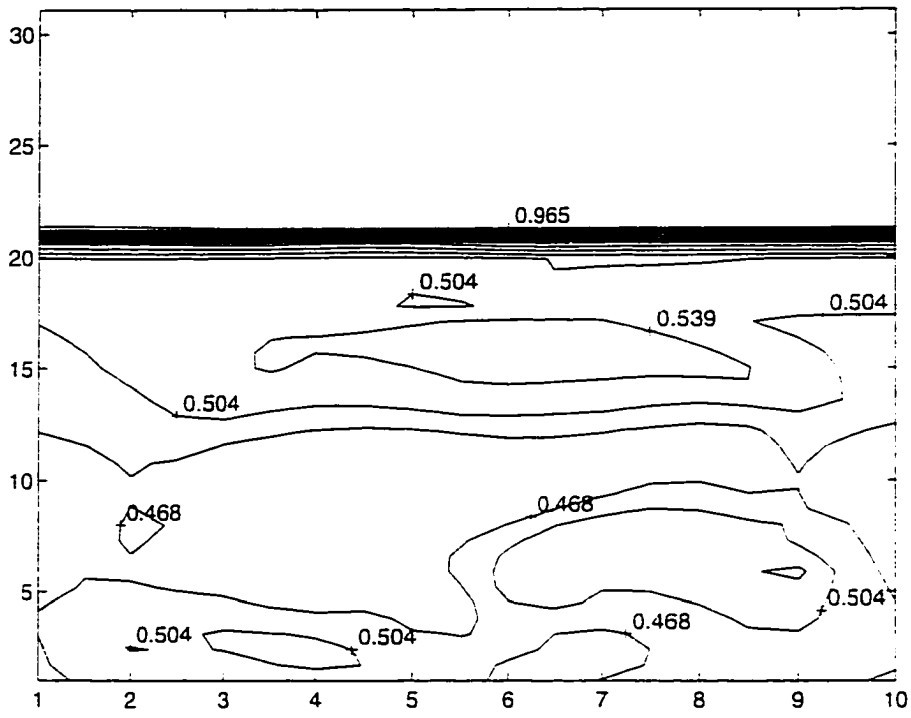

Figure 5.32: Contour plot of air void fraction of an inserted single bubble in gas-solid fluidized bed with E=0 kV, at t=1.5 s
(grid size 0.5X0.7 cm, U=Umf=0.49 cm/s, dp=49 micron, static bed height 19.6 cm, bed width 9.5 cm)

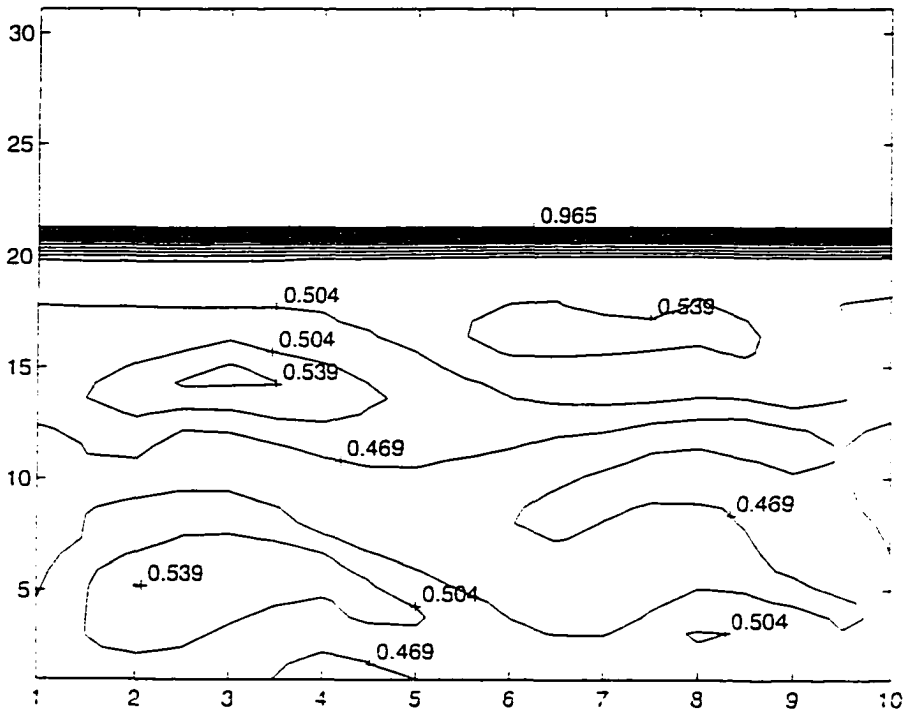

Figure 5.33: Contour plot of air void fraction of an inserted single bubble in gas-solid fluidized bed with E=100 kV. at t=1.5 s
(grid size 0.5X0.7 cm. U=Umf=0.49 cm/s. dp=49 micron, static bed height 19.6 cm, bed width 9.5 cm)

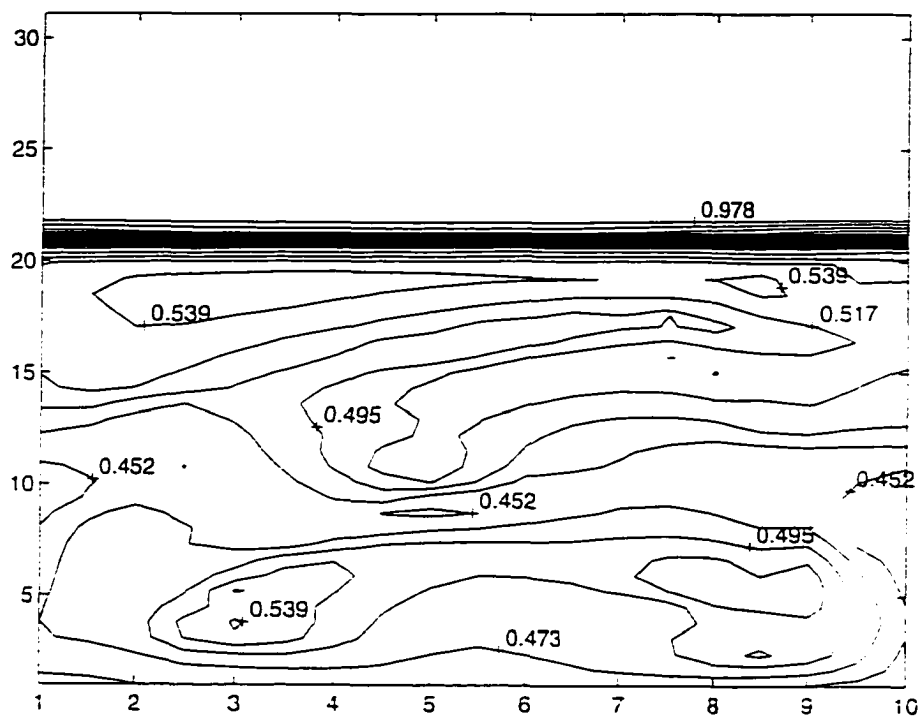

Figure 5.34: Contour plot of air void fraction of an inserted single bubble in gas-solid fluidized bed with E=0 kV, at t=2.0 s
(grid size 0.5X0.7 cm, U=Umf=0.49 cm/s, dp=49 micron, static bed height 19.6 cm, bed width 9.5 cm)

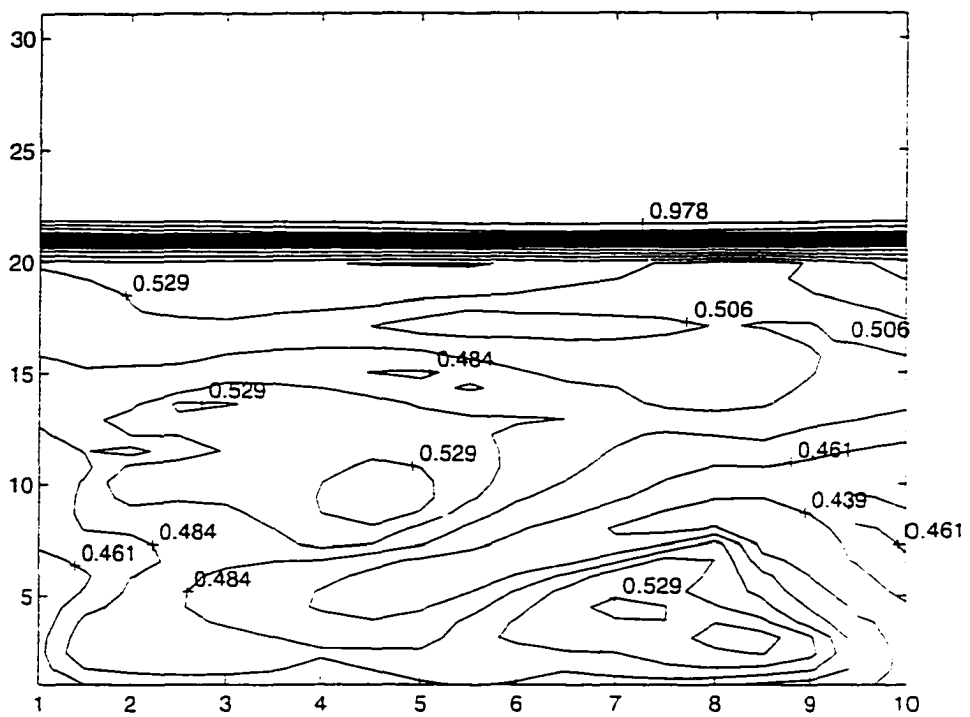

Figure 5.35: Contour plot of air void fraction of an inserted single bubble in gas-solid fluidized bed with E=100 kV, at t=2.0 s
(grid size 0.5X0.7 cm, U=Umf=0.49 cm/s, dp=49 micron, static bed height 19.6 cm, bed width 9.5 cm)

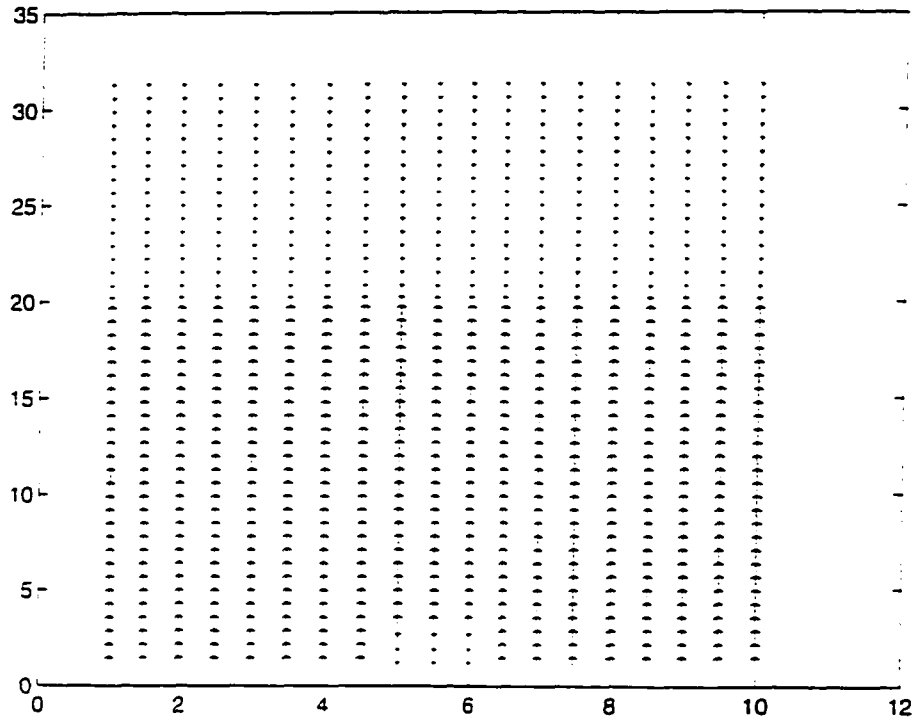

Figure 5.36: Vector plot of air velocity of an inserted single bubble in gas-solid fluidized bed with E=0 kV, at t=0.0 s (grid size 0.5X0.7 cm, U=Umf=0.49 cm/s, dp=49 micron, static bed height 19.6 cm, bed width 9.5 cm)

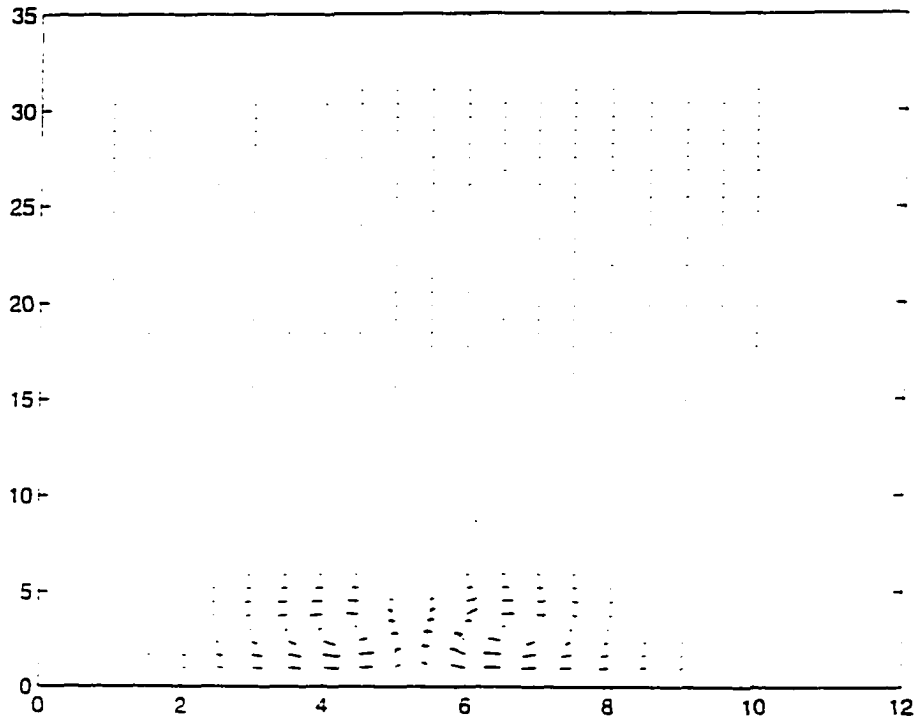

Figure 5.37: Vector plot of air velocity of an inserted single bubble in gas-solid fluidized bed with E=0 kV, at t=0.1 s (grid size 0.5X0.7 cm, U=Umf=0.49 cm/s, dp=49 micron, static bed height 19.6 cm, bed width 9.5 cm)

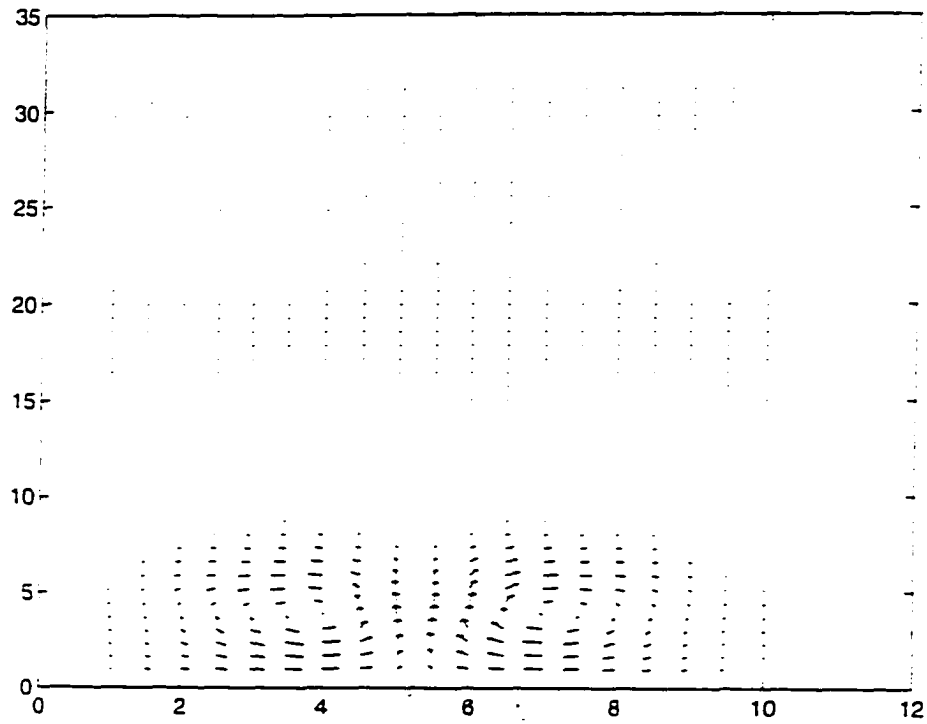

Figure 5.38: Vector plot of air velocity of an inserted single bubble in gas-solid fluidized bed with E=0 kV, at t=0.2 s
(grid size 0.5X0.7 cm, U=Umf=0.49 cm/s, dp=49 micron, static bed height 19.6 cm, bed width 9.5 cm)

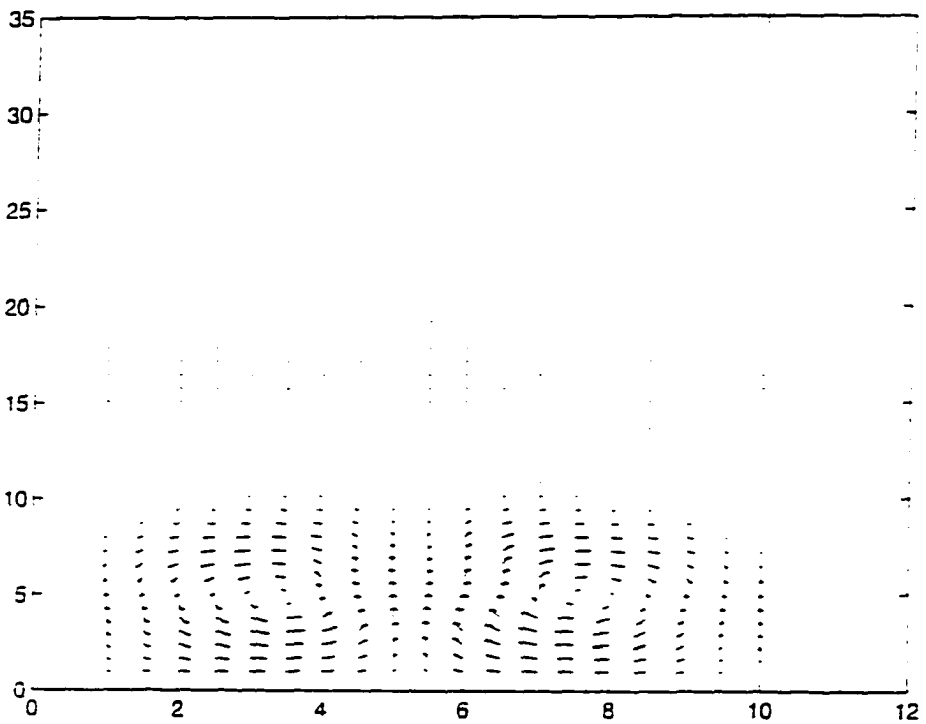

Figure 5.39: Vector plot of air velocity of an inserted single bubble in gas-solid fluidized bed with E=0 kV, at t=0.3 s (grid size 0.5X0.7 cm, U=Umf=0.49 cm/s, dp=49 micron, static bed height 19.6 cm, bed width 9.5 cm)

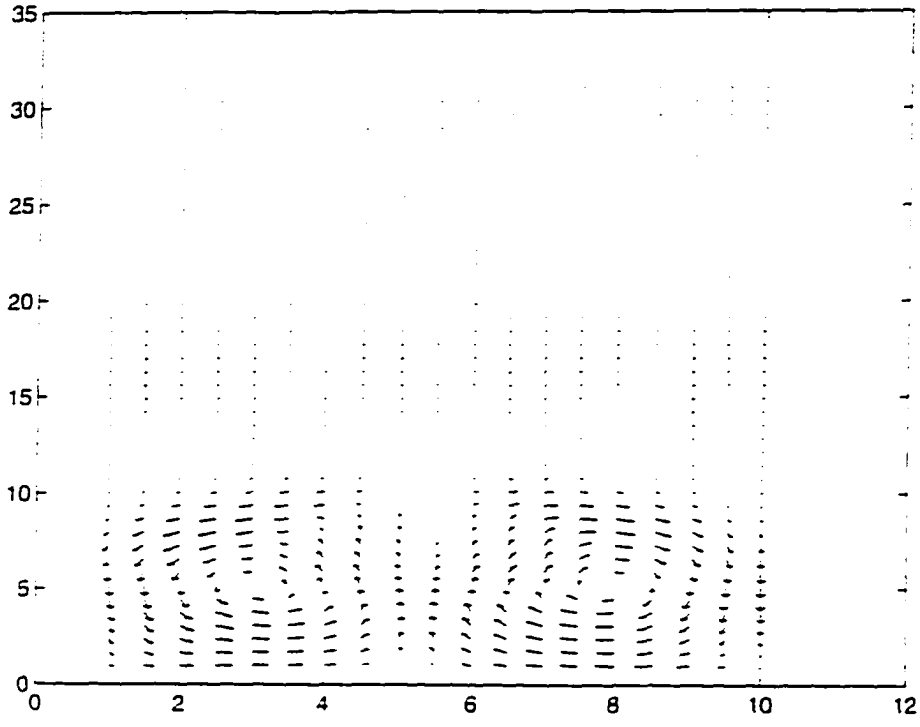

Figure 5.40: Vector plot of air velocity of an inserted single bubble in gas-solid fluidized bed with E=0 kV, at t=0.4 s (grid size 0.5X0.7 cm, U=Umf=0.49 cm/s, dp=49 micron, static bed height 19.6 cm, bed width 9.5 cm)

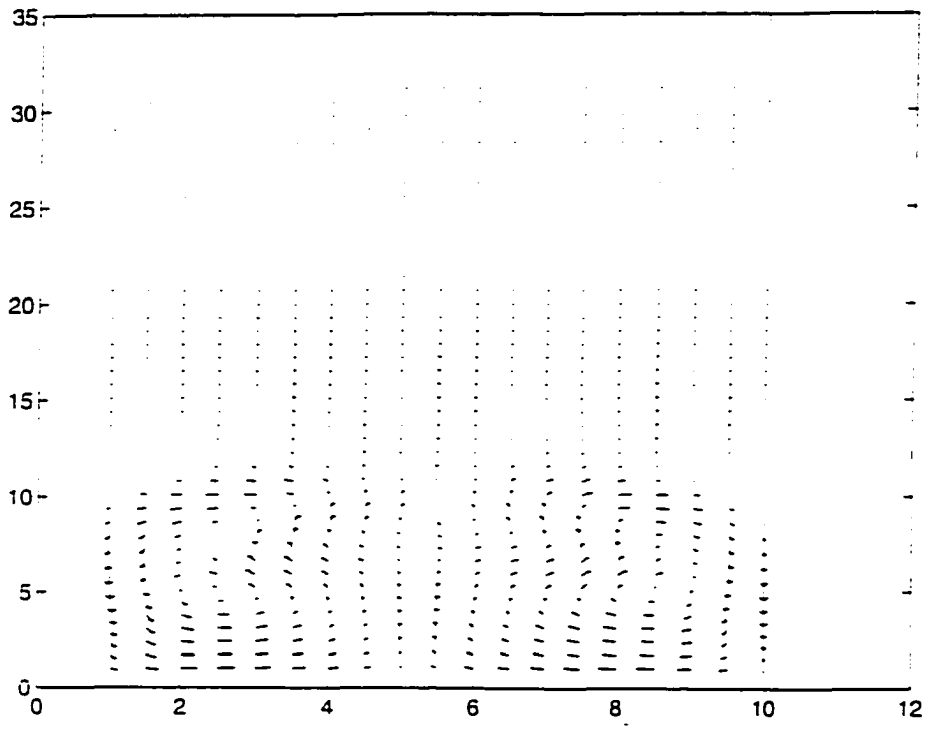

Figure 5.41: Vector plot of air velocity of an inserted single bubble in gas-solid fluidized bed with E=0 kV, at t=0.6 s (grid size 0.5X0.7 cm, U=Umf=0.49 cm/s, dp=49 micron, static bed height 19.6 cm, bed width 9.5 cm)

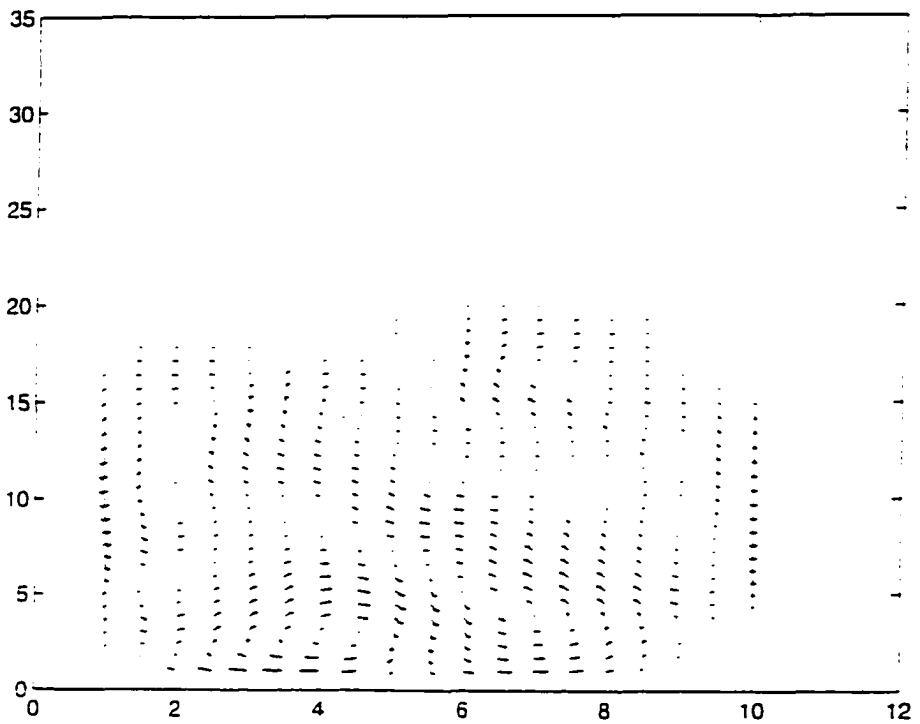

Figure 5.42: Vector plot of air velocity of an inserted single bubble in gas-solid fluidized bed with E=0 kV, at t=1.5 s (grid size 0.5X0.7 cm, U=Umf=0.49 cm/s, dp=49 micron, static bed height 19.6 cm, bed width 9.5 cm)

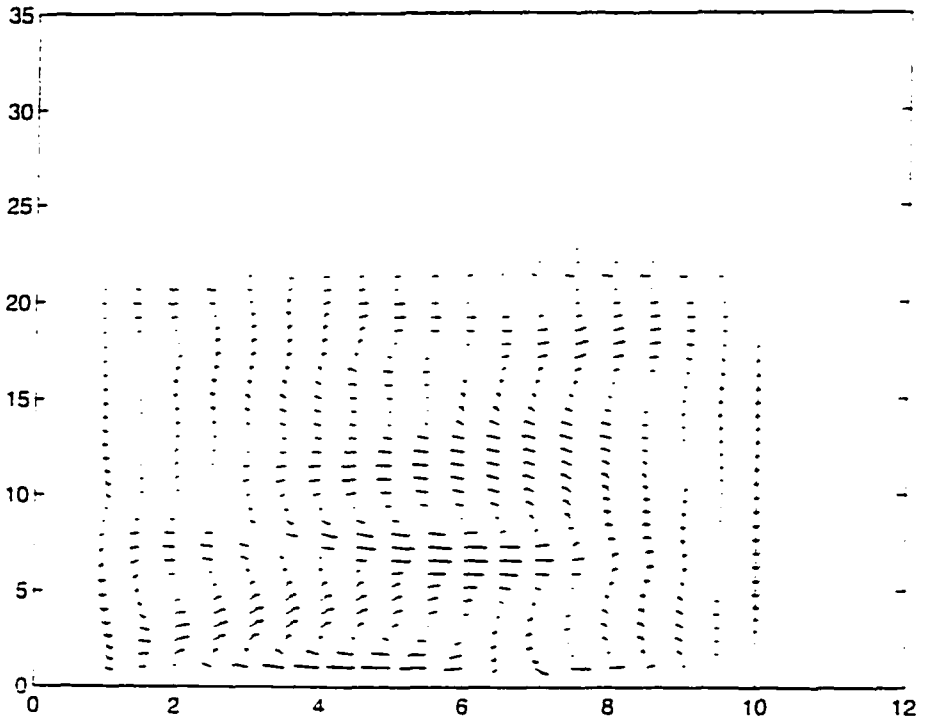

Figure 5.43: Vector plot of air velocity of an inserted single bubble in gas-solid fluidized bed with E=0 kV, at t=2.0 s (grid size 0.5X0.7 cm, U=Umf=0.49 cm/s, dp=49 micron, static bed height 19.6 cm, bed width 9.5 cm)

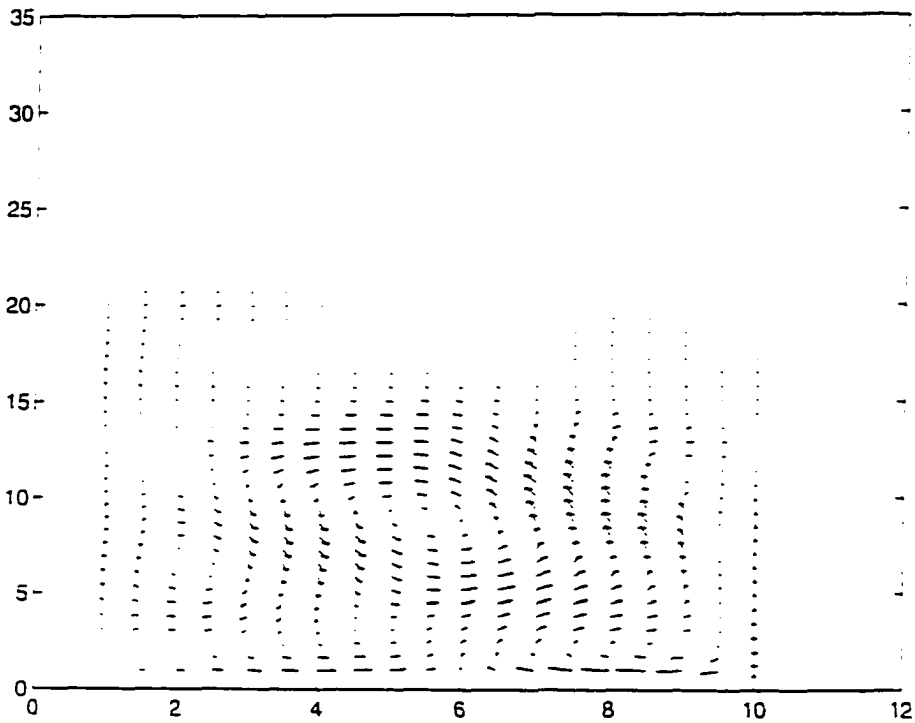

Figure 5.44: Vector plot of air velocity of an inserted single bubble in gas-solid fluidized bed with E=0 kV, at t=3.0 s (grid size 0.5X0.7 cm, U=Umf=0.49 cm/s, dp=49 micron, static bed height 19.6 cm, bed width 9.5 cm)

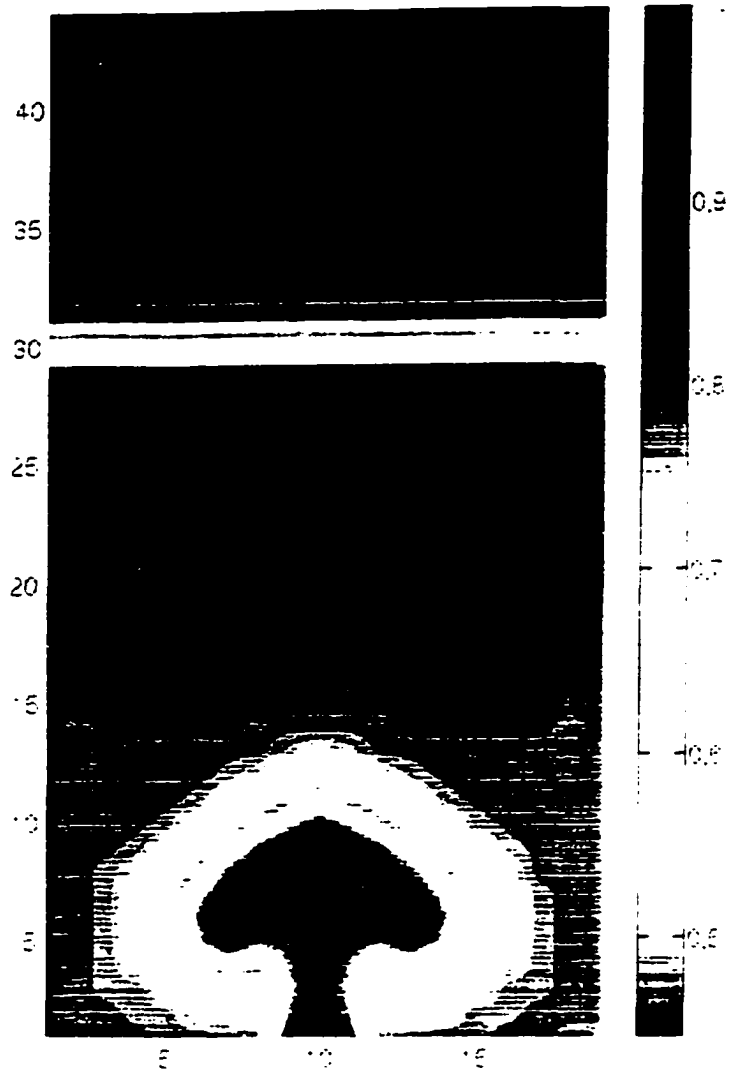

Figure 5.45: Shading plot of Air Void fraction of a jet velocity = 49.49 cm/s in Gas-Solid Fluidized bed with E=0 kV, at t=0.2 s
(Grid size 0.5X0.7 cm, U=Umf=0.49 cm/s, dp=49 micron, static bed height 19.6 cm, bed width 9.5 cm)

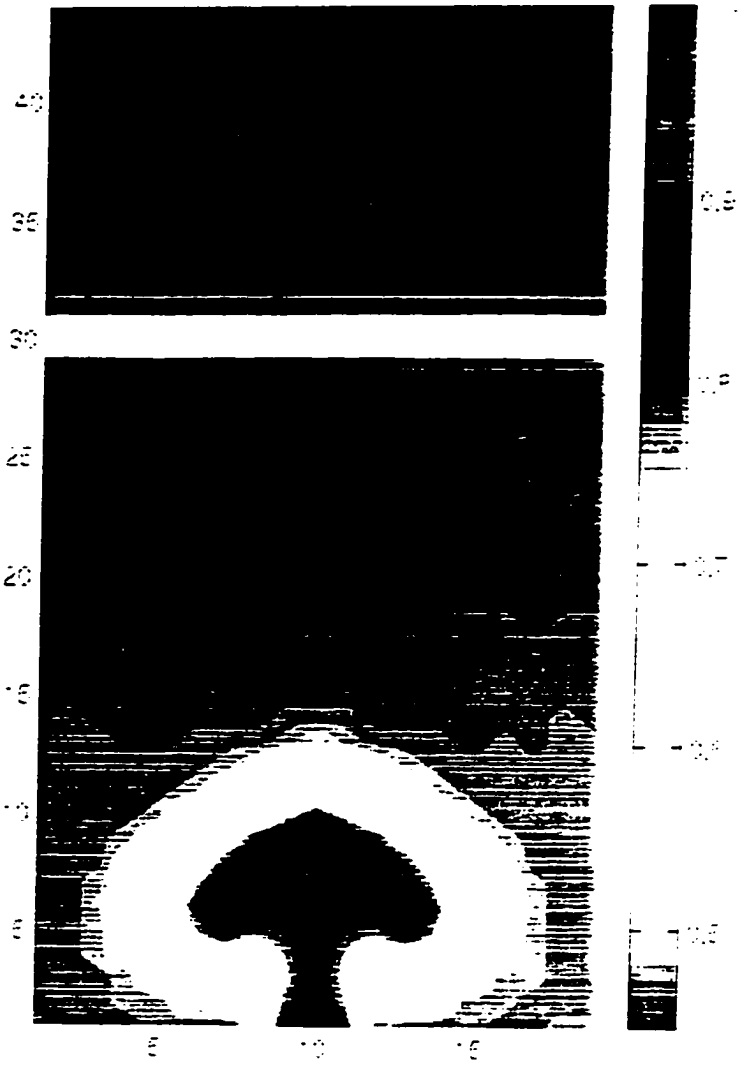

Figure 5.46: Shading plot of Air Void fraction of a jet velocity = 49.49 cm/s in Gas-Solid Fluidized bed with E=100 kV. at t=0.2 s
(Grid size 0.5X0.7 cm. U=Umf=0.49 cm/s. dp=49 micron. static bed height 19.6 cm. bed width 9.5 cm)

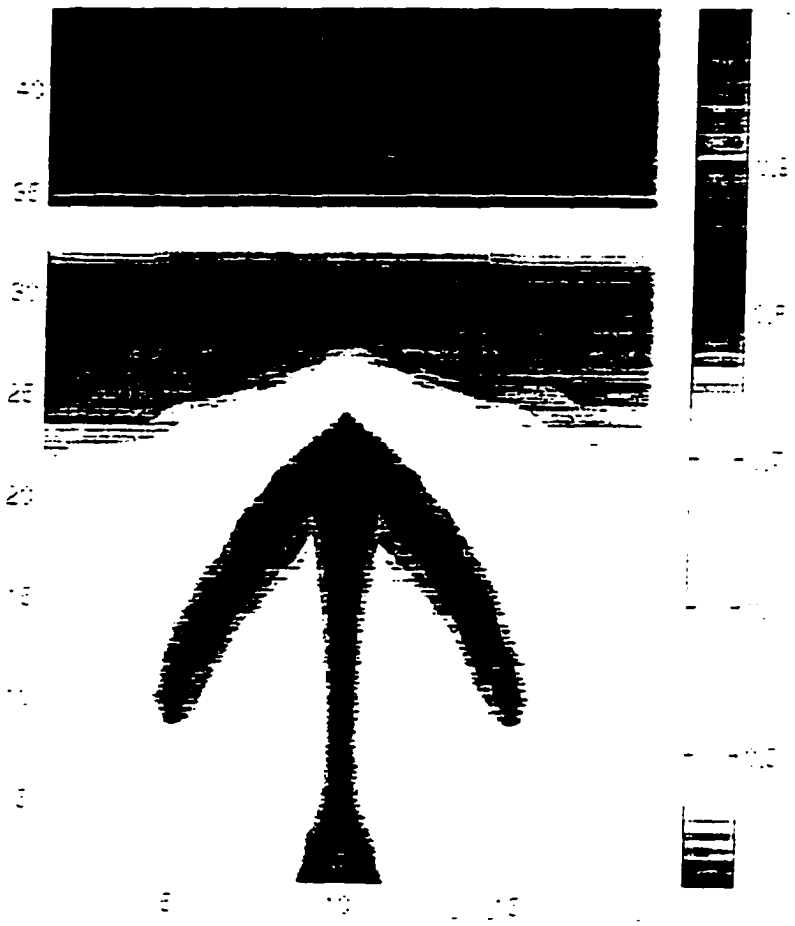

Figure 5.47: Shading plot of Air Void fraction of a jet velocity = 49.49 cm/s in Gas-Solid Fluidized bed with E=0 kV. at t=0.4 s
(Grid size 0.5X0.7 cm. U=Umf=0.49 cm/s. dp=49 micron. static bed height 19.6 cm. bed width 9.5 cm)

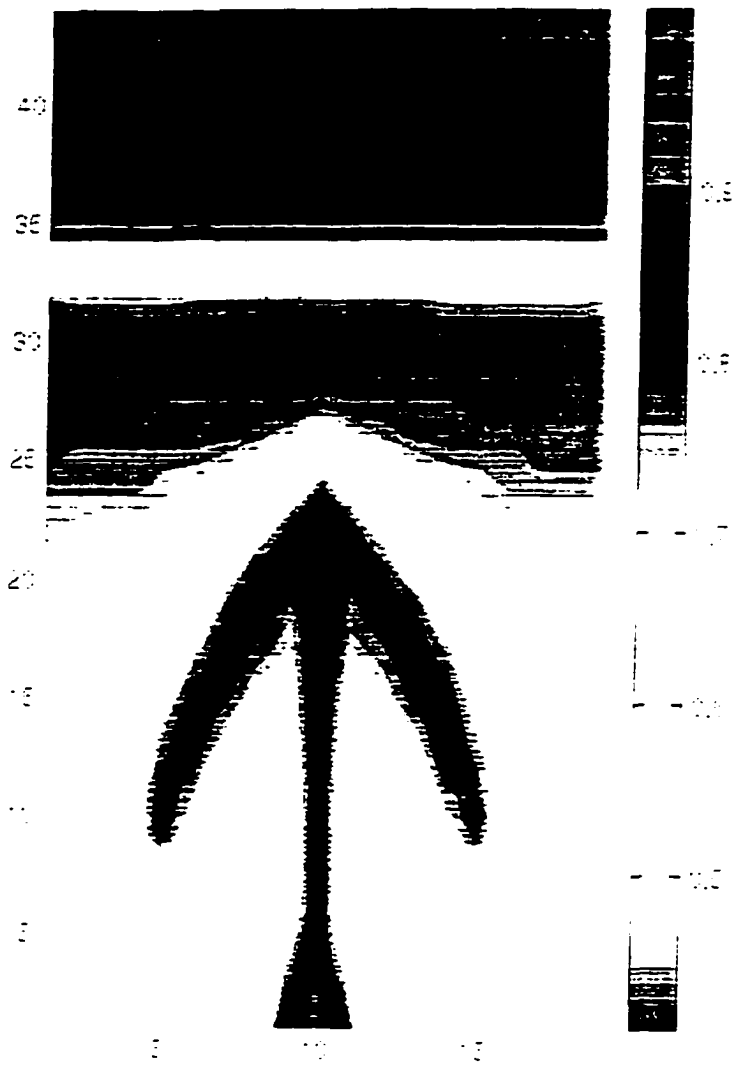

Figure 5.48: Shading plot of Air Void fraction of a jet velocity = 49.49 cm/s in Gas-Solid Fluidized bed with E=100 kV, at t=0.4 s
(Grid size 0.5X0.7 cm, U=Umf=0.49 cm/s, dp=49 micron, static bed height 19.6 cm, bed width 9.5 cm)

Figure 5.49: Shading plot of Air Void fraction of a jet velocity = 49.49 cm/s in Gas-Solid Fluidized bed with E=0 kV. at t=0.6 s
(Grid size 0.5X0.7 cm. U=Umf=0.49 cm/s. dp=49 micron. static bed height 19.6 cm. bed width 9.5 cm)

Figure 5.50: Shading plot of Air Void fraction of a jet velocity = 49.49 cm/s in Gas-Solid Fluidized bed with E=100kV, at t=0.6 s
(Grid size 0.5X0.7 cm, U=Umf=0.49 cm/s, dp=49 micron, static bed height 19.6 cm, bed width 9.5 cm)

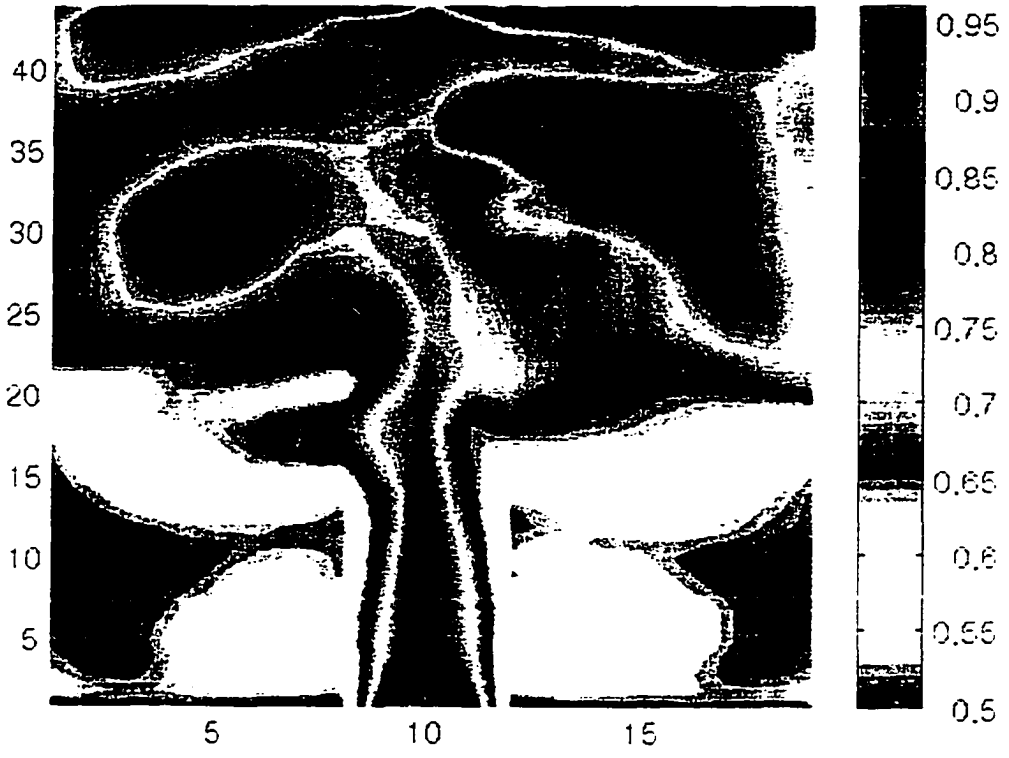

Figure 5.51: Shading plot of air void fraction of a jet velocity = 49.49 cm/s in gas-solid fluidized bed with E=0 kV, at t=1.5 s
(grid size 0.5X0.7 cm, U=Umf=0.49 cm/s, dp=49 micron, static bed height 19.6 cm, bed width 9.5 cm)

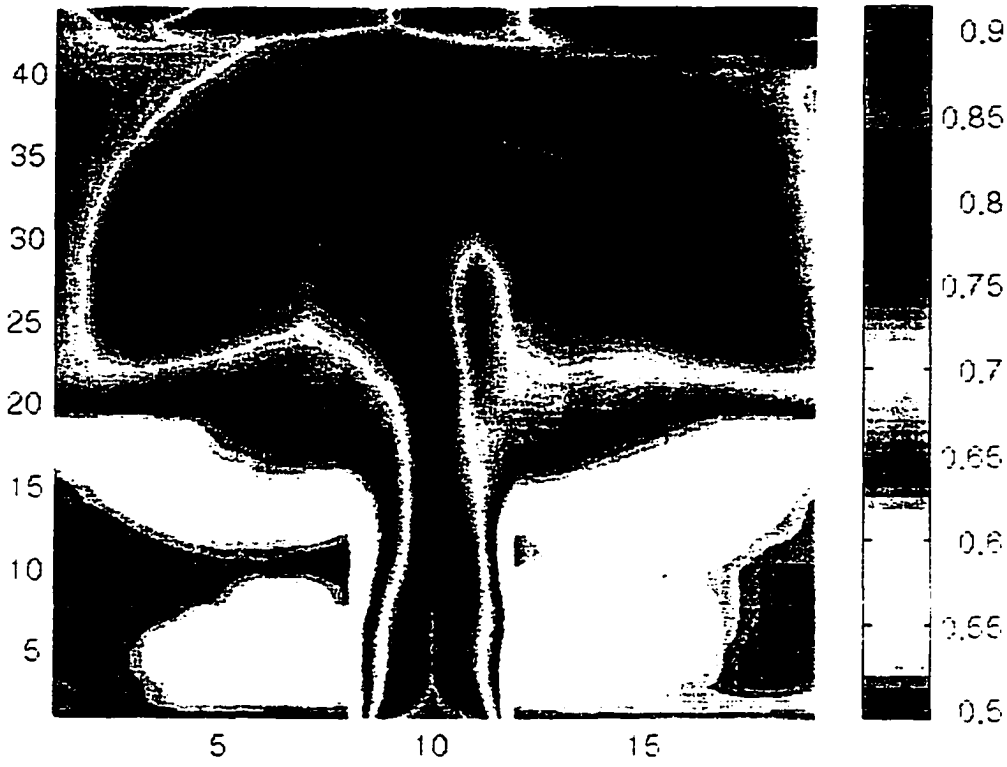

Figure 5.52: Shading plot of air void fraction of a jet velocity = 49.49 cm/s in gas-solid fluidized bed with E=100 kV, at t=1.5 s
(grid size 0.5X0.7 cm, U=Umf=0.49 cm/s, dp=49 micron, static bed height 19.6 cm, bed width 9.5 cm)

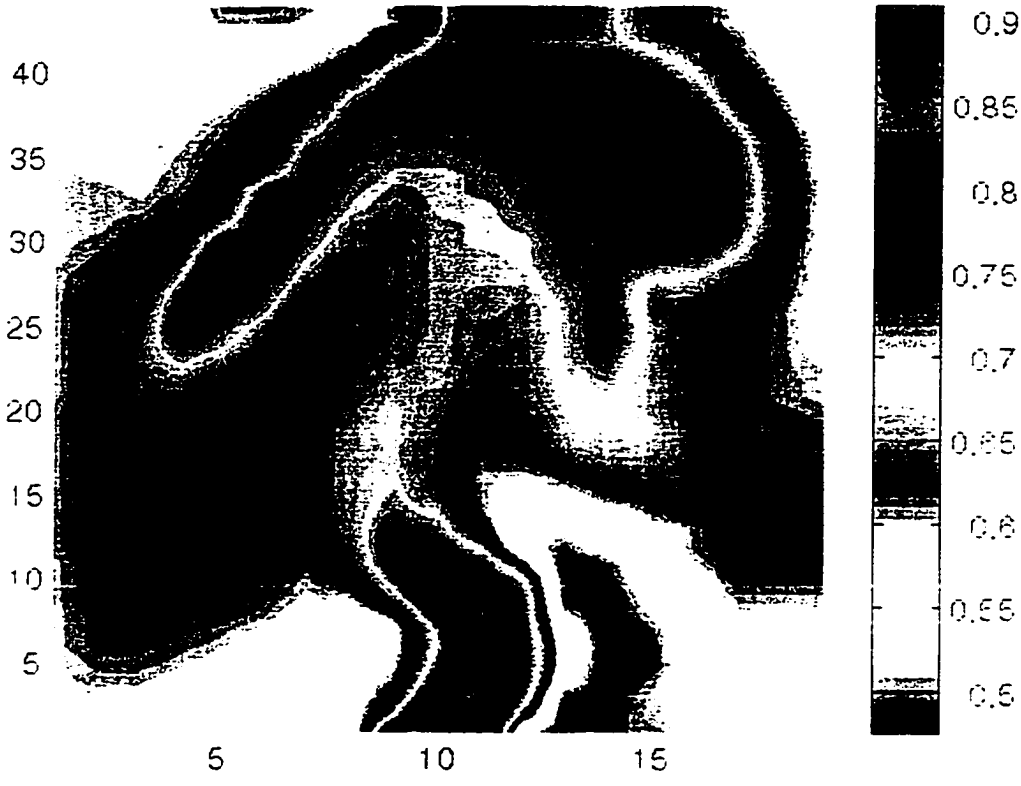

Figure 5.53: Shading plot of air void fraction of a jet velocity = 49.49 cm/s in gas-solid fluidized bed with E=0 kV, at t=3.0 s
(grid size 0.5X0.7 cm, U=Umf=0.49 cm/s, dp=49 micron, static bed height 19.6 cm, bed width 9.5 cm)

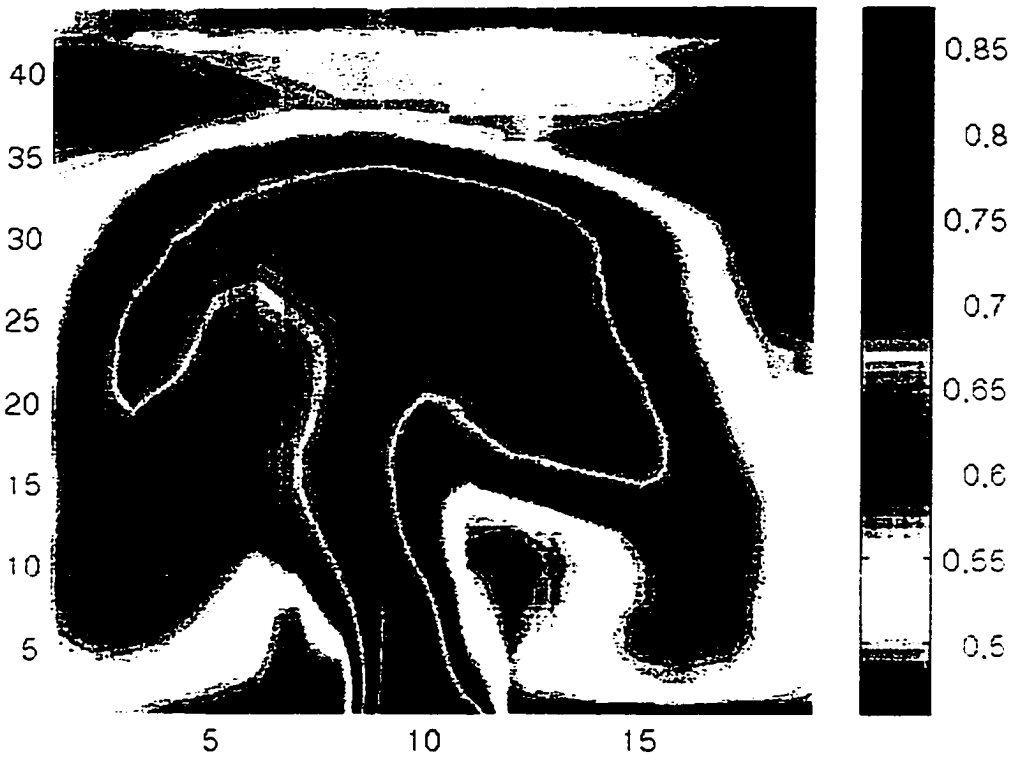

Figure 5.54: Shading plot of air void fraction of a jet velocity = 49.49 cm/s in gas-solid fluidized bed with E=100 kV. at t=3.0 s
(grid size 0.5X0.7 cm. U=Umf=0.49 cm/s, dp=49 micron, static bed height 19.6 cm. bed width 9.5 cm)

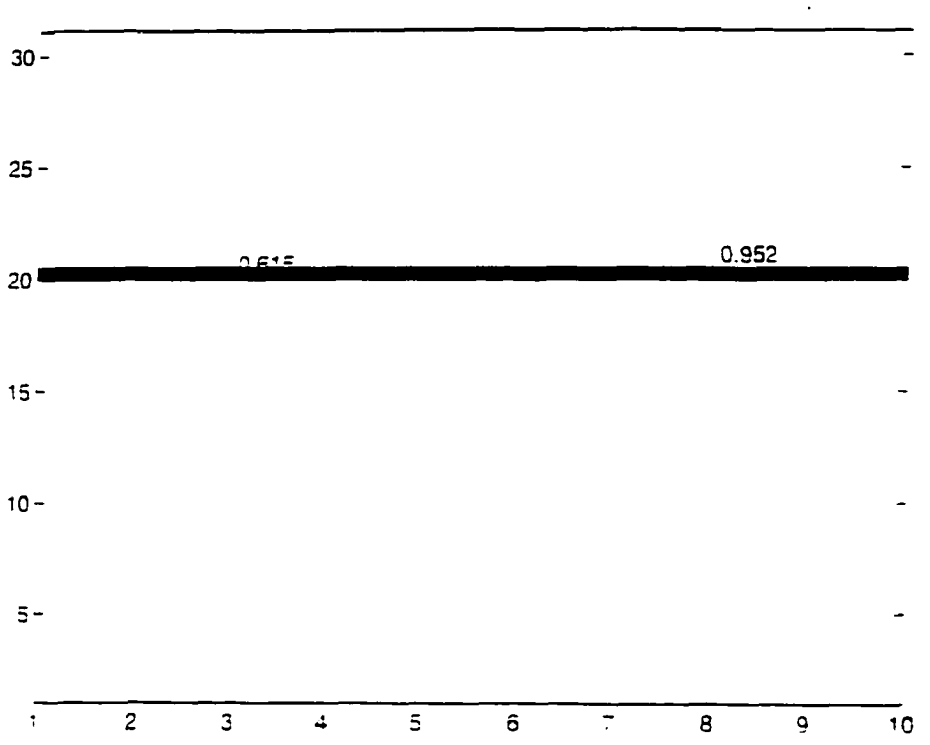

Figure 5.55: Contour plot of Air Void fraction of a jet velocity = 49.49 cm/s in Gas-Solid Fluidized bed with E=0 kV. at t=0.0 s
(Grid size 0.5X0.7 cm. U=Umf=0.49 cm/s. dp=49 micron. static bed height 19.6 cm. bed width 9.5 cm)

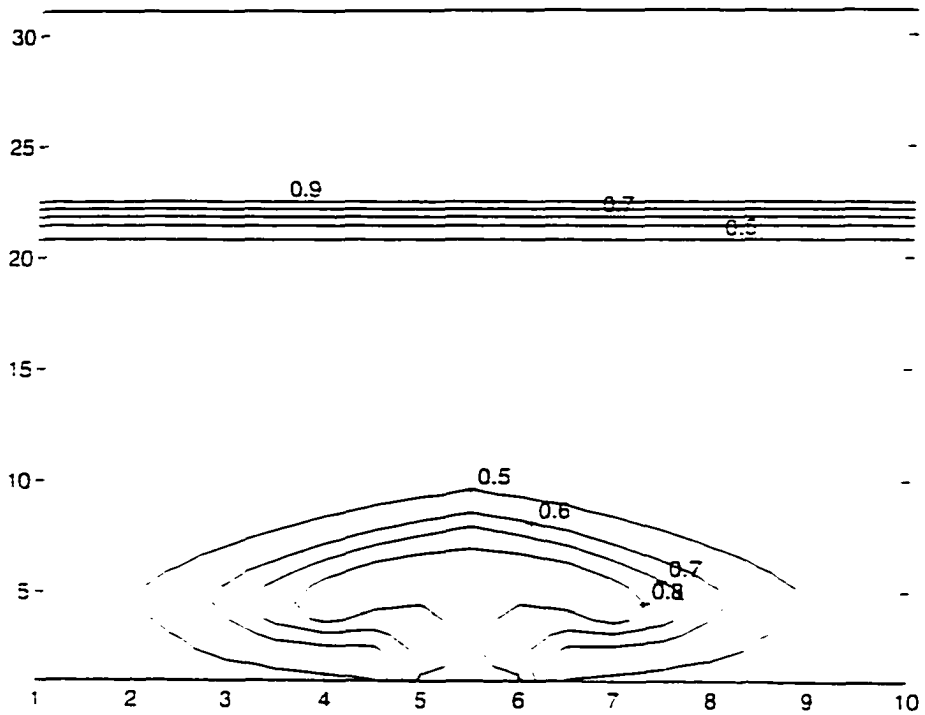

Figure 5.56: Contour plot of Air Void fraction of a jet velocity = 49.49 cm/s in Gas-Solid Fluidized bed with E=0 kV. at t=0.2 s
(Grid size 0.5X0.7 cm. U=Umf=0.49 cm/s. dp=49 micron. static bed height 19.6 cm. bed width 9.5 cm)

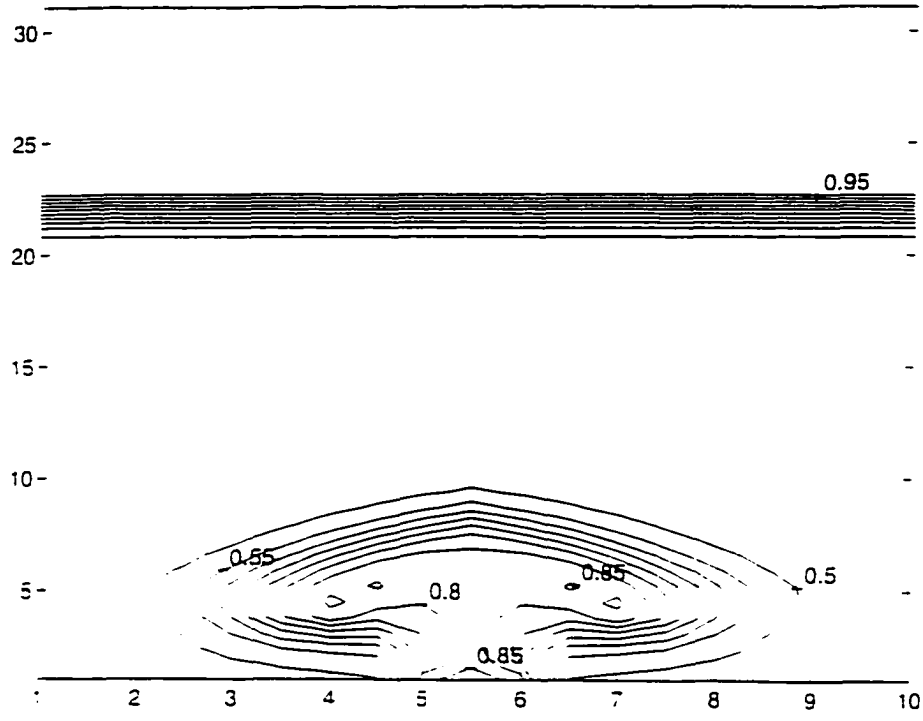

Figure 5.57: Contour plot of Air Void fraction of a jet velocity = 49.49 cm/s in Gas-Solid Fluidized bed with E=100 kV. at t=0.2 s
(Grid size 0.5X0.7 cm. U=Umf=0.49 cm/s. dp=49 micron. static bed height 19.6 cm. bed width 9.5 cm)

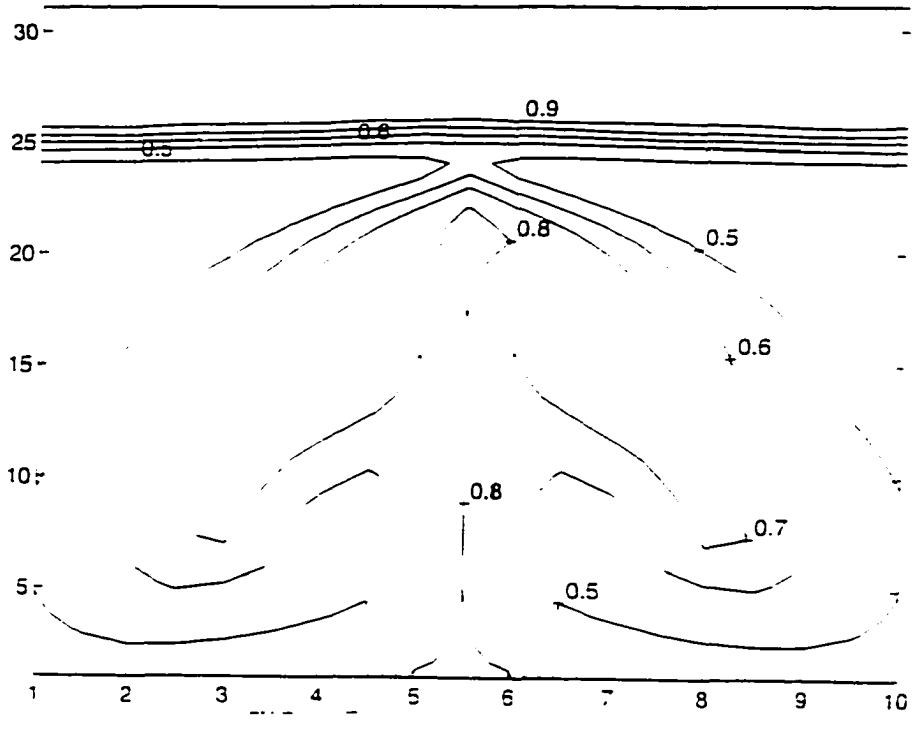

Figure 5.58: Contour plot of Air Void fraction of a jet velocity = 49.49 cm/s in Gas-Solid Fluidized bed with E=0 kV. at t=0.4 s
(Grid size 0.5X0.7 cm. U=Umf=0.49 cm/s. dp=49 micron. static bed height 19.6 cm. bed width 9.5 cm)

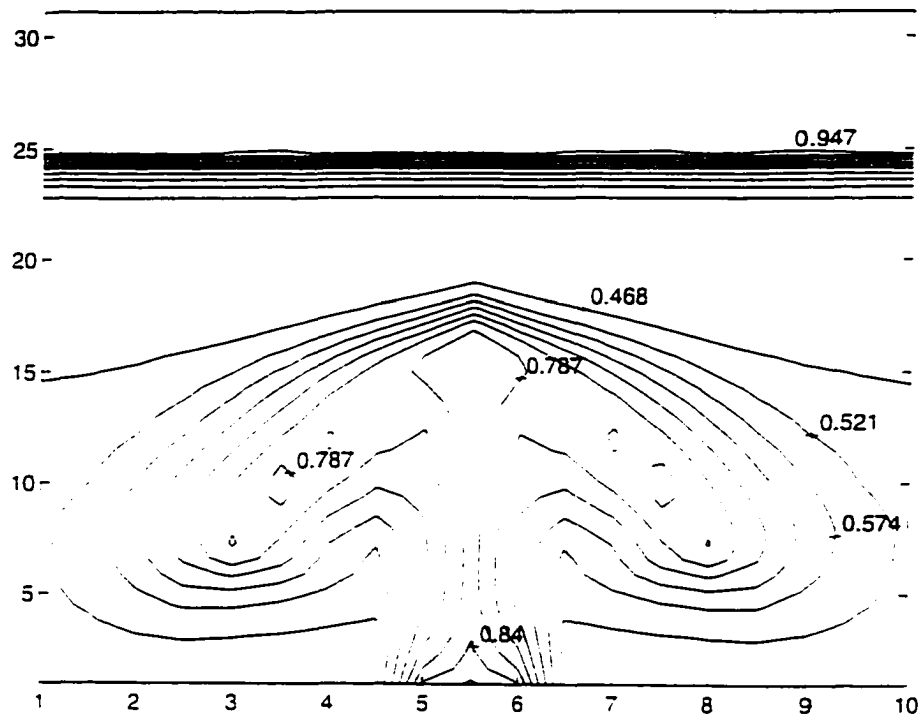

Figure 5.59: Contour plot of Air Void fraction of a jet velocity = 49.49 cm/s in Gas-Solid Fluidized bed with E=100 kV, at t=0.4 s
(Grid size 0.5X0.7 cm, U=Umf=0.49 cm/s, dp=49 micron, static bed height 19.6 cm, bed width 9.5 cm)

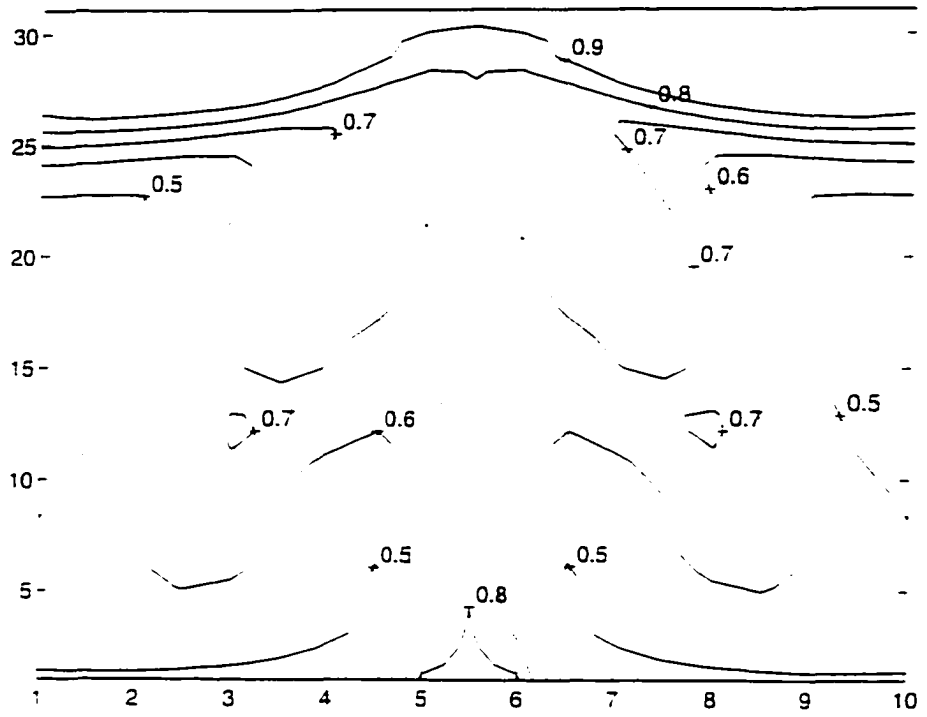

Figure 5.60: Contour plot of Air Void fraction of a jet velocity = 49.49 cm/s in Gas-Solid Fluidized bed with E=0 kV. at t=0.6 s
(Grid size 0.5X0.7 cm. U=Umf=0.49 cm/s. dp=49 micron. static bed height 19.6 cm. bed width 9.5 cm)

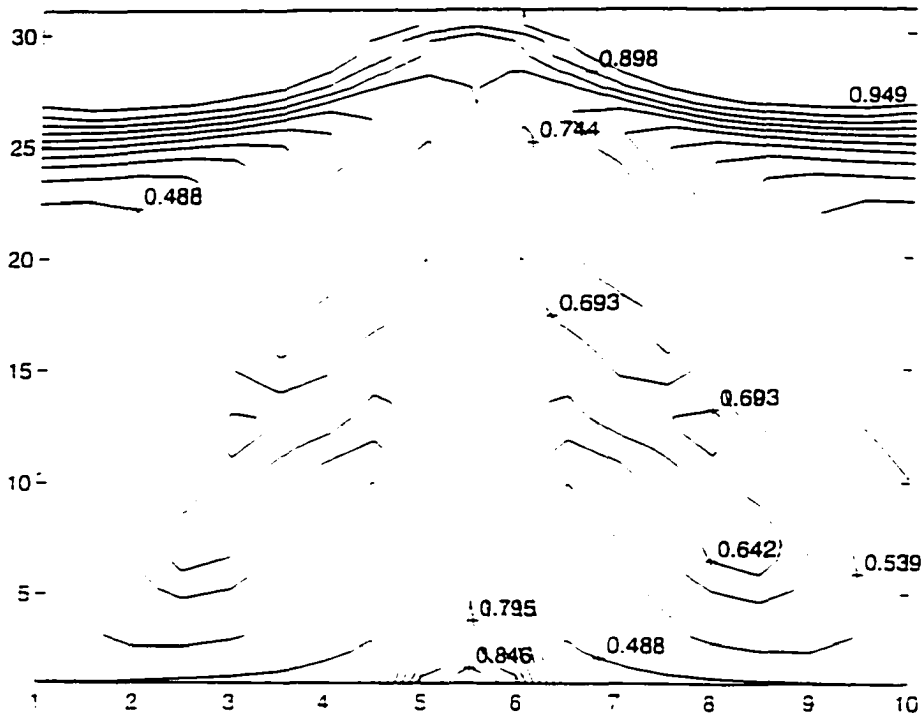

Figure 5.61: Contour plot of Air Void fraction of a jet velocity = 49.49 cm/s in Gas-Solid Fluidized bed with E=100 kV, at t=0.6 s
(Grid size 0.5X0.7 cm, U=Umf=0.49 cm/s, dp=49 micron, static bed height 19.6 cm, bed width 9.5 cm)

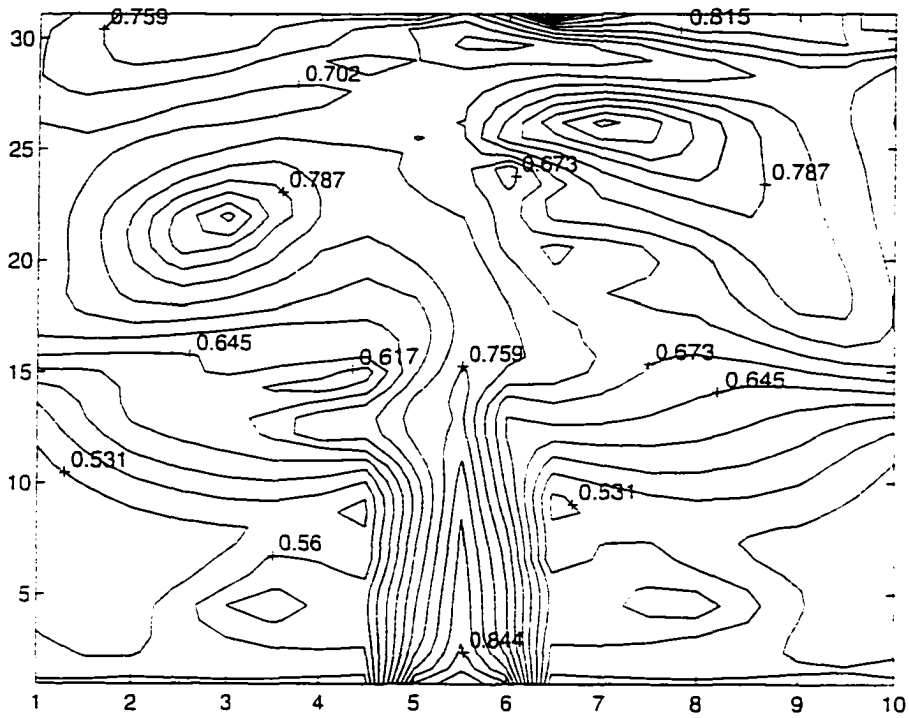

Figure 5.62: Contour plot of air void fraction of a jet velocity = 49.49 cm/s in gas-solid fluidized bed with E=0 kV, at t=1.5 s
(grid size 0.5X0.7 cm, U=Umf=0.49 cm/s, dp=49 micron, static bed height 19.6 cm, bed width 9.5 cm)

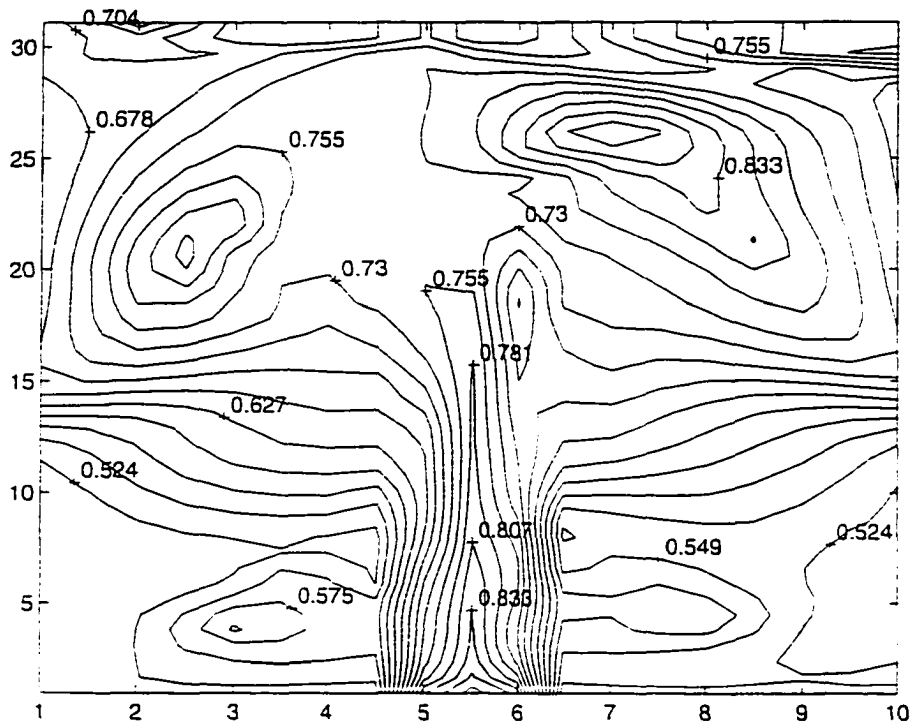

Figure 5.63: Contour plot of air void fraction of a jet velocity = 49.49 cm/s in gas-solid fluidized bed with E=100 kV, at t=1.5 s
(grid size 0.5X0.7 cm, U=Umf=0.49 cm/s, dp=49 micron, static bed height 19.6 cm, bed width 9.5 cm)

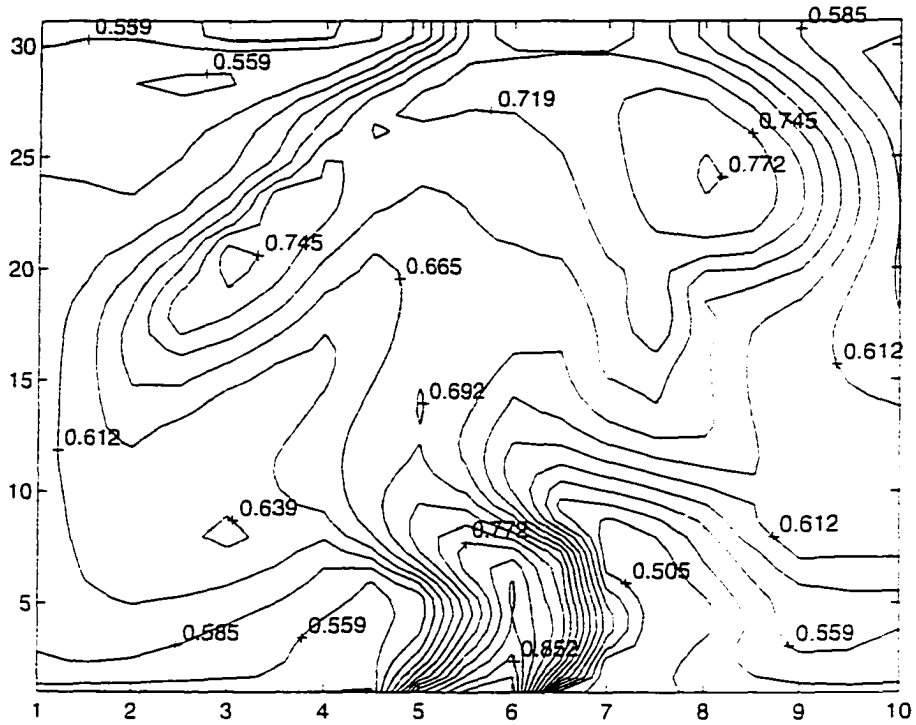

Figure 5.64: Contour plot of air void fraction of a jet velocity = 49.49 cm/s in gas-solid fluidized bed with E=0 kV, at t=3.0 s
(grid size 0.5X0.7 cm, U=Umf=0.49 cm/s, dp=49 micron, static bed height 19.6 cm, bed width 9.5 cm)

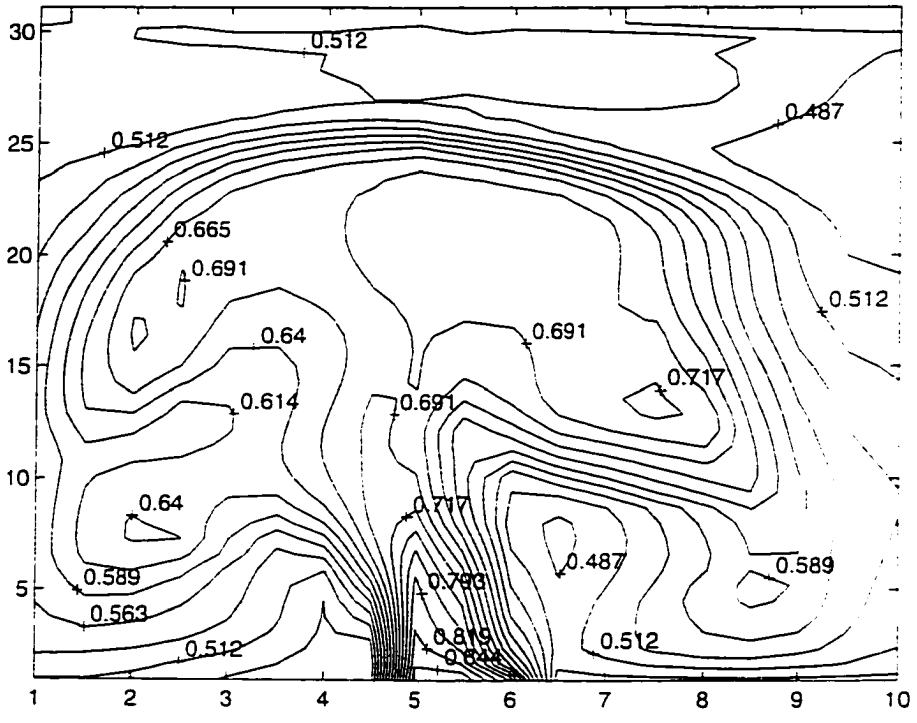

Figure 5.65: Contour plot of air void fraction of a jet velocity = 49.49 cm/s in gas-solid fluidized bed with E=100 kV, at t=3.0 s
(grid size 0.5X0.7 cm, U=Umf=0.49 cm/s, dp=49 micron, static bed height 19.6 cm, bed width 9.5 cm)

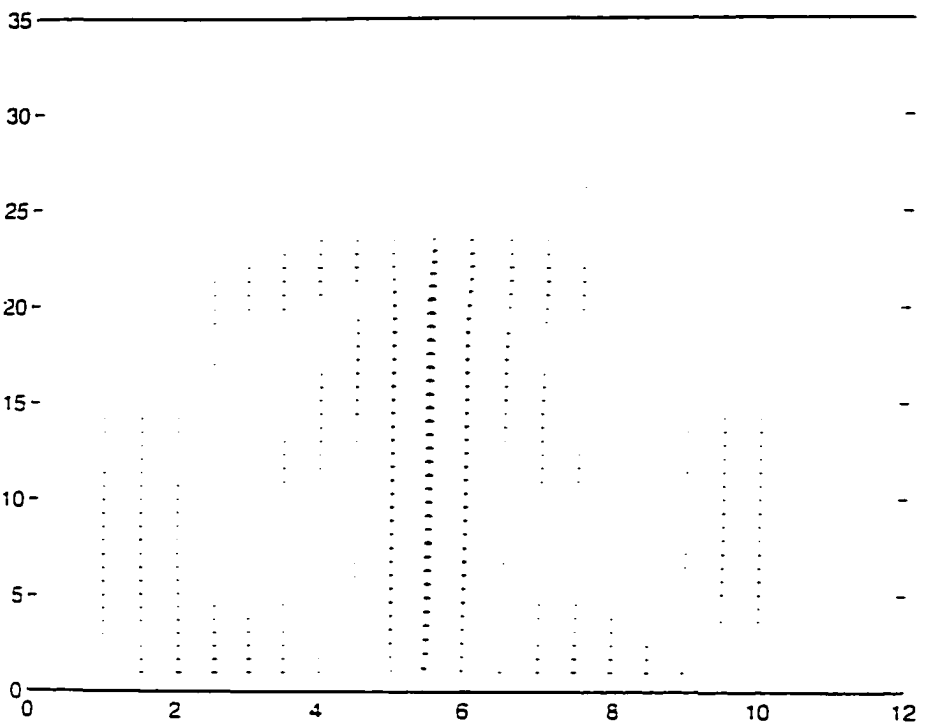

Figure 5.66: Vector plot of air velocity of a jet velocity = 49.49 cm/s in gas-solid fluidized bed with E=0 kV, at t=0.0 s (grid size 0.5X0.7 cm, U=Umf=0.49 cm/s, dp=49 micron, static bed height 19.6 cm, bed width 9.5 cm)

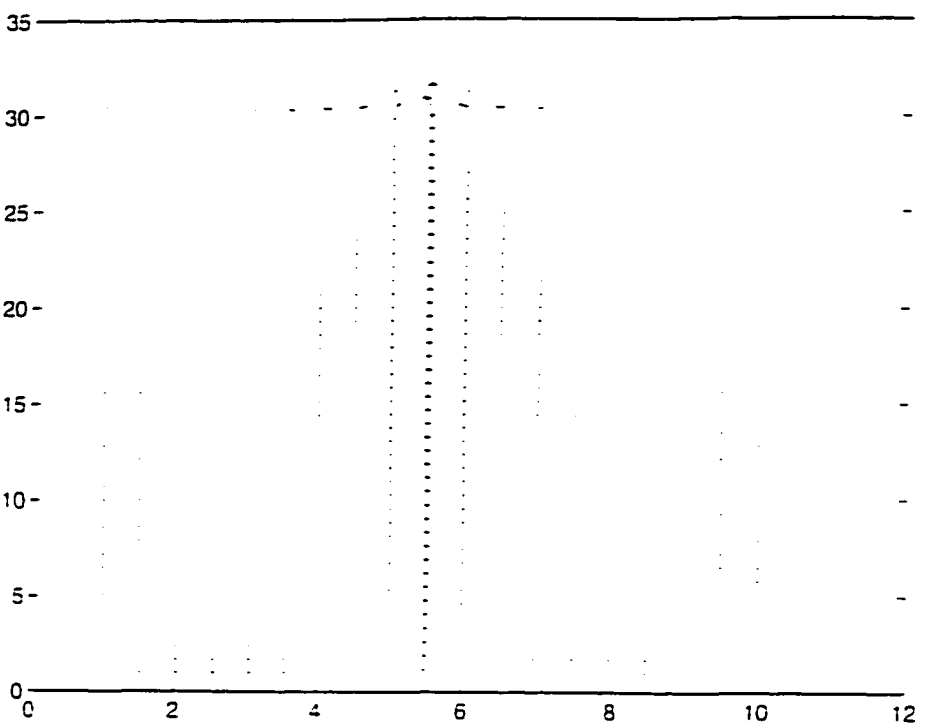

Figure 5.67: Vector plot of air velocity of a jet velocity = 49.49 cm/s in gas-solid fluidized bed with E=0 kV, at t=0.6 s (grid size 0.5X0.7 cm, U=Umf=0.49 cm/s, dp=49 micron, static bed height 19.6 cm, bed width 9.5 cm)

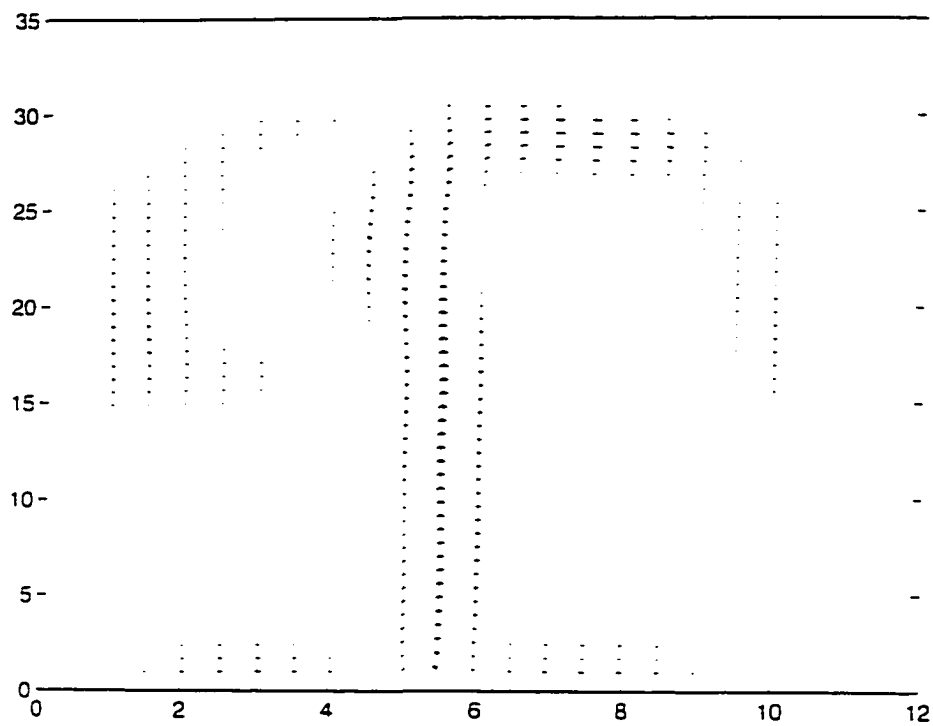

Figure 5.68: Vector plot of air velocity of a jet velocity = 49.49 cm/s in gas-solid fluidized bed with E=0 kV, at t=1.5 s (grid size 0.5X0.7 cm, U=Umf=0.49 cm/s, dp=49 micron, static bed height 19.6 cm, bed width 9.5 cm)

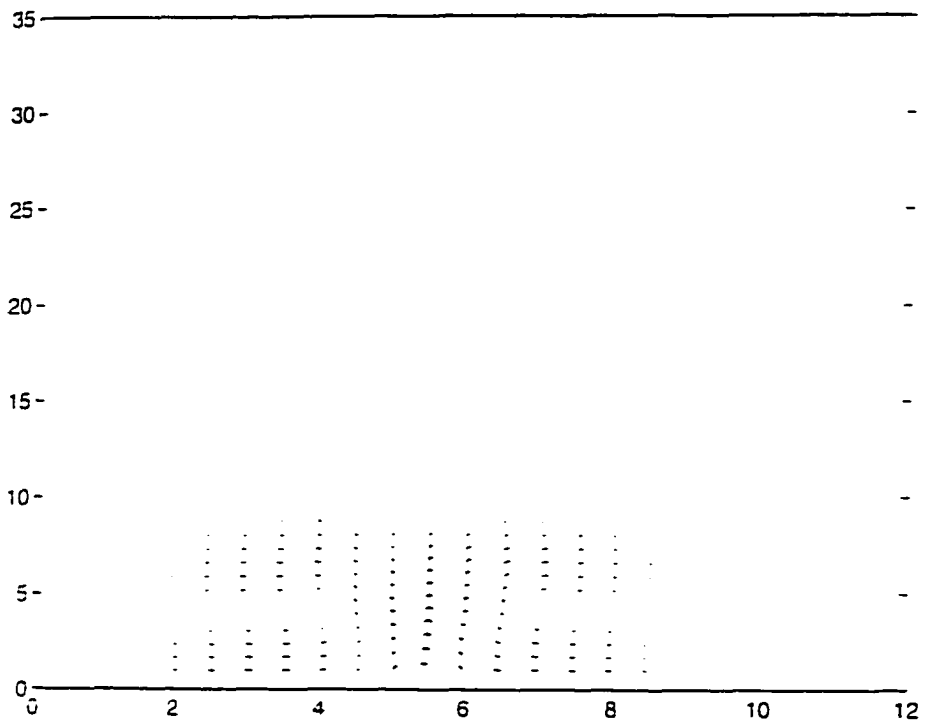

Figure 5.69: Vector plot of air velocity of a jet velocity = 49.49 cm/s in gas-solid fluidized bed with E=0 kV, at t=2.0 s (grid size 0.5X0.7 cm, U=Umf=0.49 cm/s, dp=49 micron, static bed height 19.6 cm, bed width 9.5 cm)

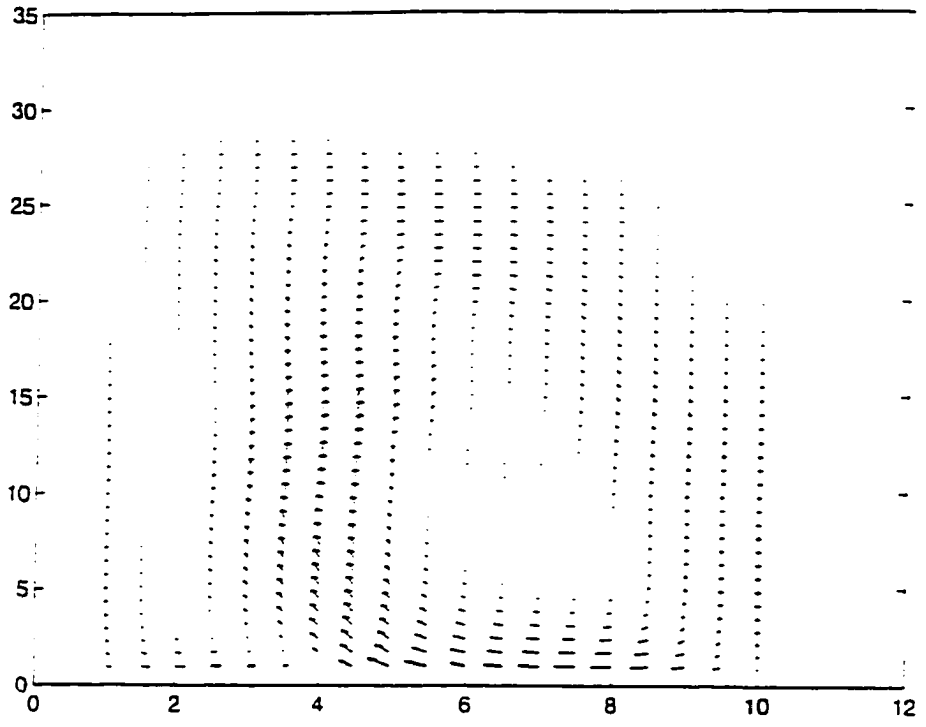

Figure 5.70: Vector plot of air velocity of a jet velocity = 49.49 cm/s in gas-solid fluidized bed with E=0 kV, at t=3.0 s (grid size 0.5X0.7 cm, U=Umf=0.49 cm/s, dp=49 micron, static bed height 19.6 cm, bed width 9.5 cm)

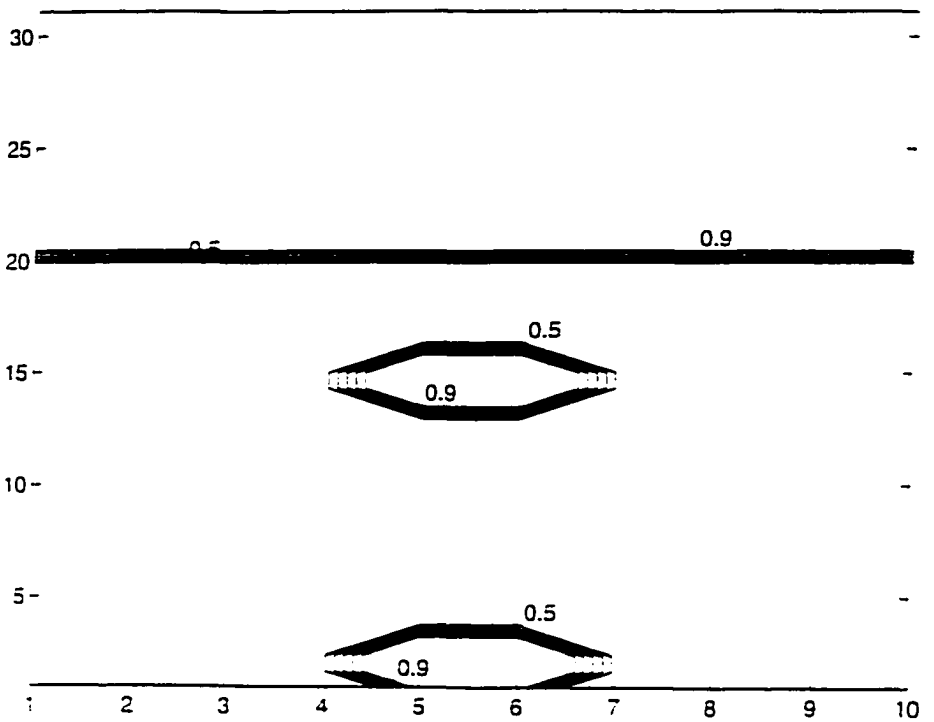

Figure 5.71: Contour plot of Air Void fraction of two inserted bubble in Gas-Solid Fluidized bed with E=0 kV. at t=0.0 s
(Grid size 0.5X0.7 cm. U=Umf=0.49 cm/s. dp=49 micron. static bed height 19.6 cm. bed width 9.5 cm)

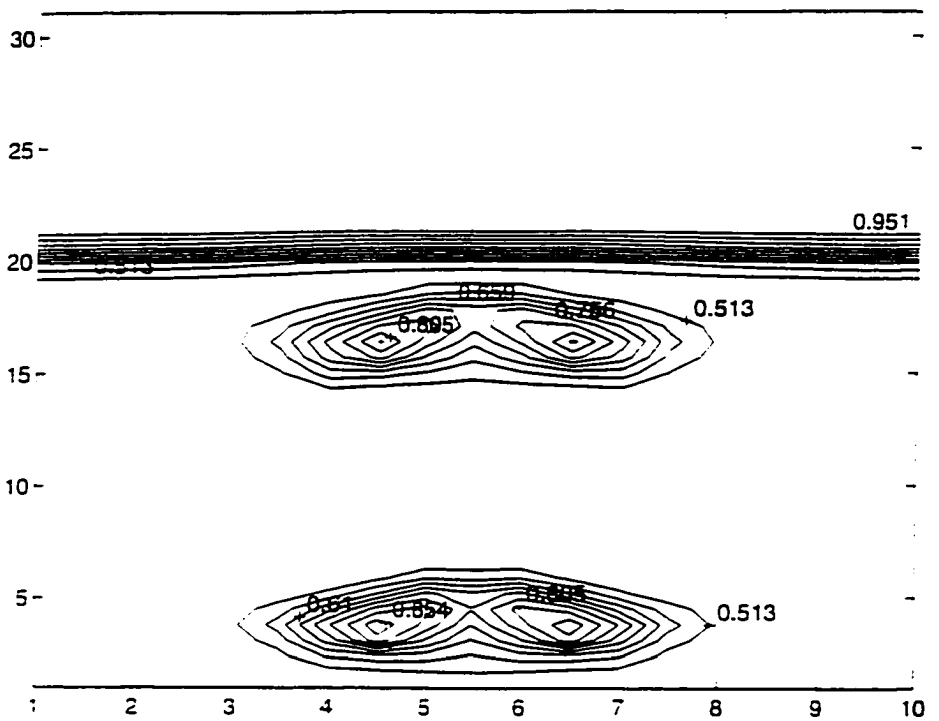

Figure 5.72: Contour plot of Air Void fraction of two inserted bubble in Gas-Solid Fluidized bed with E=0 kV. at t=0.1 s
(Grid size 0.5X0.7 cm. U=Umf=0.49 cm/s. dp=49 micron. static bed height 19.6 cm. bed width 9.5 cm)

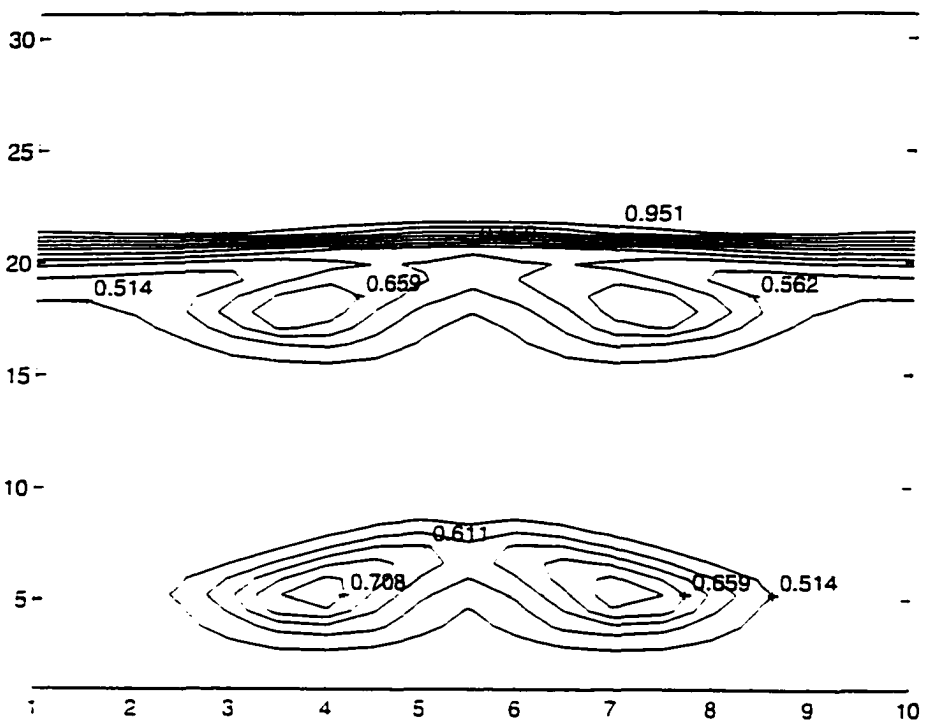

Figure 5.73: Contour plot of Air Void fraction of two inserted bubble in Gas-Solid Fluidized bed with E=0 kV. at t=0.2 s (Grid size 0.5X0.7 cm. U=Umf=0.49 cm/s. dp=49 micron. static bed height 19.6 cm. bed width 9.5 cm)

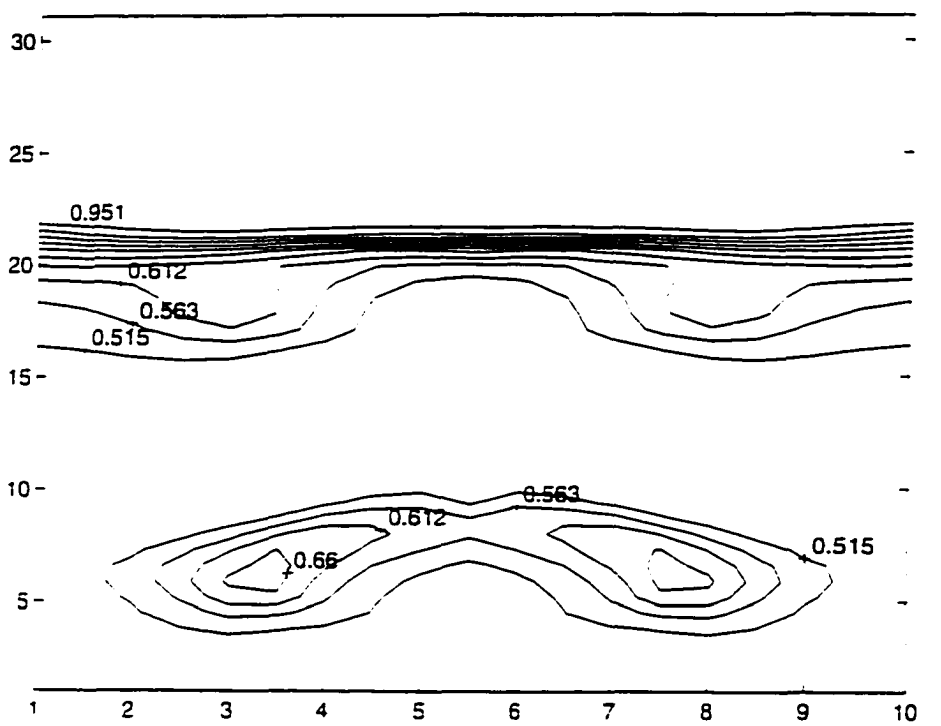

Figure 5.74: Contour plot of Air Void fraction of two inserted bubble in Gas-Solid Fluidized bed with E=0 kV. at t=0.3 s
(Grid size 0.5X0.7 cm. U=Umf=0.49 cm/s. dp=49 micron. static bed height 19.6 cm. bed width 9.5 cm)

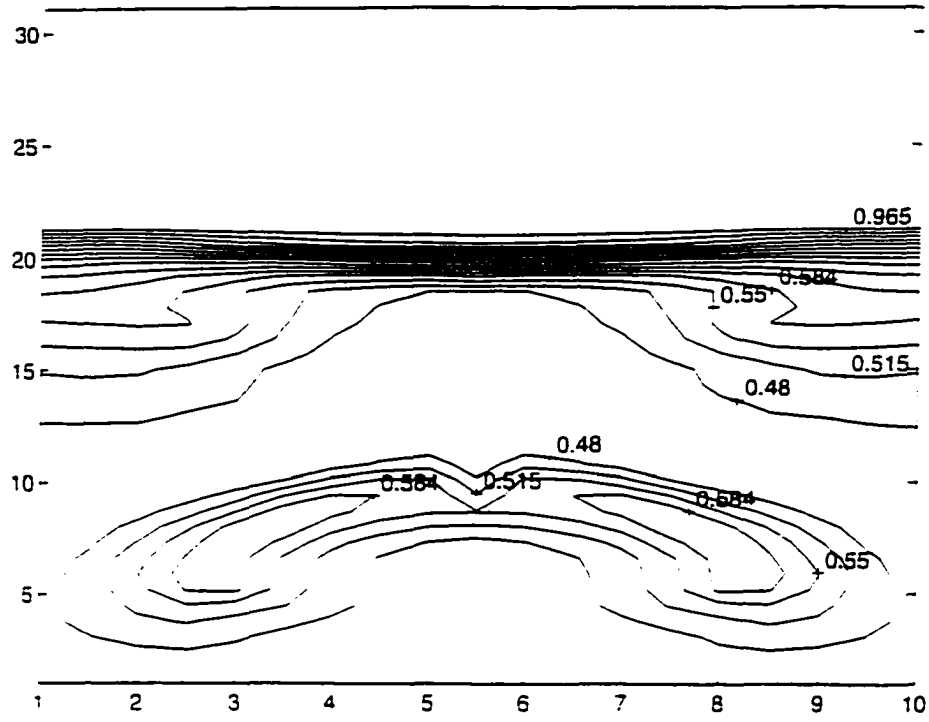

Figure 5.75: Contour plot of Air Void fraction of two inserted bubble in Gas-Solid Fluidized bed with E=0 kV. at t=0.4 s
(Grid size 0.5X0.7 cm. U=Umf=0.49 cm/s. dp=49 micron. static bed height 19.6 cm. bed width 9.5 cm)

6. CONCLUSIONS

A modified two-dimensional, unsteady state hydrodynamic computer code K-Fix is used to incorporate an electric field as an interparticle force effect to calculate the gas and solids velocities and pressure and void fraction in a solid-gas rectangular fluidized bed. The cases studied are those of a bubble free bed, single and multiple bubbles, and a bed with a central jet. It is found that the electric field is an independent variable in controlling the bed stability. The effect of the electric field is graphically illustrated by the alteration of voidage contour lines in the bed. The empirical relation for the interparticle force caused by the electric field as developed by Colver and Wang, (1994c) can be utilized to predict the stability of the bed through observation of the bubble dynamics. These particle forces help solidify the numerical stability of the code through the existence of real eigenvalues. Theoretically, the inclusion of the interparticle force term makes the ill posed set of equations well posed at low porosities by ensuring that the eigenvalues are always real. The solid pressure was essential to the stability of the hydrodynamic model. In the available literature the solid stress modulus is given only as a function of porosity. A general formulation of this term should show a functional relationship to pressure, porosity, gas velocity, and relative velocity. In addition to the developed modulus equation which incorporates a void fraction and electric field, variables such as temperature and particle diameter should be included to predict more accurately the bed behavior. Subsequently the Code will provide us with the capability to predict unsteady operation of the fluidized bed including following the development of a single bubble or a jet as well as the detailed bed circulation without

bubbles. The latter effect will be significant in heat and mass transfer studies with electric fields. However, the numerical simulation of a fluidized bed of fine semi-insulating particles subjected to an ac applied electric field appears to confirm observations made on actual beds with the ac electric fields as follows:

i) Bed circulation is reduced (particulate fluidized)

ii) Bubble rise velocity is decreased

iii) Bubbles are elongated in the direction of the electric field and dispersed

iv) Jet penetration is slowed and narrowed in the bed

Of these effects, the behavior of the jet remains to be confirmed experimentally, although bed spouting is well known to be initiated with the application of ac and dc fields of high electric field strength.

APPENDIX A: VELOCITY

Single Particle Terminal velocity

For a single particle falling through a fluid, the balance between buoyancy due to gravity and drag force on the particle (e. g. sphere) is known as the terminal velocity. Two examples given below is terminal velocities of two different particles (Gidispow,1994).

I)

$d_p = 0.127$ cm

$g = 980$ cm/s^2

$\rho_s = 2.61$ gm/cm^3

T=293 k (Air)

P=1.0129 X 10^6 pa

$C_D = 0.44$

$$\rho_g = \frac{P}{RT} = \frac{1.0129 \times 10^6}{2.87 \times 10^6 \times 293} = 0.00120 \text{ gm/cm}^3$$

$$u_t = 1.74 \sqrt{\frac{d_p\, g(\rho_s - \rho_g)}{\rho_g}} = 905.09 \text{ cm/s}$$

II)

$d_p = 0.0571$ cm

$g = 980$ cm/s^2

ρ_s=1.11 gm/cm^3

P=1.0129 X 10^6 pa T= 293 k C_D= 0.44

Using the above formula,

u_t = 395.65 cm/s

III

Minimum Fludization Velocity of a Fluidized bed

The minimum fluidization velocity is determined empirically by the intersection of the pressure drop versus the superficial velocity curve and the pressure drop equals the weight of the bed. At minimum fluidization the velocity of the solids is taken to be the velocity in the packed bed region, that is zero. The following equation (Gidispow, 1994) is used to estimate the minimum fluidization velocity.The porosity at minimum fluidization is determined from the height of the bed at minimum fluidization.

$$u_{mf} = \frac{d_p^2(\rho_s - \rho_g)g}{150\mu} \times \frac{\varepsilon_{mf}^3 \varphi_s^2}{1-\varepsilon_{mf}}$$

d_p= 0.127 cm

g= 980 cm/s^2

ρ_s=2.61 gm/cm^3

ρ_g=0.0012 gm/cm^3

$\mu = 1.8 \times 10^{-4}$ gm/cm.s

$\varphi_s = 1.0$

$\varepsilon_{mf} = 0.44$

$u_{mf} = 220.15$ cm/s

APPENDIX B: NUMERICAL METHODS

The Newton-Raphson Method

Perhaps the most widely used of all root locating formulas is the Newton-Raphson equation Figure B.1. If the initial guess at the root is x_i , a tangent can be extended from the point $[x_i, f(x_i)]$. The point where this tangent crosses the x axis usually represents an improved estimate of the root.

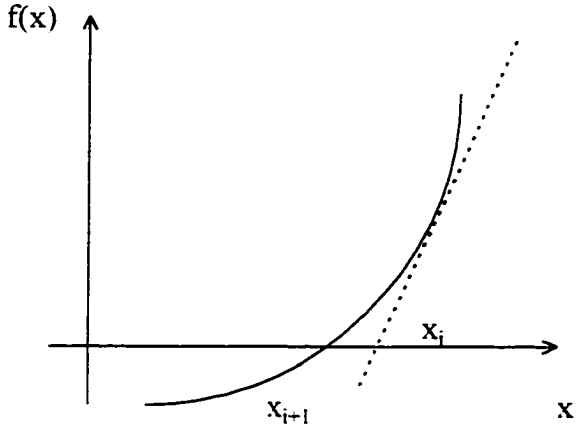

Figure B.1: Root estimation in Newton-Raphson Method

The Newton-Raphson method can be derived on the basis of this geometrical interpretation. As in Figure B.1, the first derivative at x_i is equivalent to the slope:

$$f'(x_i) = \frac{f(x_i) - 0}{x_i - x_{i+1}}$$

which can be rearranged to yield

$$x_{i+1} = x_i - \frac{f(x_i)}{f'(x_i)}$$

which is called the Newton-Raphson formula.

The Secant Method

A potential problem in implementing the Newton-Raphson method is the evaluation of the derivative. Although this is convenient for polynomials and many other functions. there are certain functions whose derivatives may be difficult to evaluate . For these cases . the derivative can be approximated by a finite divided difference. as in Figure B.1

$$f'(x_i) \cong \frac{f(x_{i-1}) - f(x_i)}{x_{i-1} - x_i}$$

This approximation can be substituted into previous formal to yield the following iterative equation:

$$x_{i+1} = x_i - \frac{f(x_i)(x_{i-1} - x_i)}{f(x_{i-1}) - f(x_i)}$$

The above equation is the formula for the secant method. Notice that the approach requires two initial estimates of x. However. because $f(x)$ is not required to change signs between the estimates. it is not classified as a bracketing method.

Stopping craters for the two methods are as follows:

$$\left|\frac{x_{i+1} - x_i}{x_{i+1}}\right| \leq \varepsilon \quad \text{and for the Secant Method} \quad \left|\frac{x_{i+1} - x_i}{x_{i+1}}\right| \leq \varepsilon$$

Gauss-Jordan Method

In this method for solving simultaneous equation the elements above the diagonal elements are made zero at the same time that zeros are created below the diagonal elements also. Usually the diagonal elements are assigned unity at the same time that the reduction is performed. this transforms the coefficient matrix into the identity matrix. When this has been accomplished , the column of the equation matrix has been transformed into the solution vector. Pivoting is normally employed to preserve arithmetic accuracy. For example. for the system of equations.

$$2x_2 + x_4 = 0.$$

$$2x_1 + 2x_2 + 3x_3 + 2x_4 = -2.$$

$$4x_1 - 3x_2 + x_4 = -7.$$

$$6x_1 + x_2 - 6x_3 - 5x_4 = 6.$$

The augmented coefficient matrix is

$$\begin{bmatrix} 0 & 2 & 0 & 1 & 0 \\ 2 & 2 & 3 & 2 & -2 \\ 4 & -3 & 0 & 1 & -7 \\ 6 & 1 & -6 & -5 & 6 \end{bmatrix}$$

After doing some algebraic operations of rows . the solution form becomes

$$\begin{bmatrix} 1 & 0 & 0 & 0 & -0.49999 \\ 0 & 1 & 0 & 0 & 1.00010 \\ 0 & 0 & 1 & 0 & 0.33326 \\ 0 & 0 & 0 & 1 & -1.9999 \end{bmatrix}$$

APPENDIX C: PROGRAM ORGANIZATION

The K-Fix FORTRAN code used for numerical bubble simulation are organized in following Figure C.1: . The program is in modular form. The input files in this program are GCOM and Multim.dat. GCOM file contain all the global declared variables for each module. Multim.dat file contains all the input values for numerical simulation.

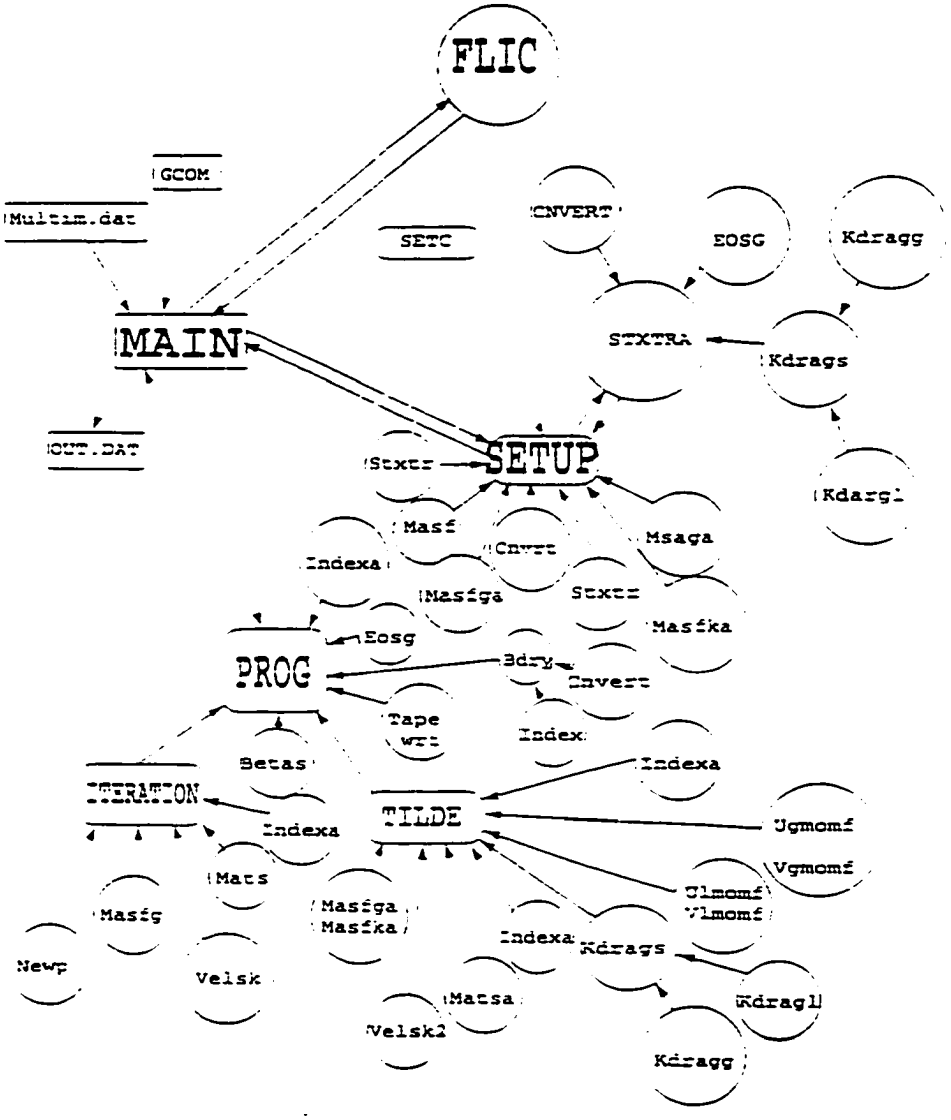

Figure C.1: K-Fix FORTRAN Computer code organization

Figure C.2 represents the rectangular divisions of computing regions of interests with cell indices and cell flags. Cell flags are designated to the computing cells to identify the cell types. The cell flags used in this numerical simulation work are 1, 3, 5, and 7. These numbers are identified by the code as Fluid, Solid cell with no-slip boundaries, Specified influx inflow, and Specified outflow pressure cells.

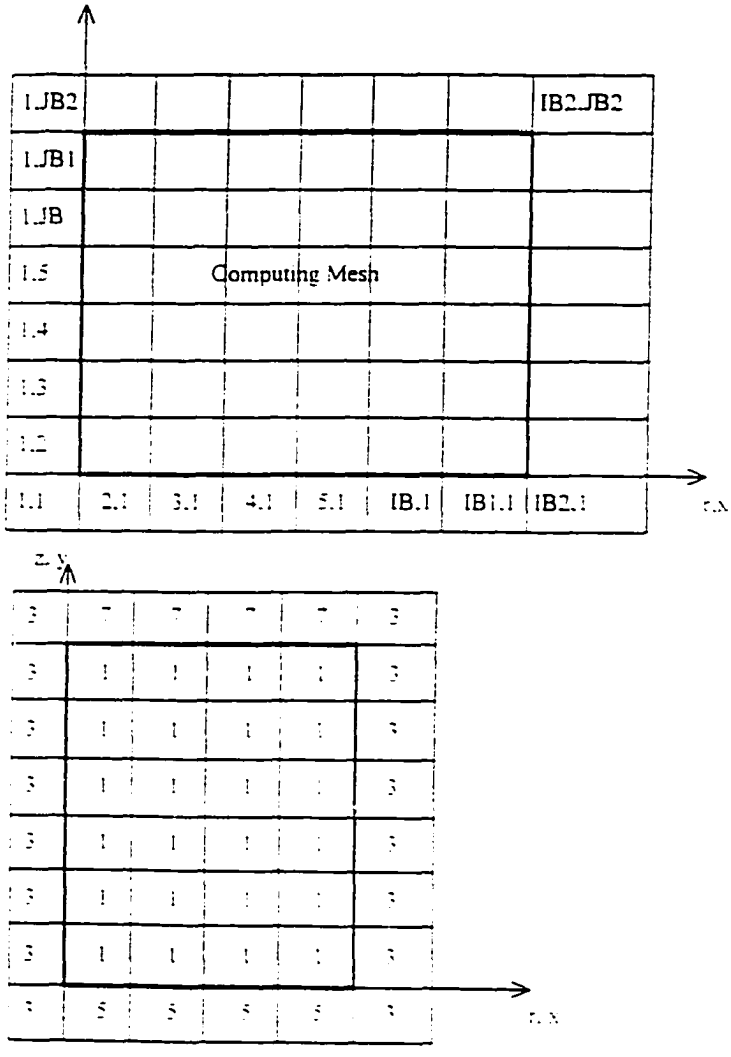

Figure C.2: Problem Setup for Computation

APPENDIX D: SECANT METHOD

The pressure corrections are done using a constrained two sided secant method as illustrated in figure D.1. Given the three points 1, 2, and 3 of which 1 and 2 bracket the desired pressure and 3 lies between them, the pressure P_A, and P_B are determined by straight line extrapolation and interpolation, respectively. The new estimate of the advanced time pressure is then computed as ${}^{n+1}P^j_i = 0.5\,(P_A + P_B)$. If the pressure P_A should lie outside the interval P_1 to P_3, it is given the value $0.5\,(P_1 + P_3)$. After ${}^{n+1}P^j_i$ is estimated, point 2 is discarded and points 1 and 3 are retained as improved bounds for the next pressure estimate.

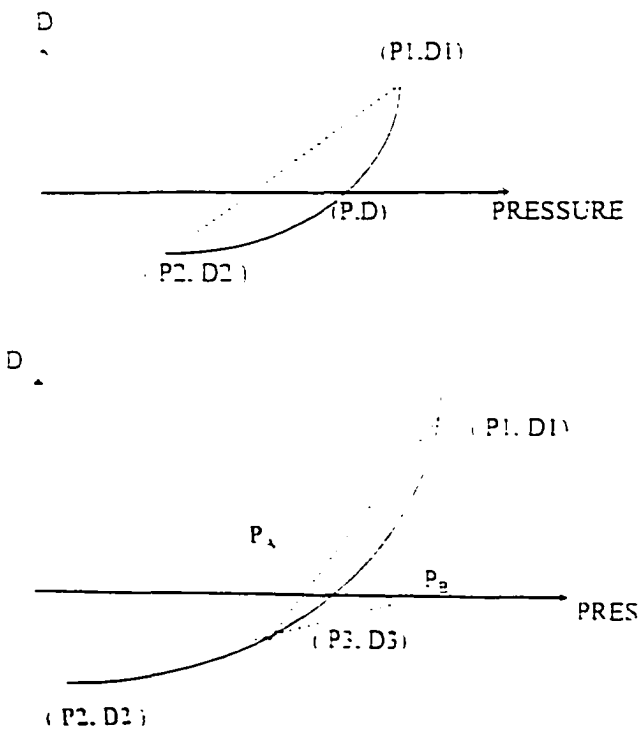

Figure D.1: Secant Method used to speed up the convergence (Rivard and Torrey, 1977)

BIBLIOGRAPHY

Anderson, D. A., Tannehill, J. C., and Pletcher, R. H., Computational Fluid Mechanics and Heat Transfer, New York: Taylor & Francis, 1984.

Colver, G. M., "Dynamic and Stationary Charging of Heavy Metallic and Dielectric Particles Against a Conducting Wall in the Presence of a DC Applied Electric Field", J. Applied Physics 47, no. 11 (1976): 4839-4849.

Colver, G. M., "Bubble Control in Gas-Fluidized Beds with Applied.Electric Fields, Analogies and Mechanisms", 2nd Powder and Bulk Solids Conf., Chicago, May 10-12, 1977a.

Colver, G. M., "Bubble Control in Gas-Fluidized Beds with Applied Electric Fields", J. Powder Technology, no. 17 (1977b): 9-18.

Colver, G. M., "The Influence of Electric and Magnetic Fields on Air-Fluidized Beds", NSF Workshop, Fluidization and Fluid Particle System Research Needs and Priorities, Rensselaer Polytechnic Inst., Troy, NY, 17-19 Oct., 1979.

Colver, G. M., and Bosshart, G. S., "Heat and Charge Transfer in an AC Electrofluidized Beds", Multiphase transport: Fundamentals, Reactor Safety, Applications, Vol. 1-5 (1980): 2215-2243.

Colver, G. M., and Donahoe, T. S., "Bubble-Rise Velocity in AC and DC Electrofluidized Beds", IEEE Trans. Industry Applications 20, no. 2 (1984): 259-266.

Colver, G. M., and Liu, X. M., "Capture of Fine Particles on Charged Moving Spheres: A New Electrostatic Precipitator", IEEE Trans. Industry Applications 27, no. 5 (1991): 807-815.

Colver, G. M., Tucholski, D. R., Soetomo, F., and Wang, J. S., "Electrostatics in Powders and Related High Temperature Phenomena", IFPRI Annual Meeting, Harrogate England, May 31-June 5, 1992a.

Colver, G. M., and Wang, J. S., "Bubble and Elutriation Control in Fluidized Beds with Electric Fields", IFPRI Annual Report, AAR 24-02, Dec. 31, 1992b.

Colver, G. M., and Wang, J. S., "Electrostatics in Powders and Related High Temperature Phenomena: Fluidized beds and Elutriation", IFPRI Annual Meeting, Pasadena, California, June 27-30, 1993a.

Colver, G. M., and Wang, J. S., "Bubble and Elutriation Control in Fluidized Beds with Electric Fields", IFPRI Annul Report, AAR24-03, Dec. 31, 1993b.

Colver, G. M., and Wang, J. S., "Electric Field Control of Powders", IFPRI Annual Meeting, Goslar Germany, June 12-16, 1994a.

Colver, G. M., and Wang, J. S., "Bubble Stability Modeling in Fluidized Beds Utilizing Electric Fields", lst International Particle Technology Forum, Denver, Colorado, August 17-19, 1994b.

Colver, G. M., and Wang, J. S., "Bubble and Elutriation Control in Fluidized Beds with Electric Fields", IFPRI Annual Report, ARR24-04, Dec. 31, 1994c.

Colver, G. M., and Wang, J. S., "Electric Field Control of Powders", IFPRI Annual Meeting Allea Hotel, Nancy France, June 9-14, 1996.

Davidson, J. F., Clift, R., and Harrison, D., Fluidization, London: Academic Press, 1985.

Dietz, P. W., "Fields and Forces of a Macroscopic Sphere above a Ground Plane in a Sinusoidally Varying Electric Field", J. Applied Physics 48, no. 3 (1977): 1036-1040.

Dietz, P. W., and Melcher, J. M., "Interparticle Electrical Forces in Packed and Fluidized Beds", Ind. Eng. Chem. Fundamental. 17, no. 1 (1978a): 28-32.

Dietz, P. W., and Melcher, J. M., "Momentum Transfer in Electrofluidized Beds", AIChE Symposium of Air Pollutants-NO_x and Particulate Emissions 74, no. 175 (1978b): 166-174.

Ettehadieh, B., "Hydrodynamics Analysis of Gas-Sold Fluidized Bed", Ph.D. Dissertation Illinois Institute of Technology, Chicago (1982).

Fan, L. -S., "Summary Paper on Fluidization and Transport Phenomena", Powder Technology 88(1996) 245-253.

Geldart, D., Gas Fluidization Technology, New York: John Wiley & Sons, 1986.

Gidaspow, D., Multiphase Flow and Fluidization, San Diego: Academic Press, 1994.

Jackson, R., "The Mechanics of Fluidized Beds: The Stability of the State of Uniform Fluidization", Trans. Inst. Chem. Eng., 41, 13-21(1963)

Johnson, T. W., and Melcher, J. M., "Electromechanics of Electrofluidized Beds", Ind. Eng. Chem. Fundam. 14, no. 3 (1975): 146-153.

Katz, H., and Sears, J. T., "Electric Field Phenomena in Fluidized and Fixed Beds", Canadian J. Chem. Eng. 47, Feb. (1969): 50-53.

Kos, P. , "Gravity Thickening of Water Treatment Plant Sludges", Journal AWWA. pp. 272-282 (1977).

Kunii, D., and Levenspiel, O., Fluidization Engineering, Stoneham: Butterworth-Heinemann, 1991.

Moissis, A. A., and Zahn, K., "Electrofluidized Bed Responses to Small Signal Excitations", IEEE Trans. Industry Application 22, no. 6 (1986): 1396-1403.

Murray, J. D., "On the Mathematics of Fluidization", J. Fluid Mech., 21, 465-493(1965).

Nayfeh, M. H., and Brussel, M. K., Electricity and Magnetism, New York: John Wiley & Sons, 1985.

Pigford, R. L. and Baron, T., "Hydrodynamic Stability of a Fluididizd Bed", Ind. Eng. Chem. Fundam., 4, 81-87 (1965).

Pritchett, J. W., H. B. Levine, T. R. Blake, S. K. Garg, "A Numerical Model of Gas Fluidized Beds", Presented at the AIChE Symposium Series Volume No. 176, 74, pp. 134, 148 (1978).

Reitema, K., The Dynamics of Fine Powders, Essex: Elsevier Science, 1991.

Richardson, J. F. and Zaki, W. N. 1954, "Sedimentation and Fluidization: Part I.", Trans. Instn Chem. Engrs 32.

Rivard, W. C. and Torrey, M. D., 1977. "K-Fix a computer program for transient two dimensional fluid flow.", Los Alamos Scientific Laboratory Report, LA-NUREG-6623 (1977).

Ruckenstein, E. and Tzeculescu, M., "Proceedings of the International Symposium on Fluidization in Eindhoven", Drinkenburg, A. A. H., ed., Netherlands University Press, 180, 1967/1968.

Soo, S. L., Fluid Dynamics of Multiphase Systems, Waltham, MA, Blaisdell Publishing Corp., 1967.

Syamlal, M., "Multiphase Hydrodynamics of Gas-Solid Flow", Ph.D. Dissertation, Illinois Institute of Technology, Chicago (1985).

Wang, Jiun-Shen, "Bubble and Elutriation Control in Fluidized Beds with Electric Fields", Ph.D. Dissertation, Department of Mechanical Engineering, Iowa State University, Ames, Iowa (1995).

Xie, H. Y., and Geldart, D., "The Role of Interparticle Forces in the Gas Fluidization of Fine Powders", IFPRI Annual Report, ARR15-07, 1993.

Xie, H. Y., and Geldart, D., "Interparticle Forces in Fine Particle Fluidization", IFPRI Annual Report, ARR15-06, Dec. 1992.

Zahedi, K. and Melcher, J. R., "Electrofluidized Beds in the Filtration of Submicron Aerosols", APCA Journal, Vol. 26 (1976): 345-351.

ACKNOWLEDGMENTS

I would like to express my sincere gratitude to my research advisor, Dr. Gerald M. Colver, for his guidance and much helpful advice during this work. I would also like to extend my deep appreciation to Dr. Richard H. Pletcher, Dr. Michael B. Pate, Dr. William D. James, and Dr. J. M. Vogel for their willingness to be committee members and for their valuable discussions and suggestions.

I am also grateful to the department of Mechanical Engineering for my teaching assistantship to complete my graduate study, through which I learned a lot as an instructor.

IMAGE EVALUATION
TEST TARGET (QA–3)

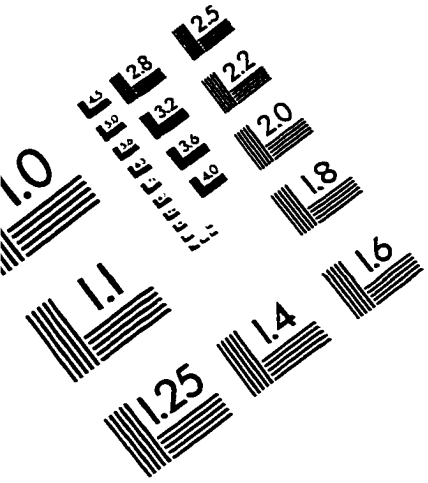

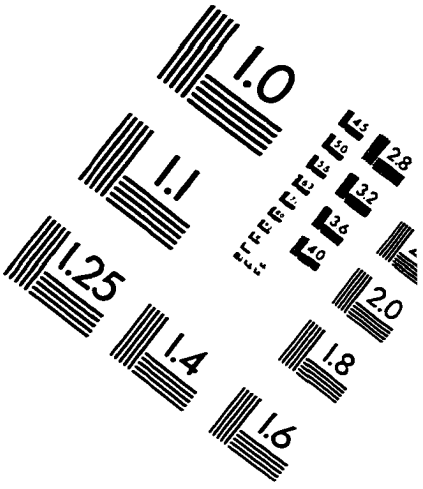

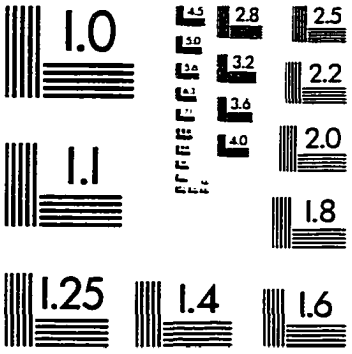

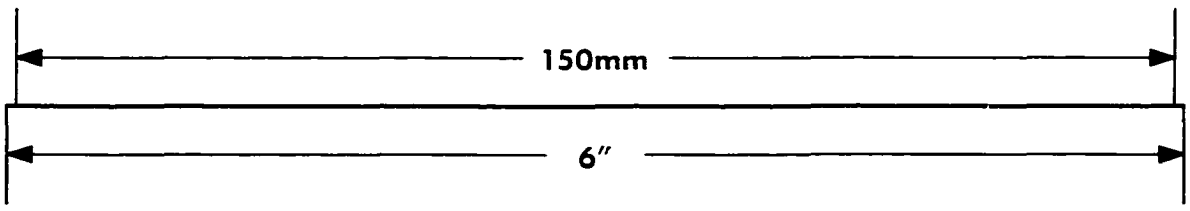

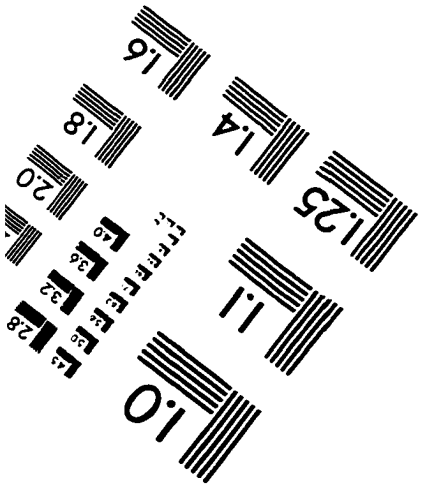

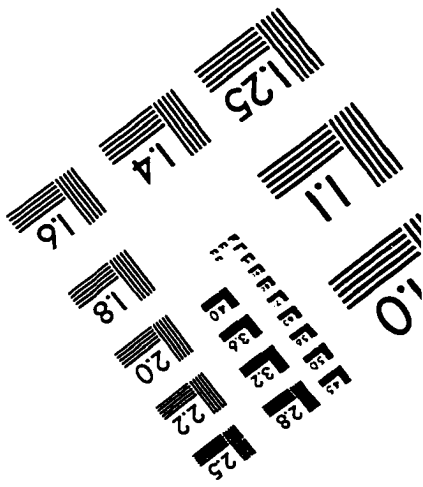

APPLIED IMAGE, Inc
1653 East Main Street
Rochester, NY 14609 USA
Phone: 716/482-0300
Fax: 716/288-5989